A TRIDENT SCHOLAR PROJECT REPORT

NO. 261

"Design, Construction, and Analysis of a Flat Heat Pipe"

UNITED STATES NAVAL ACADEMY
ANNAPOLIS, MARYLAND

This document has been approved for public release and sale; its distribution is unlimited.

20000424 149

DTIC QUALITY INSPECTED 3

REPORT DOCUMENTATION PAGE

Form Approved
OMB No. 074-0188

Public reporting burden for this collection of information is estimated to average 1 hour per response, including g the time for reviewing instructions, searching existing data sources, gathering and maintaining the data needed, and completing and reviewing the collection of information. Send comments regarding this burden estimate or any other aspect of the collection of information, including suggestions for reducing this burden to Washington Headquarters Services, Directorate for Information Operations and Reports, 1215 Jefferson Davis Highway, Suite 1204, Arlington, VA 22202-4302, and to the Office of Management and Budget, Paperwork Reduction Project (0704-0188), Washington, DC 20503.

1. AGENCY USE ONLY (Leave blank)	2. REPORT DATE	3. REPORT TYPE AND DATE COVERED
	5 May 1999	

4. TITLE AND SUBTITLE
Design, construction, and analysis of a flat heat pipe

5. FUNDING NUMBERS

6. AUTHOR(S)
Boughey, Britt W.

7. PERFORMING ORGANIZATION NAME(S) AND ADDRESS(ES)
U.S. Naval Academy
Annapolis, MD

8. PERFORMING ORGANIZATION REPORT NUMBER
USNA Trident Scholar project report no. 261 (1999)

9. SPONSORING/MONITORING AGENCY NAME(S) AND ADDRESS(ES)

10. SPONSORING/MONITORING AGENCY REPORT NUMBER

11. SUPPLEMENTARY NOTES
Accepted by the U.S. Trident Scholar Committee

12a. DISTRIBUTION/AVAILABILITY STATEMENT
This document has been approved for public release; its distribution is UNLIMITED.

12b. DISTRIBUTION CODE

13. ABSTRACT: Thermophotovoltaic (TPV) energy conversion utilizes photons from a thermal radiator to convert photonic energy to electrical energy. Due to the nature of the system, the thermal radiator must emit uniform radiation and therefore maintain a uniform temperature profile in order to achieve maximum efficiency. Heat pipe technology can effectively meet the demand for an isothermal emitter as it utilizes near isobaric phase changes to transfer heat at a uniform temperature. In this project, heat pipes are explored for use in TPV energy conversion systems. A flat heat pipe offers many advantages over the conventional cylindrical design. These include increased surface area to volume ratio in order to maximize power density, as well as the ability to stack or layer the system with photovoltaic (PV) cells on both sides of the flat heat pipe to utilize available energy. Not only do flat heat pipes present unique engineering demands inherent in their operation to counteract pressure differences across their vessel walls, but they are also difficult to construct. To date, only limited analyses of their thermal characteristics have been done for use in performance predictions. Therefore, it is necessary to conduct analyses to enable consideration of heat pipes for implementation into TPV systems. This report details the design and construction of a flat heat pipe analysed both in symmetric and asymmetric heating conditions, involving a low temperature version of future emitter designs due to safety considerations. Water was used as a working fluid instead of the liquid metal required to achieve the temperatures of a functional emitter. Despite this difference in working fluid, the data presented is valuable to both TPV and heat pipe research.

14. SUBJECT TERMS
heat pipe, emitter, isothermal, thermophotovoltaic

15. NUMBER OF PAGES

16. PRICE CODE

17. SECURITY CLASSIFICATION OF REPORT	18. SECURITY CLASSIFICATION OF THIS PAGE	19. SECURITY CLASSIFICATION OF ABSTRACT	20. LIMITATION OF ABSTRACT

U.S.N.A. — Trident Scholar project, report; no. 261 (1999)

"Design, Construction, and Analysis of a Flat Heat Pipe"

by

Midshipman Britt W. Boughey, Class of 1999
United States Naval Academy
Annapolis, Maryland

Britt Boughey
(signature)

Certification of Advisors' Approval

Professor Keith W. Lindler
Department of Naval Architecture, Ocean and Marine Engineering

Keith W. Lindler
(signature)

5/4/99
(date)

Associate Professor Martin R. Cerza
Department of Naval Architecture, Ocean and Marine Engineering

Martin R. Cerza
(signature)

5/4/99
(date)

Acceptance for the Trident Scholar Committee

Professor Joyce E. Shade
Chair, Trident Scholar Committee

J. E. Shade
(signature)

6 May 1999
(date)

ABSTRACT

Thermophotovoltaic (TPV) energy conversion utilizes photons from a thermal radiator to convert photonic energy to electrical energy. Due to the nature of the system, the thermal radiator must emit uniform radiation and therefore maintain a uniform temperature profile in order to achieve maximum efficiency. Heat pipe technology can effectively meet the demand for an isothermal emitter as it utilizes near isobaric phase changes to transfer heat at a uniform temperature. In this project, heat pipes are explored for use in TPV energy conversion systems. A flat heat pipe offers many advantages over the conventional cylindrical design. These include increased surface area to volume ratio in order to maximize power density, as well as the ability to stack or layer the system with photovoltaic (PV) cells on both sides of the flat heat pipe to utilize available energy. Not only do flat heat pipes present unique engineering demands inherent in their operation to counteract pressure differences across their vessel walls, but they are also difficult to construct. To date, only limited analyses of their thermal characteristics have been done for use in performance predictions. Therefore, it is necessary to conduct analyses to enable consideration of heat pipes for implementation into TPV systems. This report details the design and construction of a flat heat pipe analysed both in symmetric and asymmetric heating conditions, involving a low temperature version of future emitter designs due to safety considerations. Water was used as a working fluid instead of the liquid metal required to achieve the temperatures of a functional emitter. Despite this difference in working fluid, the data presented is valuable to both TPV and heat pipe research.

KEYWORDS: heat pipe, emitter, isothermal, thermophotovoltaic

TABLE OF CONTENTS

ABSTRACT		1
TABLE OF CONTENTS		2
LIST OF FIGURES		4
NOMENCLATURE		6
1.0	INTRODUCTION	9
	1.1 OBJECTIVES	
	1.2 METHODOLOGY	
2.0	THERMOPHOTOVOLTAICS BACKGROUND	11
	2.1 PHOTOVOLTAIC PHYSICS	
	2.2 TPV EFFICIENCY	
3.0	HEAT PIPE INTRODUCTION	15
	3.1 STEADY-STATE LIMITS	
	3.2 WICK DESIGNS	
4.0	FLAT HEAT PIPE PROPERTIES	22
	4.1 FLAT HEAT PIPE HEATING LIMITS	
	4.2 FLAT HEAT PIPE STRUCTURAL CONSIDERATIONS	
5.0	USNA FLAT HEAT PIPE DESIGN	26
	5.1 CALCULATED LIMITS	
	5.2 HEAT TRANSFER CALCULATIONS	
6.0	SUBSCALE FLAT HEAT PIPE	32
	6.1 SUBSCALE HEAT PIPE CONSTRUCTION	
	6.2 SUBSCALE HEAT PIPE TESTING	
	6.3 SUBSCALE HEAT PIPE TESTING RESULTS	
	6.4 IMPLICATIONS FOR FULLSCALE HEAT PIPE	
7.0	FULLSCALE HEAT PIPE CONSTRUCTION	37
	7.1. FULLSCALE HEAT PIPE CONSTRUCTION DETAILS	
8.0	EXPERIMENTAL SETUP AND PROCEDURE	40
	8.1 EXPERIMENTAL SETUP	
	8.2 EXPERIMENTAL PROCEDURE	

9.0 DATA ANALYSIS 50

9.1 HORIZONTAL TESTS/ HEAT PIPE VERIFICATION
9.2 ORIENTATION EFFECTS
9.3 CHARGING EFFECTS
9.4 START-UP TRANSIENTS
9.5 ASYMMETRIC TESTING
9.6 VARIABLE CONDUCTANCE EFFECTS

10.0 CONCLUSIONS AND MODELLING 65

10.1 GOALS MET
10.2 RECOMMENDATIONS

11.0 REFERENCES 67

APPENDICES 68

APPENDIX 1 - CAPILLARY LIMIT DERIVATIONS
APPENDIX 2 - BOILING LIMIT DERIVATION
APPENDIX 3 - SONIC LIMIT DERIVATION
APPENDIX 4 - DEFLECTION DERIVATIONS AND SPREADSHEET
APPENDIX 5 - MATHCAD MODELLING OF FIN VS HEAT PIPE

ACKNOWLEDGMENTS 99

LIST OF FIGURES

		PAGE
FIGURE 1.	BASIC TPV SYSTEM	11
FIGURE 2.	PLANCK'S LAW	12
FIGURE 3.	AXIAL FLOW TPV- HEAT PIPE SYSTEM	14
FIGURE 4.	BASIC HEAT PIPE	15
FIGURE 5.	GAS LOADING EFFECTS	16
FIGURE 6.	HEATING LIMITS	18
FIGURE 7.	WETTING ANGLE	19
FIGURE 8.	SUBCALE HEAT PIPE EXTERIOR	28
FIGURE 9.	SUBSCALE HEAT PIPE DETAIL	29
FIGURE 10.	FULLSCALE FLAT HEAT PIPE EXTERIOR	30
FIGURE 11.	FULLSCALE FLAT HEAT PIPE DETAIL	31
FIGURE 12.	CHARGING ASSEMBLY	34
FIGURE 13.	SUBSCALE HEAT PIPE PHOTO	35
FIGURE 14.	PHOTO OF INFRARED CAMERA	36
FIGURE 15.	CLOSE-UP PHOTO OF VESSEL	38
FIGURE 16.	COMPLETED HALVES	38
FIGURE 17.	SCREEN SIDE VIEW WITH BENT SIDE	39
FIGURE 18.	SHEET WITH PINS	39
FIGURE 19.	PHOTO OF SYMMETRIC HEATER MOUNTING	41
FIGURE 20.	PHOTO OF ASYMMETRIC HEATER MOUNTING	41
FIGURE 21.	PHOTO OF HEAT PIPE END FITTING WITH PRESSURE TRANSDUCER	42
FIGURE 22.	PHOTO OF HEAT PIPE END FITTING WITH ANALOG PRESSURE GAUGE	43
FIGURE 23.	PHOTO OF HEAT PIPE TEST STAND	44
FIGURE 24.	PHOTO OF TEST STAND CLAMP MOUNTED TO HEAT PIPE	45
FIGURE 25.	THERMOCOUPLE PLACEMENT BY NUMBERS	46
FIGURE 26.	PHOTO OF THERMOCOUPLES MOUNTED	47
FIGURE 27.	PHOTO OF DATA ACQUISITION SETUP	47
FIGURE 28.	HEAT PIPE TESTING ORIENTATIONS	49
FIGURE 29.	HEAT TRANFER REJECTION MODES FOR HEAT INPUT	51
FIGURE 30.	STANDARD FIN VS IDEAL HEAT PIPE FIN AND ACTUAL HEAT PIPE (400 W STEADY-STATE, HORIZONTAL)	52
FIGURE 31.	IR PHOTO OF HORIZONTAL HEAT PIPE, 800W, 125% CHARGE	53
FIGURE 32.	NEAR ISOTHERMAL CASE TEMPERATURE VS TIME, HORIZONTAL, 600W, 100% CHARGE	53
FIGURE 33.	HEAT PIPE TEMPERATURE VS. ANGLE, 400W	55
FIGURE 34.	IR PHOTOGRAPH, VERTICAL (5), 600W	56
FIGURE 35.	VERTICAL GRADIENT, 400W, 125% CHARGE	56
FIGURE 36.	TEMPERATURE VS TIME, 400W, 125% CHARGE	57
FIGURE 37.	TEMPERATURE VS TIME, 400W, 100% CHARGE	58
FIGURE 38.	TEMPERATURE VS TIME, 400W, 75% CHARGE	58

FIGURE 39.	VARYING CHARGES TEMPERATURE VS. TIME, 400W, HORIZONTAL	59
FIGURE 40.	THEORETICAL HEAT PIPE START-UP	60
FIGURE 41.	TEMPERATURE VS TIME FOR 100% CHARGE, 400-800W, HORIZONTAL	61
FIGURE 42.	ASYMMETRIC, HORIZONTAL, 200W	62
FIGURE 43.	ASYMMETRIC, HORIZONTAL, 400W	62
FIGURE 44.	ASYMMETRIC, HORIZONTAL 600W	63
FIGURE 45.	ASYMMETRIC, INCLINED, 400W	63
FIGURE 46.	ASYMMETRIC, INCLINED, 400W	64

NOMENCLATURE

General Terms

A	area (usually cross-sectional) (m^2)
a	acceleration (m/s^2)
C	constant value in an equation
c	integration constant
F	function of, or friction coefficient
f	function of, or friction
g	acceleration due to gravity (m/s^2)
Gr	Grashof number
H	height (m)
h	heat transfer convection coefficient [W/(m K)]
K	permeability (m^2)
k	thermal conductivity [W/(m K)]
L	length (m)
l	length of subsection (m)
m	mass (kg), term in fin equation
$\dot{m}$	mass flow rate (kg/s)
Ma	Mach number
N	Screen mesh number
n	number of repeated elements
Nu	Nusselt number
P	pressure (N/m^2), perimeter (m)
Pr	Prandtl number
Q	heat rate (W)
R	gas constant for given vapor [kJ/(kg K)]
r	radius (m), radius of curvature (m)
Ra	Rayleigh number
Re	Reynolds number
s	spacer distance (m)
T	temperature (K)
t	time (s), thickness (m)
U	overall heat transfer coefficient [W/(m^2 K)]
V	volume (m^3), velocity (m/s)
v	specific volume (m^3/kg)
W	width (m)
We	Weber number
x	cartesian coordinate
y	cartesian coordinate
z	cartesian coordinate

Specific Terms

A_l	cross-sectional area of liquid flow path (m^2)
A_s	total wetted surface area of wick (m^2)
A_v	vapor flow cross-sectional area (m^2)
A_x	area in x-direction (m^2)
C_1	first radiation constant (3.7415×10^{-16} W m^2), first constant of integration
C_2	second radiation constant (1.4388×10^{-2} m K), second constant of integration
c_0	speed of sound evaluated at evaporator end cap temperature (m/s)
D_v	diameter of vapor core (m)
E_b	total emissive power (W/m^2)
$E_{b\lambda}$	blackbody emissive power at absolute temperature T for a single wavelength (W/m^3)
F_l	liquid frictional coefficient
F_v	frictional coefficient for vapor
g	acceleration due to gravity (m/s^2)
h_{fg}	latent heat of vaporization (kJ/kg)
K'	ratio of specific heats
k_l	thermal conductivity of working fluid in liquid phase [W/(m K)]
k_{eff}	effective thermal conductivity of the wick [W/(m K)]
k_s	thermal conductivity of wick material [W/(m K)]
k_v	thermal conductivity of vapor [W/(m K)]
k_w	thermal conductivity of vessel wall material [W/(m K)]
L_e	Evaporator length (m)
L_{eff}	effective fluid return length (m)
L_t	total length (m)
$\dot{m}_l$	liquid mass flow rate (kg/s)
$\dot{m}_v$	vapor mass flow rate (kg/s)
P_o	pressure at evaporator end (N/m^2)
Q_b	maximum heat rate at boiling limit (W)
Q_{ent}	maximum heat rate at entrainment limit (W)
Q_s	maximum heat rate at sonic limit (W)
Q_{vis}	maximum heat rate at viscous limit (W)
QL	heat transport capability (W m)
$\dot{q}_e$	maximum heat flux into evaporator section (W/m^2)
$R_{h,w}$	hydraulic radius of wick surface pore (m)
R_i	inner radius of pipe wall (m)
R_v	vapor space radius (m)
$V_{p,l}$	liquid velocity through wick screen pores (m/s)
T_{amb}	temperature of ambient environment (K)
T_h	temperature of hot (radiating) body (K)
T_{local}	local temperature (K)
T_{ss}	steady-state temperature (K)
t_v	vessel wall thickness (m)

t_w	wick thickness (m)
$\Delta p_{cap,max}$	maximum capillary pumping pressure (N/m^2)
Δp_g	pressure drop due to gravitational force (N/m^2)
Δp_l	liquid pressure drop (N/m^2)
Δp_v	pressure drop in vapor (N/m^2)
ΔT_{crit}	Wall Superheat temperature difference (K)

Greek Symbols

δ_v	thickness of vapor flow cross-section (assume uniform for entire heat pipe) (m)
β	coefficient of thermal expansion (1/K)
ε	surface emissivity
λ	wavelength (m)
λ_{max}	wavelength at which an ideal radiator emits maximum amount of energy
μ_l	liquid viscosity($N\ s/m^2$)
ρ_0	vapor density evaluated at evaporator end cap temperature (kg/m^3)
ρ_l	density of liquid (kg/m^3)
ρ_v	vapor density (kg/m^3)
σ	liquid surface tension (N/m), Stefan-Boltzmann constant [5.67×10^{-8} $W/(m^2 K^4)$]
ϕ	angle of heat pipe from horizontal (degrees)
φ	wick porosity

1.0 INTRODUCTION

This project report entails the design, construction, and both the theoretical and experimental thermal performance investigation of a flat heat pipe using water as the working fluid. The project's findings will help determine the viability of implementing flat heat pipes into thermophotovoltaic energy conversion systems.

1.1 OBJECTIVES

The flat heat pipe was designed to meet the following criteria (as determined by both the sponsors of the project and the research team):

1. Design and construct the heat pipe entirely out of Monel 400.
2. Exhibit two-dimensional heat transfer behavior.
3. Feature ultimate dimensions of 4 feet long (1.22 m) by 1 foot wide (30.48 cm) by ½ inch thick (1.27 cm).
4. Maintain an operating temperature of up to 212°F (100°C).
5. Possess a means of internal support for structural rigidity without sacrificing two-dimensional flow capabilities.
6. Operate without the presence of any noncondensable gases, such as air, inside of the heat pipe (gas loading).

The following experimental and theoretical goals were set:

1. Monitor the condenser region temperature profile as closely as possible, via thermocouples and infrared video camera.
2. Test asymmetric heating conditions and different heat inputs.
3. Test performance at different heat inputs, fluid charges, and varying inclination angles.
4. Modify important heat pipe equations for flat geometry.
5. Model experimental and theoretical heat pipe performance against a conventional fin of the same dimensions.
6. Analyze experimental data to determine overall performance and feasibility of flat heat pipes for a TPV energy conversion system.

1.2 METHODOLOGY

The design, experimental, and theoretical goals were met in the following manner:

Step 1: Research and Design

A literature search was conducted to determine the mechanisms of heat transfer in heat pipes and how they might differ in a flat heat pipe from a cylindrical heat pipe. Several experts in the field, with specialties ranging from design and theoretical analysis to

fabrication, were consulted and their recommendations considered. Suppliers of the necessary materials were located. The final design was completed incorporating all of the above research.

Step 2: Construction and Testing

A subscale model of the final design was submitted to Technical Support Department (TSD) at USNA for construction to allow fabrication difficulties to be solved before attempting the final design. Instrument calibration and basic heat pipe operational procedures, such as fluid charging, were perfected with this model. The subscale model also served to provide insight that was incorporated in revisions for the fullscale model. Finally, the fullscale heat pipe was constructed, tested, and analyzed under the test conditions.

Step 3: Analysis

The raw data from the experiments were collected and reduced. The infrared camera data was used to aid in explaining the purely quantitative thermocouple data as well as provide visual understanding of heat pipe phenomena. The temperatures of regions at the same distance axially from the heater end were compared to other equidistant regions and analyzed for thermal performance assessment at varying heat inputs, fluid charge, and angles of inclination. A traditional fin, with the same dimensions as the fullscale heat pipe, was modelled against the heat pipe's performance. This demonstrated the heat pipe's ability to transfer large quantities of heat with a near isothermal profile; a quality not found in a traditional fin.

2.0 THERMOPHOTOVOLTAICS (TPV) BACKGROUND

TPV energy conversion is a phenomenon by which infrared thermal radiation is converted into electrical power with no moving parts. The basic components of the system include the thermal radiator and a semiconductor diode (thermophotovoltaic cell) that converts thermal radiation into electrical power. Only photons with energy greater than the bandgap, or threshold energy of the TPV cell, can be converted into electrical energy. The radiation not converted either creates heat in the cell or is recycled to the radiator via reflection if such a system (known as spectral control) exists. The bandgap energy is determined by the TPV cell material and is not a variable parameter (Erickson, 1997). For a schematic of the basic TPV system, see Figure 1.

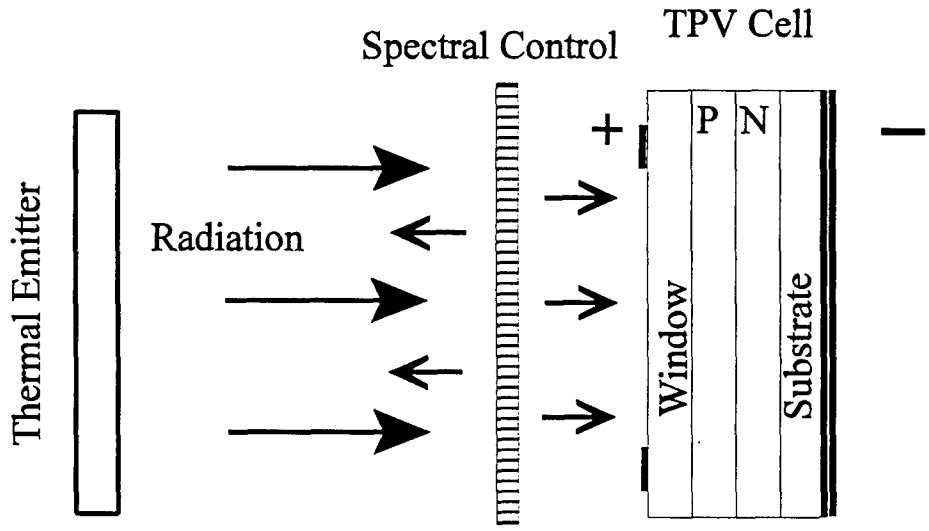

Figure 1. Basic Thermophotovoltaic Energy Conversion System

Figure 2 shows the emissive power over differing wavelengths for theoretical blackbodies at different temperatures. A blackbody, or ideal radiator, is an object that emits the maximum possible amount of radiation at any given wavelength. The emissive power is a function of only the temperature of the emitter. The emissive power for a single wavelength is given by Planck's law in equation 2.1:

(2.1)

$$E_{b\lambda} = \frac{C_1}{\lambda^5 (e^{C_2/\lambda T} - 1)}$$

From Figure 2 it is apparent that increasing temperature will increase the emissive power of the blackbody for a given wavelength. The wavelength at which the emissive

power is maximized (which corresponds to the peak of the curve for each temperature in Figure 2) is found by Wien's displacement law given in equation 2.2:

(2.2)

$$\lambda_{max} = \frac{2.898x10^{-3} m\ K}{T}$$

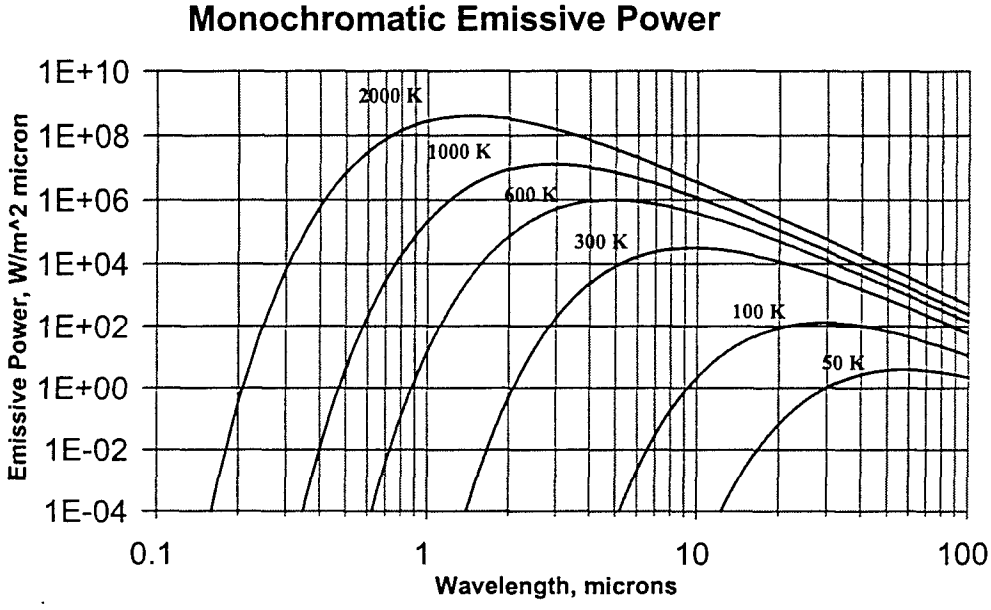

Figure 2. Planck's Law

The total emissive power of a blackbody at a given temperature is the area underneath the curve corresponding to the given temperature in Figure 2. This is represented in equation 2.3, the Stefan-Boltzmann law (where σ is the Stefan-Boltzmann constant):

(2.3)

$$E_b(T) = \sigma T^4$$

Since power is proportional to temperature to the fourth power, small changes in the temperature of an emitter can have great effects on emissive power.

2.1 PHOTOVOLTAIC PHYSICS

The physical mechanism within the TPV cells that governs the conversion of photons into electrical energy is the photoelectric effect, the same principle which standard photovoltaic (PV) cells (also known as solar cells) utilize. The active layer of these cells is

constructed of a semiconductor material with a P-N (Positive-Negative) junction. The material used to produce the active cell layers determines the bandgap energy, or the energy necessary to dislodge an electron from the material's outermost electron shell. As photons from the thermal radiator travel into the TPV cell, they travel through the "window" and are absorbed by the semiconductor. If the energy of the photon striking the semiconductor is sufficient, the semiconductor will eject an electron from its outer shell, leaving a "hole." If not, it will cause the temperature of the material to rise. If the difference in energy between the "hole" and the ejected electron is greater than the bandgap energy of the material, the pair (electron and hole) will cross the voltage barrier of the cell. When this charge-carrying pair moves towards similarly charged regions and moves away from layers of unlike charge, it becomes an electrical current, or usable electrical energy. The amount of energy available to be converted into electricity by the photoelectric effect is determined by Planck's law (see equation 2.1). Only photons that have energy (emissive power) greater than bandgap energy can produce an electron-hole pair (and therefore produce electricity) (Coutts and Fitzgerald, 1998).

As established, PV (and therefore TPV) cells can only convert certain wavelengths of electromagnetic radiation into usable energy. Therefore, the system efficiency is a function of the wavelengths emitted by the thermal radiator. As shown in Figure 2, wavelength is a function of temperature. Therefore, TPV cell efficiency is a function of radiator temperature. Methods do exist of reflecting back emitted wavelengths that cannot be utilized by the TPV cells for reabsorption into the emitter. This is known as spectral control. It ensures that the TPV cells receive only usable wavelengths of photons, and results in higher energy conversion efficiencies. However, spectral controls cannot moderate the amounts of radiation that come from different regions of the emitter (corresponding to locations on the emitter of different temperature) (Borowsky and Dziendziel, 1996).

2.2 TPV CELL EFFICIENCY

TPV and PV cells must be linked together in series to produce an appreciable voltage, as the voltage output of a single cell is small. Since the cells are in series, the same amount of current must flow through each cell. Experience has shown that if one cell in a series of TPV cells receives fewer photons above bandgap energy than the other cells (due to a low temperature region on the emitter) then the performance of the entire series of cells is downgraded (Lindler, 1999). Therefore, the emitter must exist at a uniform temperature for maximum efficiency. This presents a substantial problem for emitter design in TPV energy conversion systems. Combustion processes can have inherent non-isothermal profiles and therefore can not operate TPV cells at a high efficiency. However, heat pipes provide a means of heat transfer that maintains a nearly isothermal surface and could serve as emitters in TPV generators. Figure 3 shows just such a system. Heat pipes are heated axially via fossil fuel combustion. Alternating heat pipes and TPV cells results in a large surface area to volume ratio.

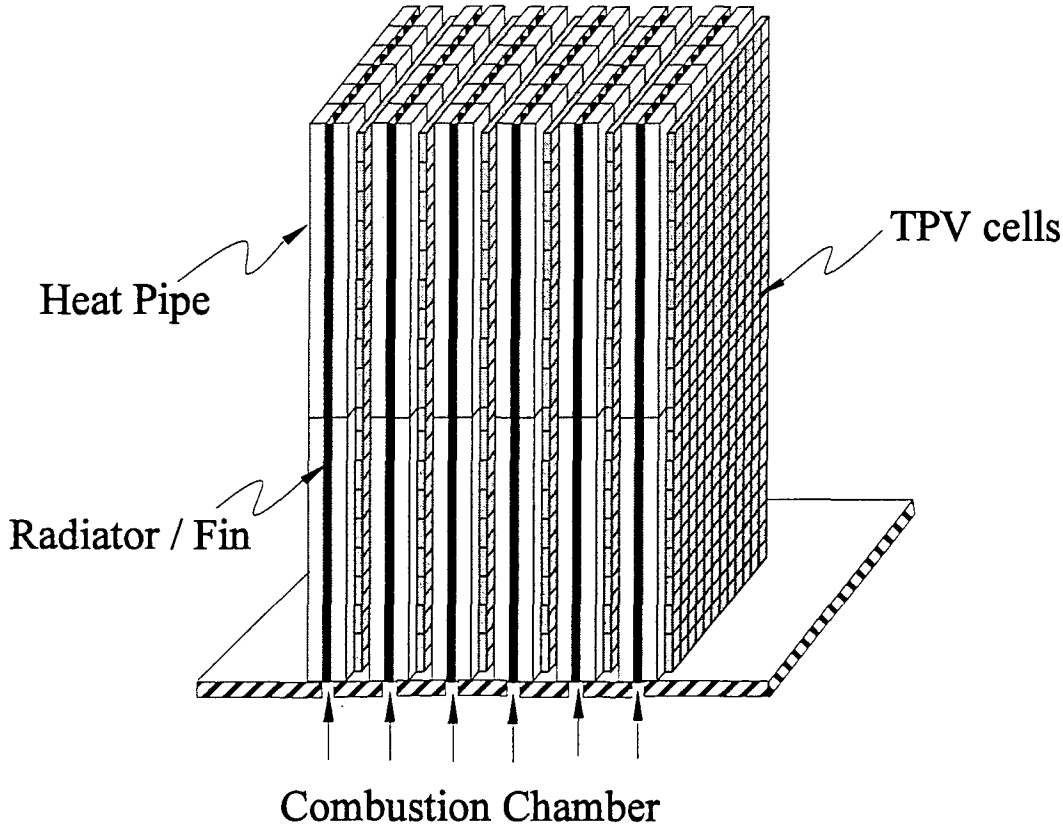

Figure 3. USNA TPV axial flow concept

3.0 HEAT PIPE INTRODUCTION

Heat pipes have existed for decades and stem from a simple principle: vapor evaporates and condenses at a uniform temperature for a given pressure. A heat pipe consists of a hermetically sealed vessel, a working fluid, and a wick that lines the vessel. The working fluid is vaporized (by an external heat source) and leaves the wick as a vapor. The vapor travels from the evaporator end to the condenser end of the heat pipe and condenses in the wick, releasing heat. Due to the change in phase of the working fluid, the heat is delivered to the condenser end at an almost isothermal profile. The fluid returns to the evaporator end from the condenser end via the capillary pumping action of the wick. Figure 4 shows the basic configuration of a cylindrical heat pipe.

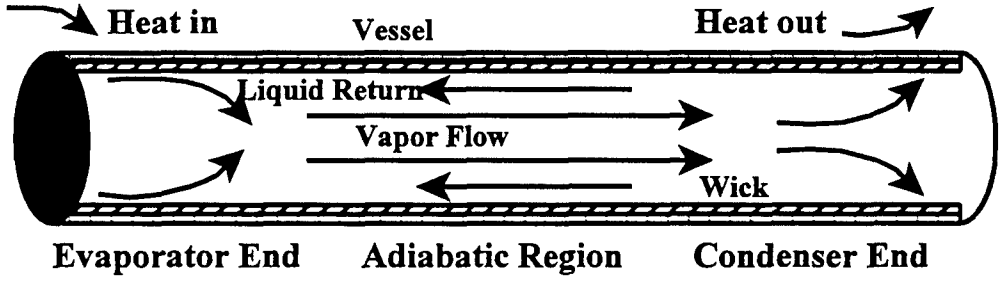

Figure 4. Basic Heat Pipe Configuration

Constructing and operating a heat pipe is an involved process, with many limitations to be considered. First, the fluid and vessel must be of high purity. If the fluid is not pure, then its heat transfer properties may fluctuate from the expected standard. Impure fluid can also deposit undesirable substances in the heat pipe vessel and vapor space, such as noncondensable gases. Undesired gases in the vapor space serve to effectively blanket the condenser area and raise the temperature of the heat pipe in the areas removed from the gas while the areas where the gas is located remain colder than the rest of the heat pipe. This effect, called gas loading, differs for varying heat inputs. Figure 5 serves to illustrate this effect (Ashcroft, 1996).

If the vessel is impure, then the working fluid may possibly erode parts of the vessel (e.g. impurities) (Ashcroft, 1996). The vessel material must also handle large compressive and tensile forces (Peterson, 1994).

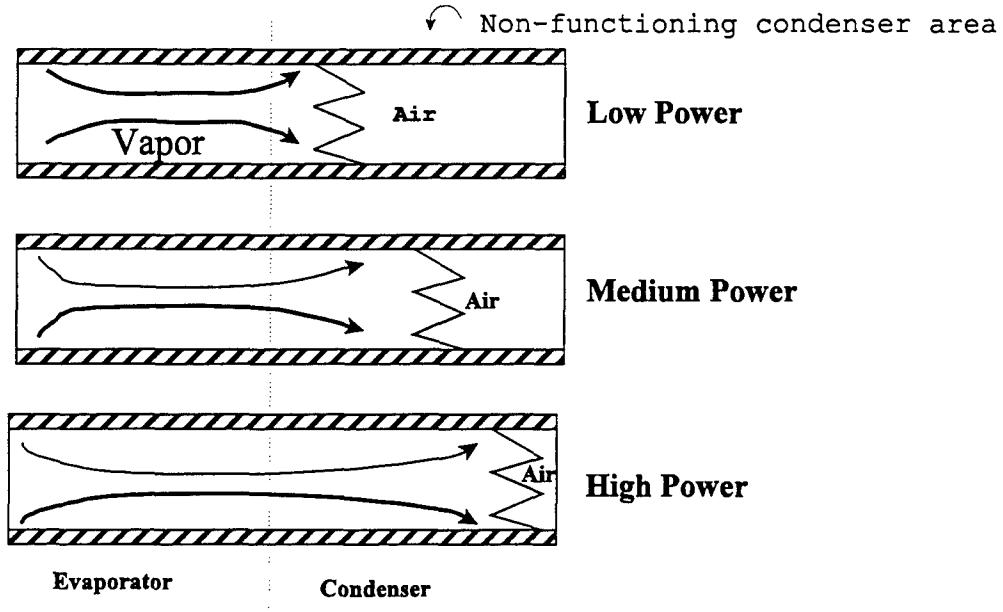

Figure 5. Gas Loading Effect

3.1 STEADY-STATE LIMITS

The heat pipe has many different operating limits for given input heating powers and operating temperatures. When too much heat is applied the working fluid is superheated and bubble formation occurs in the wick, which then dries out and interrupts heat transfer. This is known as the boiling limit and is represented by equation 3.1 (for cylindrical heat pipes) (Faghri, 1995):

$$Q_b = \frac{2\pi L_e k_{eff} \Delta T_{crit}}{\ln(\frac{R_l}{R_v})} \tag{3.1}$$

The viscous limit primarily exists in heat pipes that have startup conditions in which the working fluid is solidified (such as in high temperature liquid metal heat pipes). It is possible for the working fluid to liquefy and be vaporized from the evaporator region and condense in the condenser region without sufficiently heating the frozen fluid in the condenser region to allow flow back into the evaporator region. The evaporator will then dry out and the heat pipe will not reach normal operating conditions. In general, the viscous limit can be reached when a heat pipe is operating at temperatures below its normal operating range, when viscous forces dominate the vapor flow and vapor pressure in the condenser end is reduced to zero, limiting the heat transport capabilities of the heat pipe. The viscous limit is expressed by equation 3.2 (for cylindrical heat pipes) (Peterson, 1994):

(3.2)

$$Q_{vis} = \frac{D_v^2 h_{fg} \rho_0 P_0}{64 \mu L_{eff}}$$

At low vapor densities (and hence, low temperatures), the vapor velocity must be high to transfer the necessary heat. For a constant area duct, the vapor velocity can not exceed the local sonic velocity. Therefore, problems such as dryout, shock, and large temperature fluctuations result. The sonic limit is related as follows in equation 3.3 (Dunn and Reay, 1976):

(3.3)

$$Q_s = \frac{\rho_0 c_0 h_{fg} A_v}{\sqrt{2(K'+1)}}$$

In certain wick designs, it is also possible for the vapor that is traveling to the condenser end to capture, or entrain, the returning liquid and cause dryout. This limit, known as the entrainment limit, is expressed as (Chi, 1976):

(3.4)

$$Q_{ent} = A_v h_{fg} \left(\frac{\sigma \rho_v}{2R_{h,w}}\right)^{1/2}$$

The most important limit for design considerations, the capillary limit, is met when the vapor and liquid pressure drops exceed the maximum capillary head that the wick produces. This maximum head is related to the wick's effective pore size. The capillary limit occurs when the pumping ability of a given wicking material to provide the circulation for the working medium can no longer return fluid as fast as the evaporator vaporizes it. This limit will cause the evaporator end to dry out, resulting in damage to the vessel and wick. The capillary limit is the highest heat rate that most heat pipes can operate at to achieve minimum design operating temperature and is therefore usually the only limit given for heat pipes. See Figure 6 for the relations of temperature and heat rate to heating limits for a conventional cylindrical heat pipe. Equation 3.5, the equation for the capillary limit for a cylindrical heat pipe, neglecting the pressure drops due to evaporation and condensation, is (Faghri, 1995):

(3.5)

$$(QL)_{cap,\max} = \frac{\Delta p_{cap,\max} - \Delta p_g}{F_l + F_v}$$

$(QL)_{cap,max}$ is the heat transport capability (W m), F_l is the liquid friction loss coefficient, and

F_v is the vapor friction loss coefficient. Equations 3.6 through 3.10 further define the elements of the capillary limit equation (equation 3.5).

$$\Delta p_{cap,max} = (2\sigma)/r_{eff} \tag{3.6}$$

$\Delta p_{cap,max}$ is the maximum capillary pumping head

$$\Delta p_{cap,max} \geq \Delta p_l + \Delta p_v + \Delta p_g, \text{ where} \tag{3.7}$$

$$\Delta p_l = \frac{\mu_l l_{eff} \dot{m}_l}{\rho_l k_l A_l} \tag{3.8}$$

Δp_l is the pressure drop in liquid

$$\Delta p_v = \frac{\mu_v l'_{eff} \dot{m}_v}{\rho_v k_v A_v} \tag{3.9}$$

Δp_v is the pressure drop in the vapor

$$\Delta p_g = \rho_l g L_t \sin \phi \tag{3.10}$$

Δp_g is the pressure drop due to gravity and $\sin \phi$ = angle of inclination from horizontal

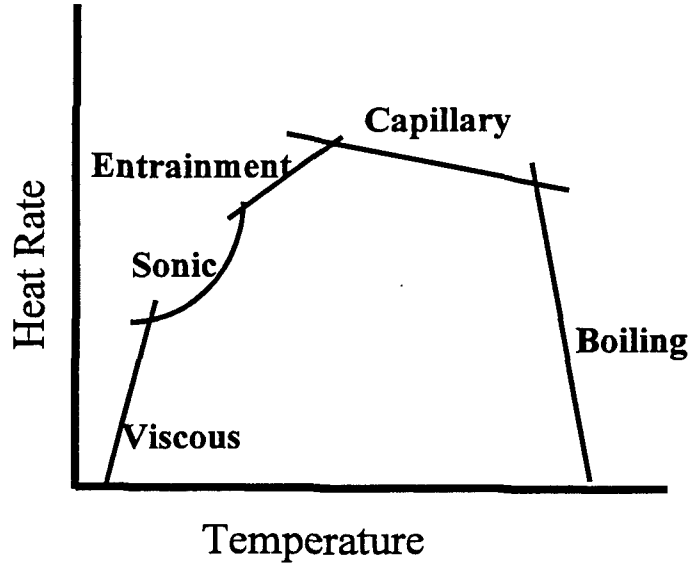

Figure 6. Heating Limits

Figure 7 depicts the wetting angle for a fluid and its interface. The maximum capillary head is calculated under the assumption that the working fluid is perfectly wetting the wick material. This assumption stipulates that the contact angle, θ, between the fluid and wick is equal to zero. A contact angle of zero means that the fluid meniscus is a perfect hemisphere, which is almost never the actual case, as most environments possess a wetting angle greater than zero. Therefore, the actual maximum capillary head is less than the value obtained by the equation 3.6. An accurate value for maximum capillary pumping head is best obtained by experimental methods (Peterson, 1994).

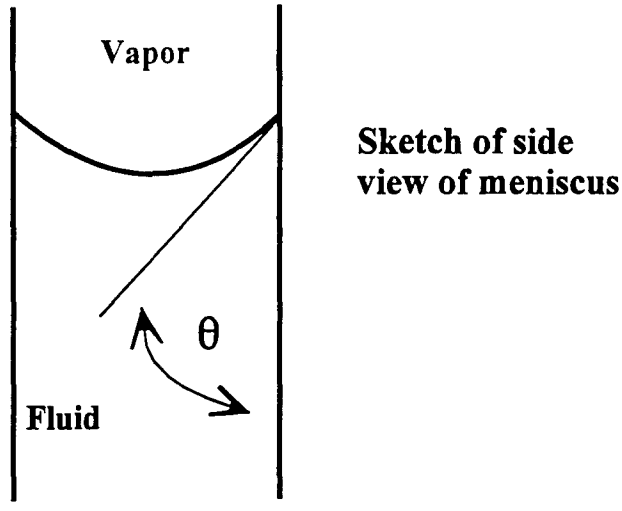

Figure 7. Wetting angle

3.2 WICK DESIGNS

For heat pipes, there are many different wicking structures that could be used to provide the path for the return of the condensate from the condenser back to the evaporator. To obtain the desired heat transport characteristics, the wick design must be optimized. This involves a trade-off of various wick characteristics. To achieve a large capillary head, the wick must have a small pore size, as shown in equation 3.6. However, in order to minimize the liquid pressure drop from the condenser end to the evaporator end the wick should have a large pore size. This minimizes F_l, in equation 3.5. The effective thermal conductivity of wicking structures is also an important consideration. Due to all of these factors of wick design, wick optimization is an involved process (Cerza, 1998).

Since the vapor condenses on the wick structure, the return liquid velocity is relatively low and heat is transported through the wick and vessel wall to the environment. The effective thermal conductivity is dependent on both the working fluid, wick material,

and number of pores per unit area. It is the effective thermal conductivity that allows for the calculation of the maximum wick thickness for desired operating temperatures since the effective thermal conductivity determines the temperature drop across the wick for given conditions. Effective thermal conductivity is found using equation 3.11 (Faghri, 1995):

$$k_{eff} = \frac{k_l[(k_l + k_s) - (1-\varphi)(k_l - k_s)]}{[(k_l + k_s) + (1-\varphi)(k_l - k_s)]} \tag{3.11}$$

where porosity, φ, is wick open area divided by total wick area.

The number of wicking structures in existence vary widely. However, they can be divided into two basic categories: homogeneous and composite wicks. A homogeneous wick is constructed of a single basic material. Common homogeneous wicks are the wrapped screen wick, which consists of one or more layers or screen in contact with the vessel wall; powdered metal wicks, which are metal powders sintered to the vessel wall; and the grooved wick, which consists of grooves machined into the inner wall of the heat pipe. Homogeneous wicks also can contain arteries, or tubes to provide liquid return paths of very low flow resistance. Composite wicks are made up of several wick materials combined to form a composite wick structure. Examples of composite wicks are overlapping screens of varying porosities or a groove wick with a fine pore screen on top of it. Many different composite wicks have been developed for specialized applications (Faghri, 1995).

The working fluid of the heat pipe itself must also be determined. For varying temperatures and heat pipe internal pressures, different working fluids will transfer unequal amounts of heat due to dissimilarities in surface tension, density, enthalpy of vaporization, and viscosity. These properties are grouped together in the figure of merit, equation 3.12 (Chi, 1976):

$$M = \frac{\rho_l \sigma_l h_{fg}}{\mu_l} \tag{3.12}$$

Equation 3.12 can be used to determine which fluid will have the greatest heat transport characteristics for the desired operating temperature. Table 1 shows various properties and figures of merit for various different fluids over various temperatures. Several computer codes exist that can predict some steady-state operating limits of a heat pipe if given the material and working fluid data for conventional, one-dimensional heat pipes.

Table 1. Figure of Merit Calculations

Ethanol							
(°F)	(°C)	(Pa)	(kg/m^3)	(J/kg)	[(N*s)/m^2]	(N/m)	(W/m^2)
	T	Pv	rho l	Hfg	Mu-l	surf. Tens	M
68	20	5.80e+03	8.00e+02	1.03e+06	1.20e-03	2.28e-02	1.568e+10
104	40	1.80e+04	7.89e+02	1.01e+06	8.19e-04	2.10e-02	2.047e+10
140	60	4.72e+04	7.70e+02	9.89e+05	5.88e-04	1.92e-02	2.486e+10
176	80	1.09e+05	7.57e+02	9.60e+05	4.32e-04	1.73e-02	2.910e+10
212	100	2.26e+05	7.30e+02	9.27e+05	3.18e-04	1.55e-02	3.298e+10
248	120	4.29e+05	7.10e+02	8.86e+05	2.43e-04	1.34e-02	3.467e+10
Water							
68	20	2.34e+03	999	2.45e+06	1.00e-02	7.29e-02	1.786e+10
104	40	7.37e+03	993.05	2.41e+06	6.51e-04	6.95e-02	2.549e+11
140	60	1.99e+04	983.28	2.36e+06	4.63e-04	6.61e-02	3.309e+11
176	80	4.74e+04	971.82	2.31e+06	3.51e-04	6.27e-02	4.008e+11
212	100	1.01e+05	958.77	2.25e+06	2.79e-04	5.89e-02	4.557e+11
248	120	1.99e+05	943.39	2.20e+06	2.30e-04	5.50e-02	4.966e+11
Ammonia							
68	20	1.06e+06	600.2	1.16e+06	1.41e-04	2.02e-02	9.966e+10
104	40	1.42e+06	584.6	1.11e+06	1.26e-04	1.80e-02	9.295e+10
140	60	2.42e+06	550.9	1.01e+06	1.02e-04	1.37e-02	7.510e+10
176	80	3.86e+06	512.3	8.95e+05	8.32e-05	9.60e-03	5.290e+10
212	100	5.87e+06	465.5	7.45e+05	6.85e-05	5.74e-03	2.906e+10
248	120	8.60e+06	400.2	5.29e+05	5.03e-05	2.21e-03	9.302e+09
Methanol							
68	20	3.00e+04	791.5	1.19e+06	5.78e-04	2.26e-02	3.686e+10
104	40	6.00e+04	774	1.16e+06	4.46e-04	2.09e-02	4.222e+10
140	60	1.10e+05	755.5	1.13e+06	3.47e-04	1.93e-02	4.750e+10
176	80	2.20e+05	735.5	1.08e+06	2.71e-04	1.75e-02	5.150e+10
212	100	4e+05	714	1.03e+06	2.14e-04	1.57e-02	5.395e+10
248	120	6.60e+05	690	9.71e+05	1.70e-04	1.36e-02	5.362e+10

4.0 FLAT HEAT PIPE PROPERTIES

Flat heat pipes are very similar to cylindrical heat pipes. The only real difference between the two is geometrical. While this may seem a minor difference, it presents many challenges from a theoretical, engineering standpoint.

Typically, heat pipes are used to transfer large amounts of heat across a large distance with only slight energy loss. The cylindrical design works well to serve this purpose. However, when designing an emitter for a TPV energy conversion system, it is advantageous to have a large surface area to volume ratio in order to maximize power density of the system. A flat heat pipe was conceived for this purpose. Flat heat pipes are a new technology, with few theoretical models. Flat heat pipes are also relatively untested for transferring heat from one end to the other (as opposed to side to side transfer). Due to the different surface area geometry, flat heat pipes also have different flow and structural design considerations than those of cylindrical heat pipes. This chapter quantifies these differences and allows for consideration of these dissimilarities in heat pipe design.

4.1 FLAT HEAT PIPE HEATING LIMITS

Flow properties in cylinders are much different from those in rectangular geometries such as flat plates and/or boxes. The flow of a thin film over a flat sheet (such as in the liquid return loop of a flat heat pipe) is not the same as the flow of a cylindrical circumferential film (which corresponds to a cylindrical heat pipe), having different friction factors and flow restrictions. Also, vapor flow through a cylindrical space differs greatly from vapor flow through an object with a rectangular cross section, having dissimilar friction factors and flow restrictions. The flow property differences can present major complications for flat heat pipe design, as they alter steady-state operating limits.

The limit most affected is the capillary limit. This is significant because the capillary limit is usually the highest heating limit that a heat pipe is designed to operate at in steady-state conditions. The capillary limit involves the flow of the liquid in the wick's return path and the pressure loss of the vapor and liquid through their respective areas of the heat pipe. Also, since the USNA flat heat pipes do not have adiabatic sections, a more accurate approximation of the mean liquid return length in the wick was needed. The derivations of the various components of the capillary limit for assumed laminar flow in a flat, rectangular heat pipe are shown in Appendix 1. The capillary limit for a flat heat pipe, when only one side of the evaporator region is heated is given in equation 4.1. In equation 4.1 q_e is maximum heat flux into evaporator section. Equation 4.2 defines K, the permeability for a wire mesh wick. To achieve a large capillary limit value r_{eff}, the effective pore size of the wire mesh in the wick, must be minimized to achieve a large capillary pumping head. Decreasing r_{eff} also decreases permeability, which can lower the capillary limit value. Proper flat heat pipe design involves optimization of both of these factors to obtain a high capillary pumping head while still maintaining an acceptable permeability value. Equations 4.1 through 4.5 were derived by Associate Professor Cerza (1999).

(4.1)

$$q_e = \frac{2\sigma h_{fg}}{r_{eff}\,\bar{L}}\left\{\frac{12\mu_v}{\rho_v A_v \delta_v^2} + \frac{\mu_l}{\rho_l A_l K}\right\}$$

(4.2)

$$K = \frac{2\mu\varphi A_x}{\rho_l V_{p,l} f(\frac{A_s}{L})}$$

The permeability of the wire mesh wick calculated by equation 4.2 can be approximated by equation 4.3. Sample calculations were performed using both equations and it was found that both equations yielded nearly equal values. Therefore, equation 4.3 is preferred due to its simplicity.

(4.3)

$$K = \frac{\varphi D_h^2}{32}$$

There are two heating configurations considered for the fullscale flat heat pipe. The first involves the entire heater section mounted to one side of the evaporator region. For this configuration, the capillary limit is found by equation 4.1. The other arrangement of the evaporator section consists of heaters mounted to both sides of the evaporator region. For this heater setup, the capillary limit is found with equation 4.4.

(4.4)

$$q_e = \frac{2\sigma h_{fg}}{r_{eff}\,\bar{L}}\left\{\frac{12\mu_v}{\rho_v A_v \delta_v^2} + \frac{\mu_l}{2\rho_l A_l K}\right\}$$

This capillary limit (two heated sides) will theoretically be higher than the limit with only one side heated, as the two sides of the heat pipe work as parallel fluid circuits, with the total resistance being less when both sides are heated versus applying heat to only one side for the same heat flux.

The boiling limit in a flat heat pipe is similar to that of a cylindrical heat pipe. Both involve pressure balances at the onset of nucleation (pressure difference from bubble to vapor space through liquid in the wick). However, since the vapor area and heat input cross section are all rectangular, the boiling limit equation for cylindrical heat pipes (equation 3.1) changes to equation 4.5 for flat heat pipes.

(4.5)

$$Q_b = \frac{2A_v RT_{sat}^2}{P_{sat} h_{fg}} \left[\frac{1}{r_b} - \frac{1}{r_w} \right] \left[\frac{t_v}{k_w} + \frac{t_w}{k_{eff}} \right]^{-1}$$

In equation 4.5, t_v is the vessel wall thickness (m), k_w is the vessel wall thermal conductivity (W/m K), and t_w is the wick thickness (m).

The boiling limit can be expected to be a very large value. Flat heat pipes are constructed of high strength metals with polished surfaces. These metals feature very small surface defect sizes and therefore minute nucleation site sizes for the onset of boiling. This drives the maximum heat input for the boiling limit up to a large value. This limit will be much higher than the capillary limit, which will be retained as the maximum heating rate for the project in consideration. However, neither of these limits will ever actually be reached, as the internal pressure (due to the temperatures reached at these heating limits) could cause structural failure of the vessel. Appendix 2 shows the boiling limit derivation.

With water as the working fluid, the entrainment and viscous limits are not an operational limit consideration, as the physical properties of water drive the entrainment and viscous limits to very large values within this project's operating parameters (20°C to 100°C condenser temperature). Furthermore, the entrainment limit is usually not a factor in well-wicked heat pipes, since the wick retains the liquid to prevent entrainment by the vapor. Being difficult to calculate, the entrainment limit is found by balancing the shear force on the liquid due to the vapor flow with the surface tension of the liquid. For most applications, the entrainment limit is calculated by assuming the Weber number equal to one, where the Weber number is a ratio of vapor inertial forces to liquid surface tension forces. One must perform this balance at the given operating point of the heat pipe to determine if entrainment is a problem (Peterson, 1994).

In the sonic limit, the vapor cannot travel faster than the local speed of sound in a constant area duct. The heat input that can be delivered is therefore limited by the maximum mass flow rate of the vapor. To see the relatively simple derivation, see Appendix 3. The sonic limit is found by equation 4.6, where T_{local} is the local temperature (K) and R is the gas constant for the vapor [kJ/(kg K)]:

(4.6)

$$Q_s = \rho_v A_v h_{fg} \sqrt{kRT_{local}}$$

4.2. FLAT HEAT PIPE STRUCTURAL CONSIDERATIONS

A flat heat pipe has structural problems that are not associated with cylindrical heat pipes. Cylindrical heat pipes are considered natural pressure vessels due to their shape, and can withstand large pressure differences as well as the resulting compressive or tensile forces on their walls. Since heat pipes can exist at pressures lower than atmospheric pressure when not in use, and can exceed atmospheric pressure at elevated, in-use temperatures, the cylindrical design has clear advantages. In this case, one of the flat heat pipe's advantages-a large surface area to volume ratio-is detrimental to its structural integrity. The heat pipe's surface area is subjected to the pressure difference created between the heat pipe internal pressure and the external environmental pressure. This may result in a large force acting on the vessel, which can cause material failure. This was clearly a design consideration that needed to be solved.

The design operating point for the flat heat pipes in this project was one atmosphere of differential pressure, with design case for loading taken at a near perfect vacuum. In this scenario, the 101.325 kPa (14.67 psia) of atmospheric pressure would be acting to deform the heat pipe with nothing more than structural supports to counteract the pressure. Since one of the project goals was to design structural supports that did not inhibit two-dimensional flow, any internal beams or walls were ruled out as internal supports. This left only pin supports as an option. Not knowing how the pins were to be fastened to the vessel wall in the final design, the pins were modelled as both welded (rigidly attached) and not welded to the vessel wall. The vessel wall was then modelled as a beam, with either the side vessel wall and a pin or two pins acting as supports. This gave the maximum expected deflection for the flat heat pipe of a given thickness, material, and spacer distance. A spreadsheet was developed to analyze deflections for many different materials, material thicknesses, and pin spacing. To view the derivations and a sample spreadsheet, see Appendix 4.

Beam deflection was not the only structural analysis conducted. To determine whether or not deflection was the limiting factor, a column buckling analysis for pins of varying lengths, diameters, materials, and types of attachments also had to be conducted. However, this calculation is only necessary to reinforce the value obtained from the deflection problem, and was performed solely on the case for which a solution was obtained via the beam deflection problem. The equations necessary for this calculation are readily found in the Strength of Materials textbook by Ferdinand Singer (1962).

5.0 USNA FLAT HEAT PIPE

The corporate sponsor funding this project instilled certain guidelines for the flat heat pipe being constructed. They determined the dimensions, which are 1.22 m (48 inches) long by 30.48 cm (12 inches) wide by 1.27 cm (½ inch) thick. They also decided that the vessel material, structural supports, and wicking material be made of Monel R-400. Due to facility limitations, safety issues, and difficulties in working with liquid metal heat pipes, the USNA heat pipe was established as a low temperature heat pipe. Therefore, distilled water was chosen to be the working fluid, as it has the highest figure of merit of any of the candidate working fluids at the operating temperature (100°C). Since effective thermal conductivity is not as important an issue to this design as maximizing capillary pumping performance, it was decided to construct the USNA flat heat pipe with a composite wick consisting of two Monel 400 screens of different porosity. The screen at the liquid-vapor interface will be 120 x 120 square mesh (N=120) to provide a large capillary pumping head, and the screen in contact with the vessel wall will be 40 x 40 (N=40) square mesh to provide a path of low flow impedance. In order to counteract the crushing force of the atmosphere when the heat pipe is not at operating temperatures, Monel pins were used for internal column supports. As discussed earlier, pins offer structural support without biasing the flow towards any direction.

Initially, the desired wall thickness and pin spacing diameter was not known. To solve these problems, two different spreadsheets were used. The first modelled the area in between the first pin from the wall. The second the spacing between the pins. The derivations of these modelling conditions and the equations that were solved for in terms of pin spacing and material thickness are included in Appendix 4 and are also discussed in section 5.2. Using a targeted maximum deformation of 0.15875 cm (1/16 of an inch), it was found that 0.127cm (0.050 inch) thick Monel sheets would be sufficient with three inch pin spacing. The three inch spacing is also convenient because three is a multiple of twelve and will allow uniform pin spacing throughout the entire pipe.

Once the pin spacing was determined, it was necessary to solve for pin diameters. Initially, the pins were only going to be welded on one side to the vessel and wick. Thus they were modelled as columns rigidly attached on one end and free on the other. A column buckling analysis was performed for the maximum loading conditions as well as compressive failure. A factor of safety was built into the analysis since it was assumed that the pins existed in a perfect vacuum (when in reality there will only exist the partial pressure of water for the given temperature) and support the entire crushing force of the atmosphere. It was also assumed that all of the pins adjacent to the pin being analyzed would fail, and that it would bear the weight of the entire grid surrounding itself to the adjacent pins. It was discovered that compressive failure would be the limiting factor for the pins, and their proper diameter was determined from this analysis. The minimum pin diameter using this method was found to be approximately 0.3556 cm (0.14 inch). However, it was not possible to locate a vendor that could supply rigid Monel pins with diameters this small. The smallest diameter readily available was 0.635cm (0.25 inch) and this is what was used to create the USNA flat heat pipe. This also provides a factor of safety for failure due to buckling.

5.1 USNA FLAT HEAT PIPE HEATING LIMITS

Using equations 4.1, 4.3, and 4.4 explained in section 5.2 and derived in the appendices, the capillary limits are as follows:

$$\dot{q}_e = 42697 \frac{W}{m^2}$$

for the case with only one side heated and

$$\dot{q}_e = 85391 \frac{W}{m^2}$$

for the case with both sides heated.

For the case with only one side heated, with the given heater area, this results in a max heat input of 3967W, and 7933W for the case with both sides heated.

The boiling limit, defined by equation 4.5 and the derivations in Appendix 2, is calculated to have a maximum heat input of 9527W assuming a typical nucleation site radius of 2.5×10^{-4} m

The sonic limit was calculated as 325,042W using HTPIPE, a one-dimensional steady-state heat limit prediction program for heat pipes. HTPIPE was not accurate for the other heating limits due to approximations that one must make to input parameters into the program which can not accurately account for the composite wick construction.

There are no standard methods of construction for flat heat pipes, as they are a relatively new and unique device. To help remedy this, a subscale model was designed and constructed to help facilitate the fabrication process with the fullscale model. Although not necessary, the subscale model will have internal pin supports. These exist solely to design the final construction procedure for attaching these pins to the vessel wall in a manner where they will provide the intended structural support. This subscale model also has a fitting on each end to perform charging experiments and perfect the evacuation and charging procedure. The subscale model will also be used to calibrate laboratory equipment while waiting for the construction of the final design. The subscale model is a fully functional flat heat pipe and will provide useful data to contribute to the overall mission of the project. Figures 8 - 11 depict the subscale and fullscale heat pipe designs.

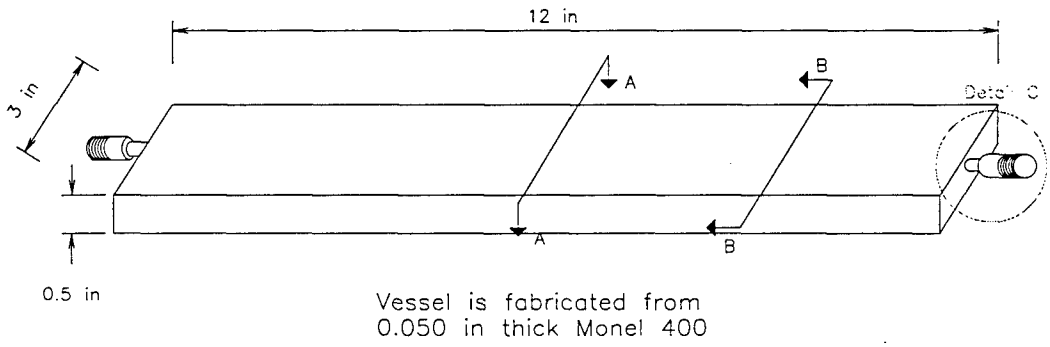

Figure 8. Subscale Heat Pipe Exterior

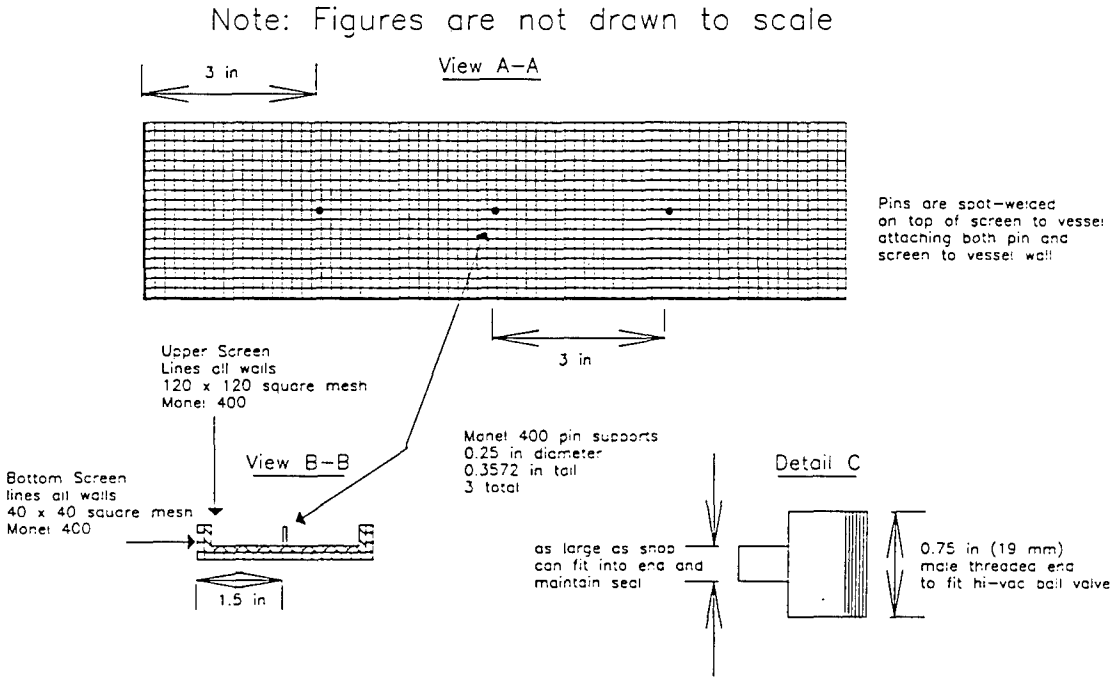

Figure 9. Subscale Heat Pipe Interior

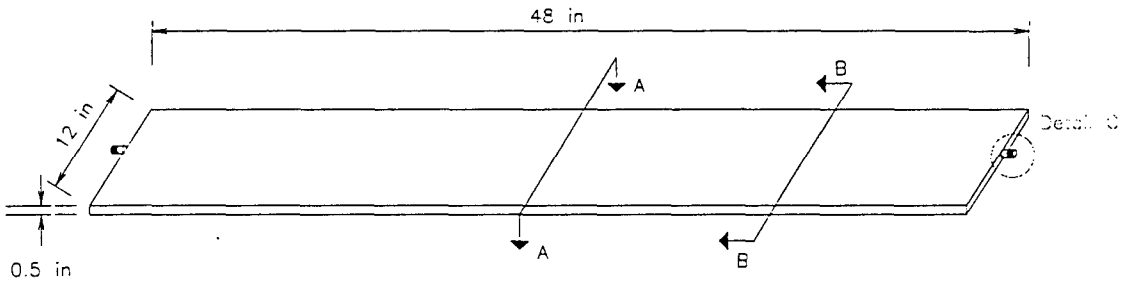

Figure 10. Fullscale Heat Pipe Exterior

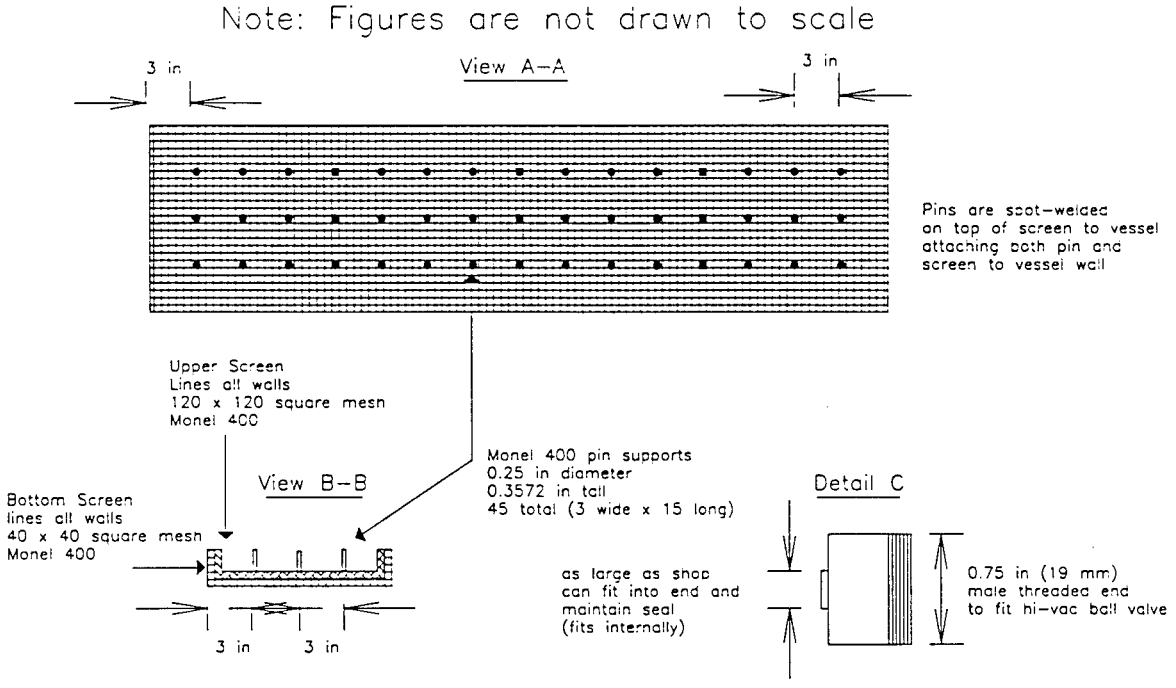

Figure 11. Fullscale Heat Pipe Interior

6.0 SUBSCALE FLAT HEAT PIPE

After the necessary supplies were obtained, the fabrication and assembly phase could be carried out. The subscale heat pipe was constructed first. Its purpose was to provide practical experience of flat heat pipe construction as well as be used to help calibrate instruments and set up the laboratory spaces. In addition, it aided in proving the practicality of the design and revealing and structural faults.

6.1 SUBSCALE FLAT HEAT PIPE CONSTRUCTION

The basic approach to construction was to assemble the heat pipe in two separate components. This involved drilling all the holes necessary for the pin supports, bending the sides of the two halves to the proper dimensions, and attaching the two layers of screen. The end pieces and fittings were also fabricated at this time and the pins were cut to the proper lengths and deburred. Then, the two sides were welded together, the ends welded on, and the fitting welded in. After this, the pins were inserted and welded to both sides of the heat pipe from the outside.

The subscale heat pipe was constructed mostly to the above parameters. The monel sheets were bent using twelve inch long copper bars with edges of fine radii. The screen was then cut to the same size using metal shears and taped to the vessel material. They were then tack-welded into place, centered halfway in between pin locations. Next, the 0.635 cm (1/4 inch) holes for the three spacers were carefully dimensioned and drilled in both halves through the vessel material and the screen. This created some problems with the screen integrity around the hole as well inducing stress around the tack weld spots. However, these were very minor and not enough to substantiate reattaching different screen material as the screen still maintained good pore integrity and contact with the vessel wall. This meant that the wick would still produce sufficient capillary pumping action and the effective thermal conductivity of the screen would remain as high as possible. The end fittings for the high vacuum ball valves were then machined and the endpieces and the pin spacers were then cut. However, they required extensive deburring and grinding so that they could fit into the 0.635 cm (1/4 inch) diameter spacer hole.

After the subscale flat heat pipe's constituent elements were readied, the two halves were welded together. The welds were staged from side to side so that the warping due to thermal stress would be minimized. The ends were then welded on, and the fittings were attached in the proper place. Following this, the pins were Tungsten Inert Gas (TIG) welded to both sides of the vessel wall from the outside.

6.2 SUBSCALE HEAT PIPE TESTING

Once completed, the subscale was pressure tested for leaks. The pins presented a problem, as did the end fittings. To make an airtight seal, the end fitting design had to be

alterred. The tubes that extended from the heat pipe were cut, and the fittings were welded directly to the ends of the heat pipe. The pins were welded to both sides of the vessel, as it would have been very difficult to attach the pins to only one side of the heat pipe. This reduced the calculated deflection substantially, and would later do the same for the final model.

The pins required re-welding several times in order to create an airtight seal at the desired 1 atmosphere of gage pressure. This problem of rewelding was found to be inherent to the design by both welder and design team. The pins were necessary for structural integrity and had to be welded from both sides to ensure structural support. Reheating of a completed weld by welding on the opposing side was determined not to be a pertinent issue since the type of welding utilized featured the use of localized heating for a short period of time. This would not be sufficient to heat the opposing weld spot to a temperature at which it could start to loosen (Monel welding wire or sheets would liquefy).

The subscale heat pipe was not intended to be used for extensive experimental data-taking, but to be used to verify that the basic heat pipe design worked, to find design flaws, and to setup laboratory equipment. Therefore, its testing regime was not very expansive. Its testing regime and objectives were as follows:

1. Design a reliable, easily repeatable method of leak-testing and make the subscale heat pipe leak-free.
2. Evacuate the heat pipe. Attach a pressure gauge to the evacuation apparatus and measure the level of evacuation achieved.
3. After successful evacuation, design and construct a charging apparatus for accurately charging the heat pipe with the correct amount of working fluid and sealing it off after charging. This method must be easily repeatable.
4. Apply a heat source to one end of the heat pipe and check for response. The condenser end will achieve a temperature nearly the same temperature as the end with the applied heat source. It is advisable not to use anything more than hot water for this test as it is conducted by hand.
5. Submerge one end of the heat pipe in a hot water bath. Monitor the water bath temperature and the heat pipe by quantifiable means. Also monitor the heat pipe performance with the infrared camera to determine if it is working properly, checking for end effects that might indicate a leak or improper charging and temperature variations that signal interior defects or improper charging.

6.3 SUBSCALE HEAT PIPE TESTING RESULTS

The leak-testing and charging consisted of the fabrication of a charging apparatus. A 0.635 cm (1/4 inch) nipple was fitted to the end of it (with necessary reducer) and mated to the compressor. The heat pipe was then pressurized for leak testing. Valve 2 in the

charging apparatus (see Figure 12) could be throttled so that excessive pressure did not build up in the heat pipe. A pressure gauge was fitted temporarily to the charging apparatus near the heat pipe to calibrate the throttling and was removed at the time of this picture. To leak test, soapy water was applied to the pressurized heat pipe in order to detect the leaks. Leaks would form bubbles in the soapy water. This assembly could be mounted and removed from the heat pipe with a few hand tools.

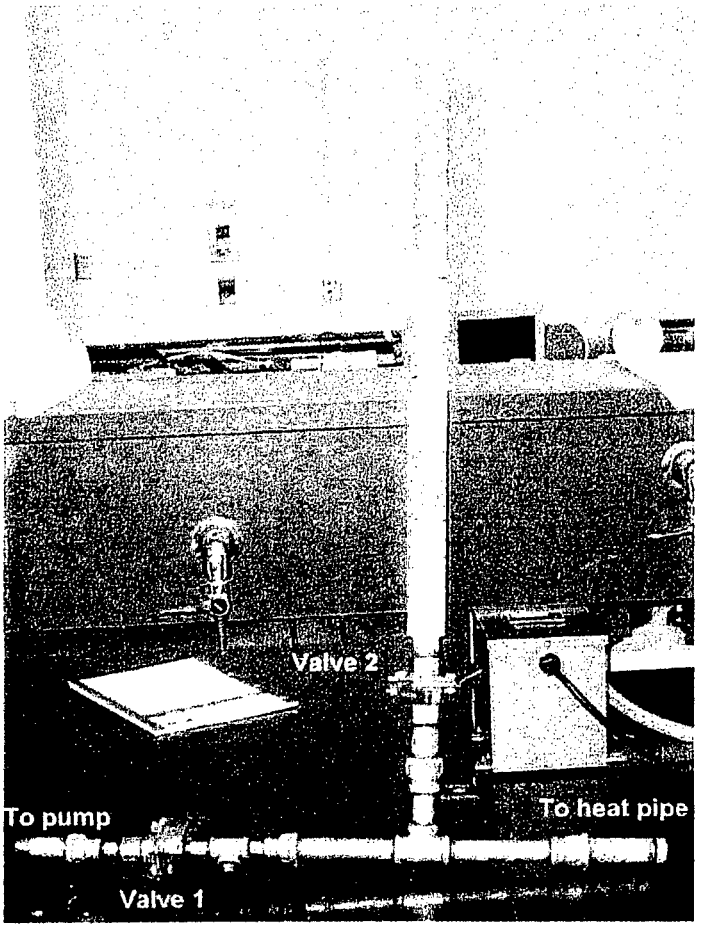

Figure 12. Charging Apparatus

Charging the heat pipe with working fluid was performed fairly simply as well. To charge a heat pipe the wick must be completely saturated. First, the heat pipe and charging assembly were mated to the vacuum pump and evacuated with valve 2 closed. In the fluid charging column was placed the correct amount of water to charge the heat pipe. These amounts were measured and marked (observe gradations on fluid charging column), taking into account the volume that would occupy the fittings as well as the heat pipe. Once evacuation was complete, valve 1 and the valve attached to the heat pipe (not pictured) were

closed, and then the vacuum pump was shut off. Valve 2 was then opened, and the vacuum inside the fittings drew the water in to fully fill the fittings. The heat pipe valve was then opened slightly to bleed in the necessary charge (as marked on the column). All valves were then closed, and the charging apparatus removed if necessary, taking care not to disturb the valve connected to the heat pipe (as it holds the heat pipe to the proper internal conditions). It is important to note that all valves used were rated for special high-vacuum service. To verify the time required for charging the heat pipe, the mass flow rate at 6.9 kPa (1psia) was calculated for water vapor through the 0.635 cm (1/4 inch) hole in the end fitting through which the pipe was evacuated. The vacuum pump's flow rate was found to be the limiting factor in evacuation, not choked flow conditions. This condition would remain true for the fullscale heat pipe as it was to have the same size end fitting.

The finished, testable model of the subscale flat heat pipe appears in Figure 13. It is shown with a valve still attached to it to show how they are mounted. Note the absence of the tube in the end fitting. The heat pipe is painted flat black to raise its surface emissivity so it can be viewed best by an infrared camera.

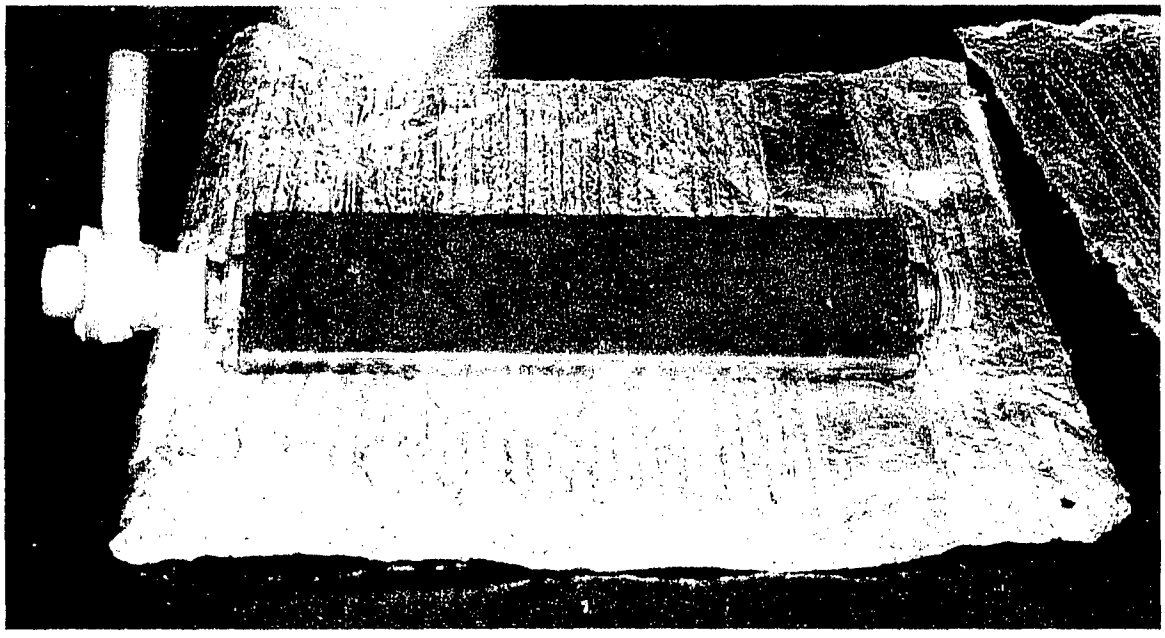

Figure 13. Subscale Heat Pipe

After all leaks were eliminated, and the heat pipe was successfully charged, it was subjected to a hot water bath. Within seconds, the other side of the heat pipe began to warm up. It worked at least as a crude heat pipe. After this, it was submerged in a pot of boiling water and monitored with the infrared camera. This facilitated a qualitative check of the heat pipe performance as well as calibrating and learning how to use the infrared camera. The subscale passed this test flawlessly, showing an almost isothermal condenser section with

marginal end effects (slightly cooler temperatures) due to the fin effect of the end fittings and the innate properties of a rectangular object (corners and ends are cooler than the middle when heated). See Figure 14 for a photo of the infrared camera.

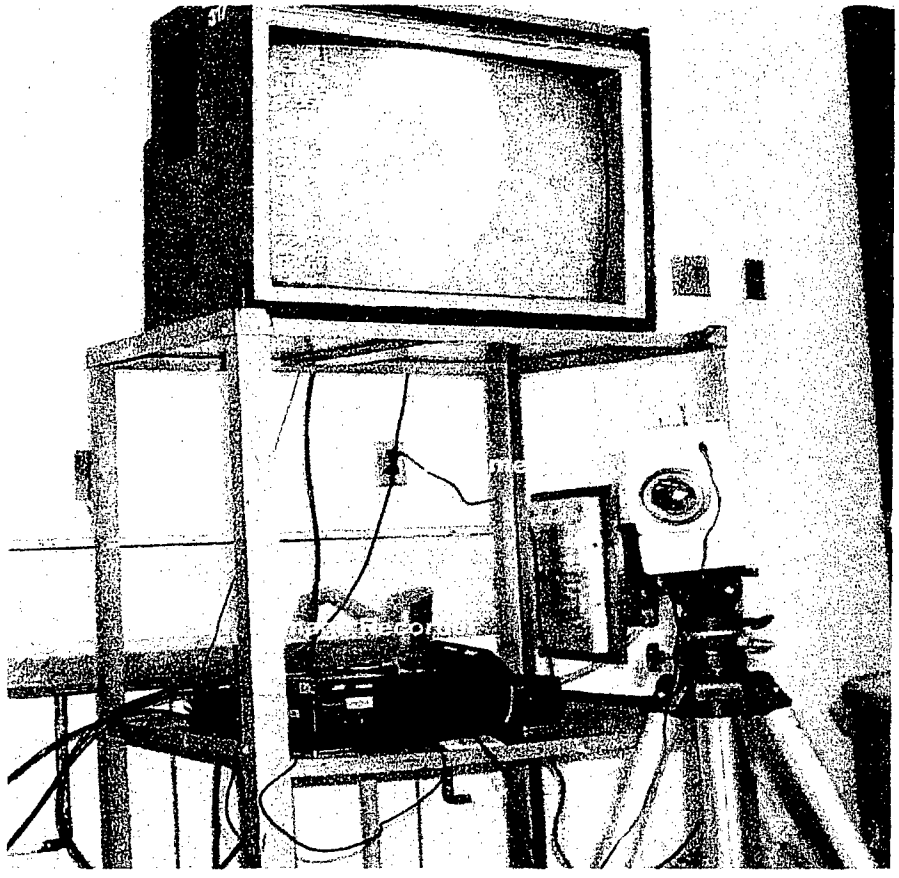

Figure 14. Infrared Camera

6.4 FULLSCALE HEAT PIPE IMPLICATIONS

After testing the subscale model, it was noted that several features initially designed into the fullscale model were no longer necessary.

Only one fitting was found necessary to perform complete leak testing, evacuation, and charging. Therefore, the fullscale has only one end fitting. The tube in the end fitting was weak and unnecessary, thus it was eliminated. Not only is it easier from a fabrication standpoint, as it aids alignment from side to side, but it also provides greater structural support. Thus, the pins were welded on both sides to the vessel (as was done in the subscale model). The shop received new equipment between construction of the two heat pipes, and this affected the construction process. See Section 7 for detail of the fullscale construction process.

7.0 FULLSCALE HEAT PIPE CONSTRUCTION

The fullscale model was to be constructed differently than the subscale model. This was due to Technical Support Department's acquisition of a new CNC Punch-Press machine as well as experimentation with the subscale and a visit from the corporate sponsor.

7.1 FULLSCALE HEAT PIPE CONSTRUCTION DETAILS

After the screens and Monel sheets were cut to the proper dimensions, their size and assigned hole placement were loaded into the CNC Punch-Press machine's user interface. The Monel sheets for the vessel wall were punched first, making holes in the locations where pins were to be welded. Next, to avoid any tearing, stretching, or any other kind of deformation in the screen, the screens were laid on top of each to other, taped to the side of thin steel sheets (30mil), and sandwiched in between the sheets. They were then loaded onto the CNC Punch-Press machine and were punched in the appropriate places, so that the steel sheets absorb the initial impact and prevent the movement and subsequent deformation of the screen. By using the computerized machine, it was possible to place all of the necessary holes in exactly the correct spots on both the sheets and the screen to ensure that the sides would line up perfectly.

Long copper bars with fine radius edges (same radius as used in construction of subscale) were obtained to facilitate bending the fullscale heat pipe to the required dimensions. The two layers of screen were then layed on top of the vessel, fastened with tape on the ends, and fastened down to the vessel by threading small screws through the pin spacer holes and attaching nuts on either sides. The screen was then tack-welded to the vessel wall in regular intervals between the pin spacer locations. Keeping the screen flush and in contact with the vessel presented a challenge, and a small portion of the screen on one side of the heat pipe ended up being not in contact with the vessel, but detached from the vessel in a small section of the heat pipe. This spot was noted in case it caused any performance problems. Figure 15 shows a close-up photo of the tack welds and the holes drilled for pins in a Monel sheet, and Figure 16 shows the two completed halves lying on top of each other. The end pieces and fitting were machined. Figure 17 shows a completed half with visible screen and bent side. The pins were then cut to the proper length, milled, and deburred to fit into the necessary space. Figure 18 shows the pins standing on the vessel wall before this process.

With all of the necessary components ready, the assembly began. First, the sides of the two separate halves were welded together, carefully sequencing the welds and using a heat trap to minimize deformation. After this, the ends were welded on, and the singular end fitting was welded snug to the end to resemble the final appearance of the subscale heat pipe. Following this, the pins were placed in their proper spots and TIG welded from either side of the heat pipe. The experimental setup then began.

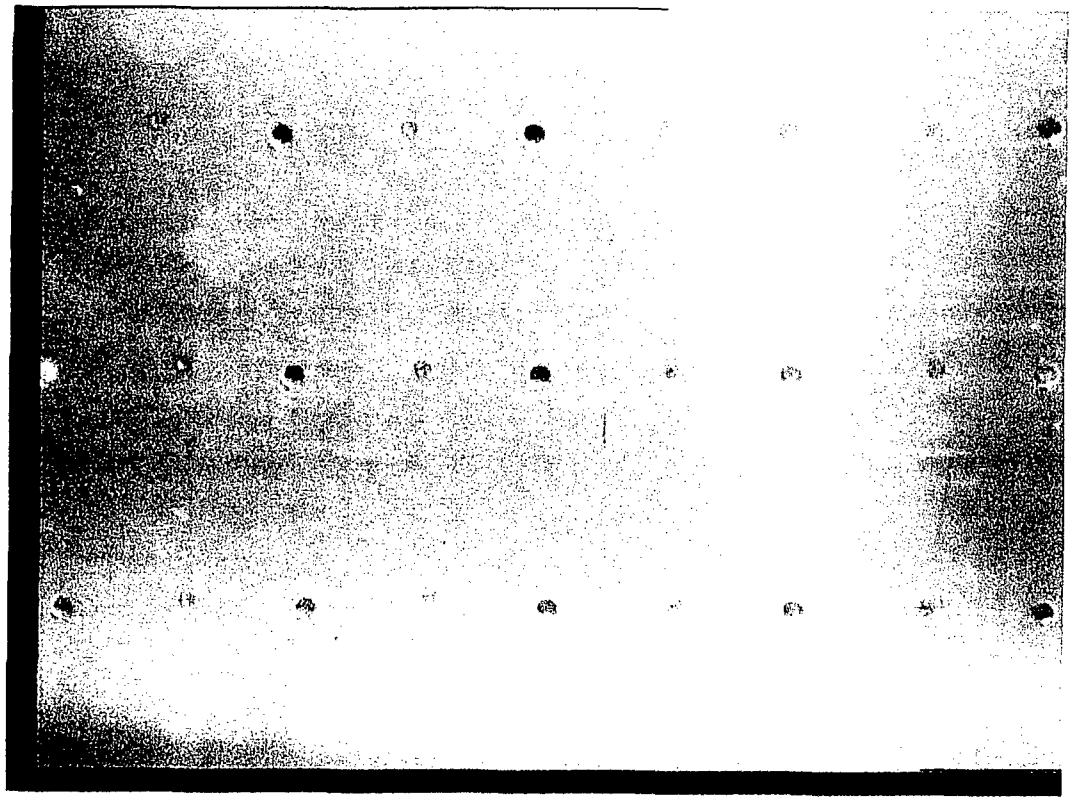

Figure 15. Monel sheet close-up

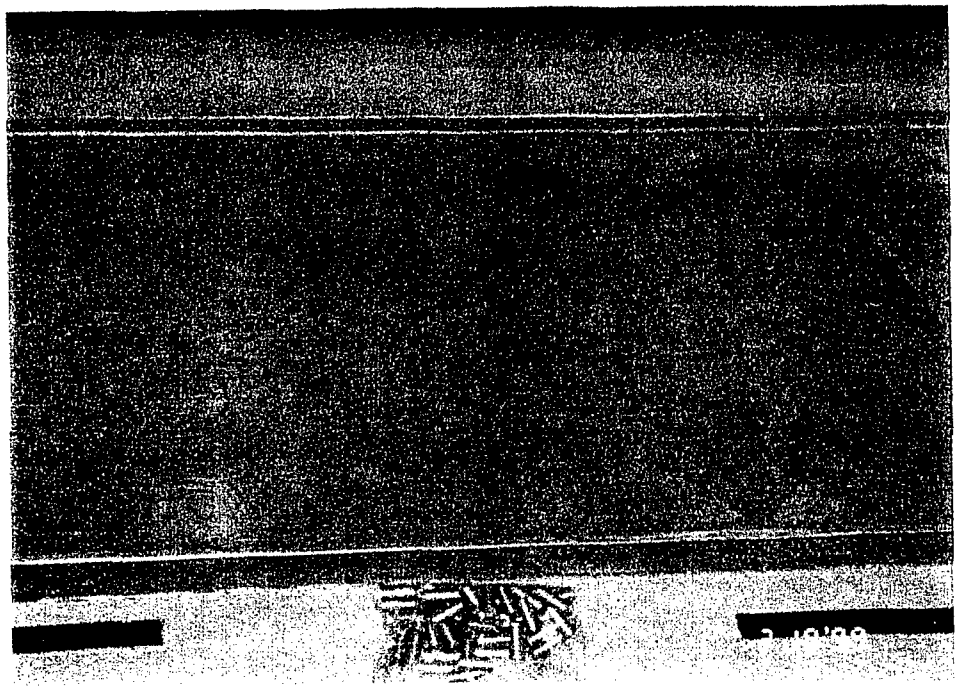

Figure 16. Completed Halves

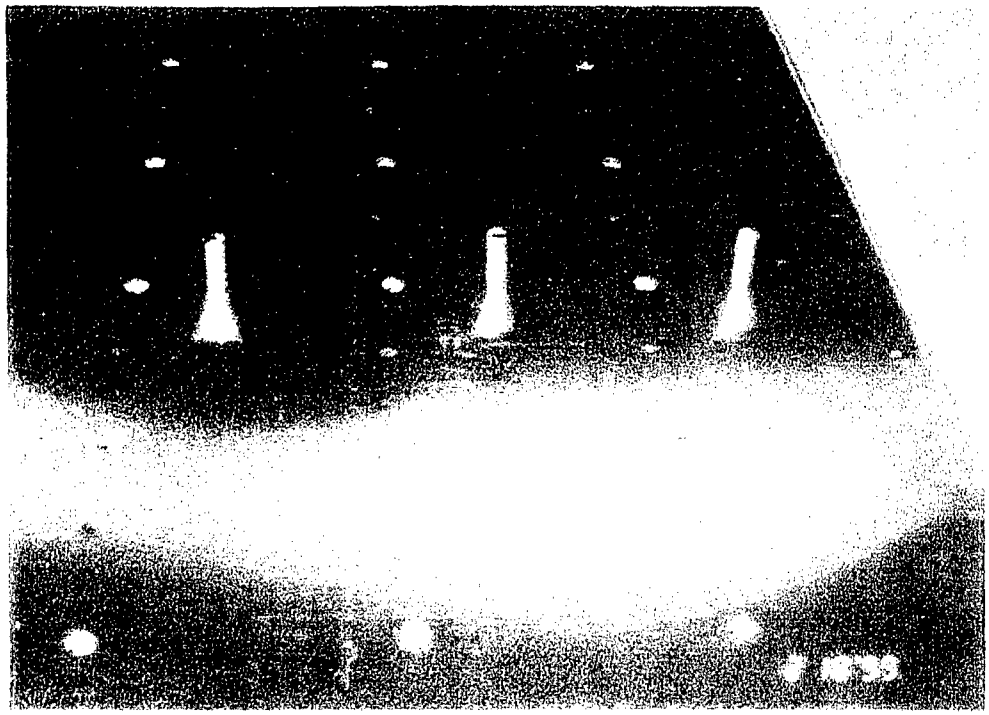

Figure 17. Screen-Side view with Bent Side

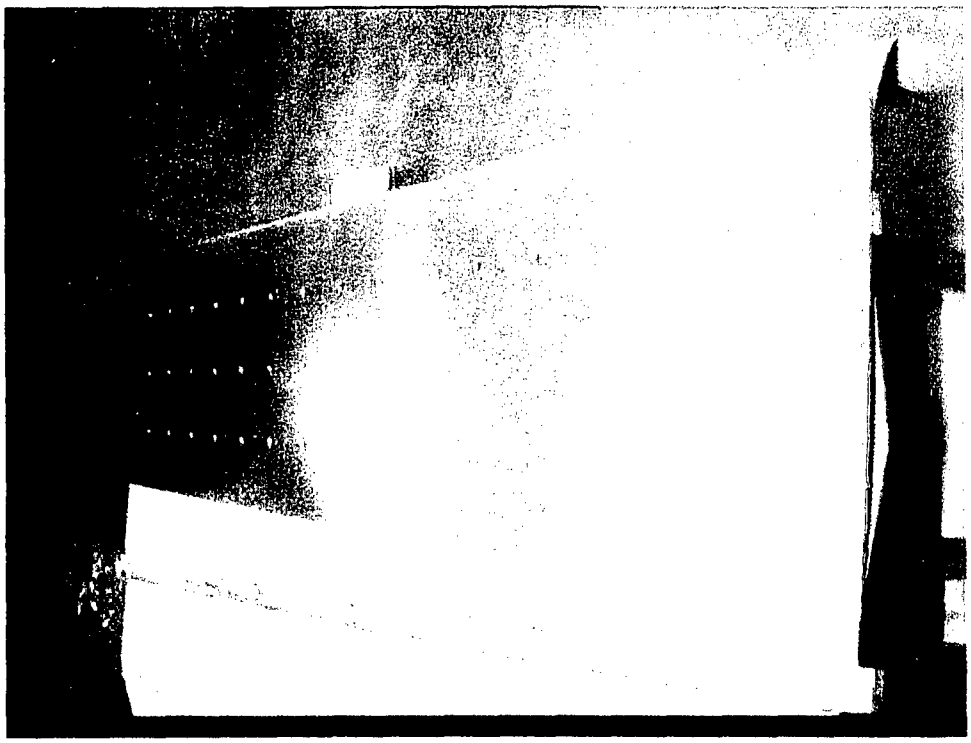

Figure 18. Sheet with Pins

8.0 EXPERIMENTAL SETUP AND PROCEDURE

The setup for experimentation as well as the procedure for experimentation were complex parts of the project and had great importance to the success of the project. It was very important to verify that the flat heat pipe does indeed perform as a heat pipe and to take data on its one-dimensional performance before proceeding on to any other tests. These one-dimensional tests were also the easiest way to understand and interpret the internal dynamics of the heat pipe as they influenced the temperature profile. Next, as the impetus behind the project was to examine two-dimensional flat heat pipe behavior, asymmetric heating conditions were imposed and the experiments run. A heat pipe is, by definition, a hermetically sealed vessel that transfers heat via phase change processes and has capillary pumping action to circulate the working fluid. It was necessary to test this capillary action. As mentioned earlier, the capillary limit is also the desired operating limit for most heat pipes. Finding the capillary limit of the heat pipe is therefore very important to not only understanding heat pipe performance but also to maximizing heat pipe performance. Experiments were conducted at differing angles of gravity assist for the liquid return path to test the capillary pumping action of the screen and gravity's effect on the heat pipe's performance.

8.1 EXPERIMENTAL SETUP

The asymmetric heating case was a unique case. The heaters had to possess the flexibility to be reconfigured and turned on and off independently to be able to satisfy both the symmetric and asymmetric heating cases. To meet this need, 16 high temperature 500 Watt strip heaters 1.905 cm (3/4 inch) inch wide with a heated section of 30 cm (11 13/16 inches) were purchased. They were wired in blocks of four to variable transformers, and could therefore be moved in blocks of four and have their heating rate adjusted independently in four blocks of four heaters each. The variable transformers were also wired to Wattmeters, which were wired into junction boxes (to be detailed later). The electric signals from the Wattmeters were recorded by the computer to which these junction boxes fed.

Thermal joint compound was spread between the heaters and the heat pipe to lower contact resistance and ensure that most of the generated heat went into the heat pipe. The heat pipe was then insulated with a ceramic tile over the heater sections with aluminum foil insulation wrapped around the entire assembly. To view the heaters being mounted with thermal joint compound in the symmetric case (all heaters on one side, covering the entire width) see Figure 19. Figure 19 does not show all of the heaters mounted to the heat pipe for the symmetric cases. Instead, Figure 19 shows ten of the heaters mounted and the thermal joint compound that was part of the heater section fabrication. Figure 20 shows the completed asymmetric mounting (half of the heaters on each side, covering only half of one end with the heaters covered with a ceramic tile and aluminum foil insulation).

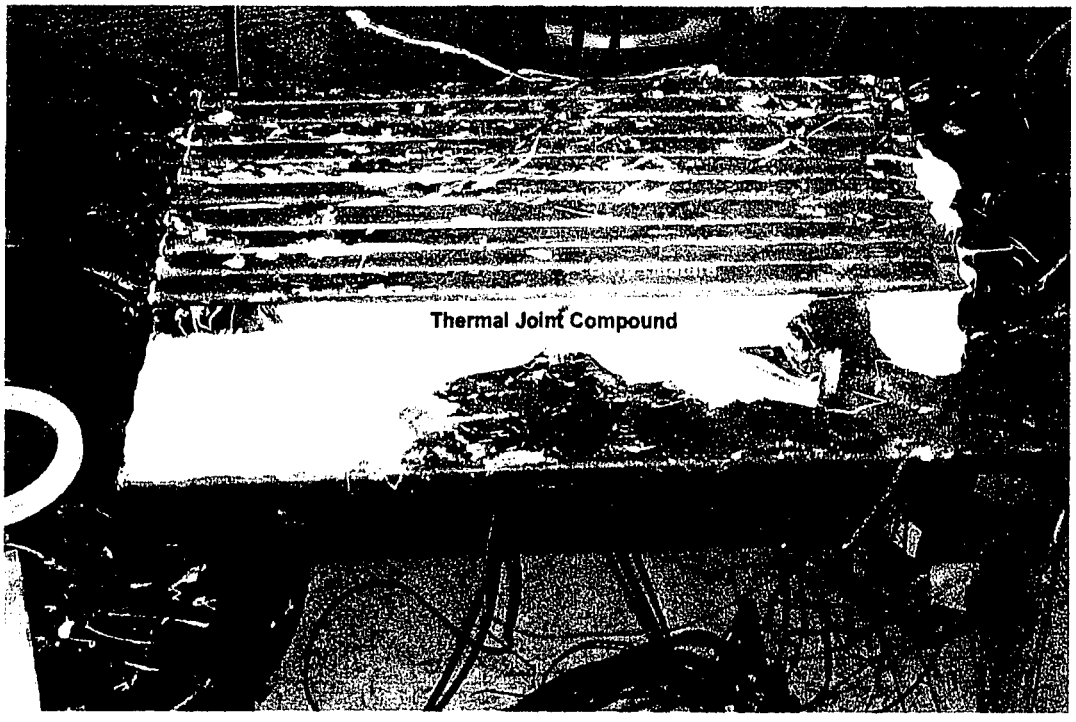

Figure 19. Symmetric Heater Mounting

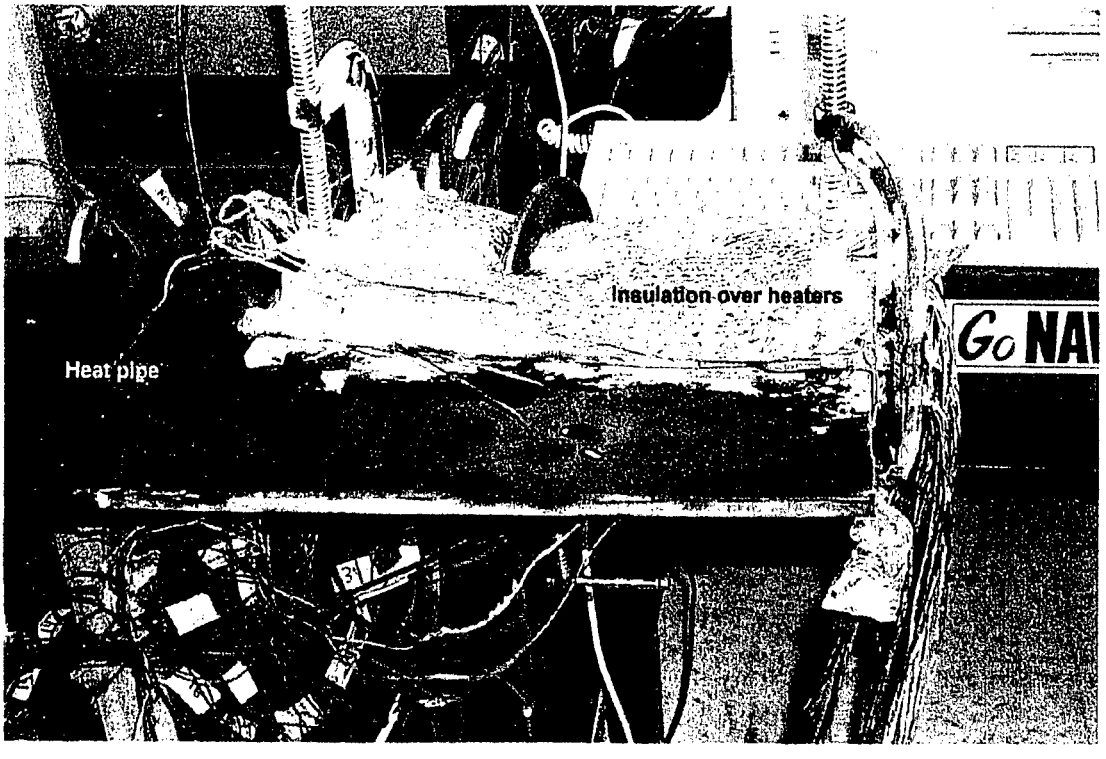

Figure 20. Asymmetric Heater Configuration

The same evacuation and charging assembly that was developed for the subscale heat pipe was used for the fullscale heat pipe. A photo of this assembly is shown in section 6. To record saturation pressures inside of the heat pipe, a pressure transducer was mounted to the end of the heat pipe in between the heat pipe valve and the heat pipe itself. Figure 21 shows this end fitting with the transducer mounted. This transducer was used to record most of the data. However, this transducer malfunctioned, and was replaced by an analog pressure gauge as seen in Figure 22.

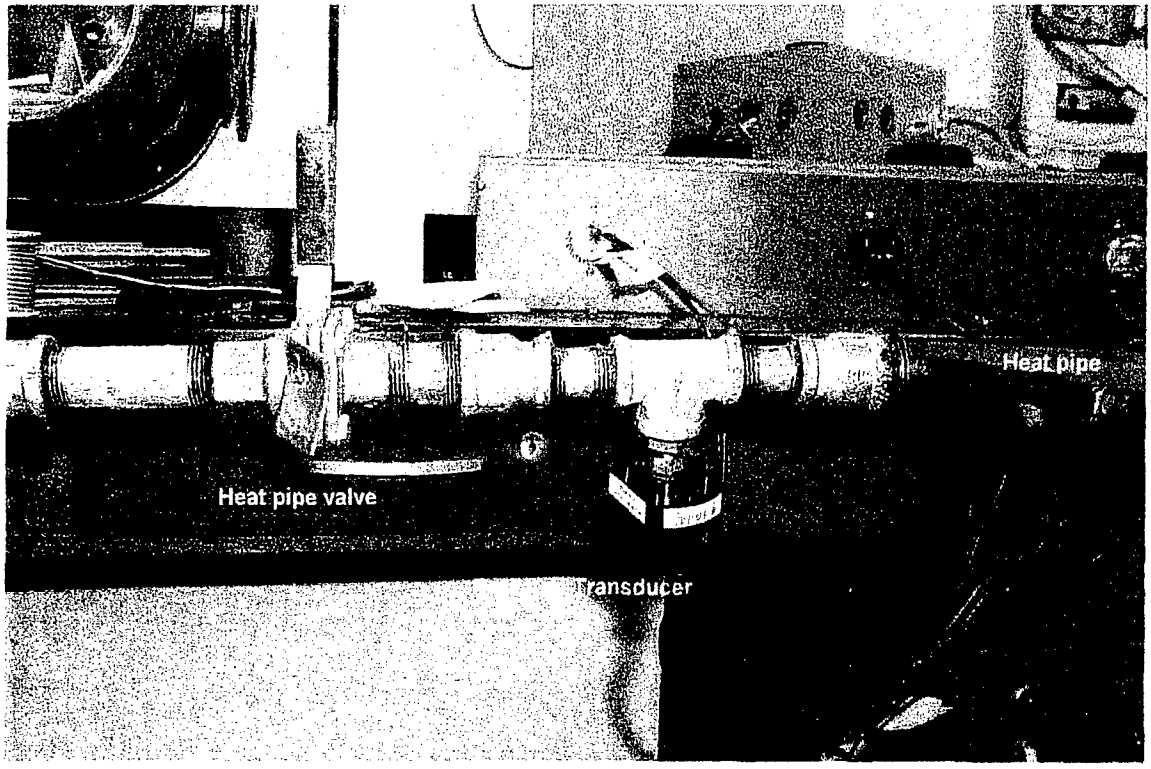

Figure 21. Heat Pipe End Fittings

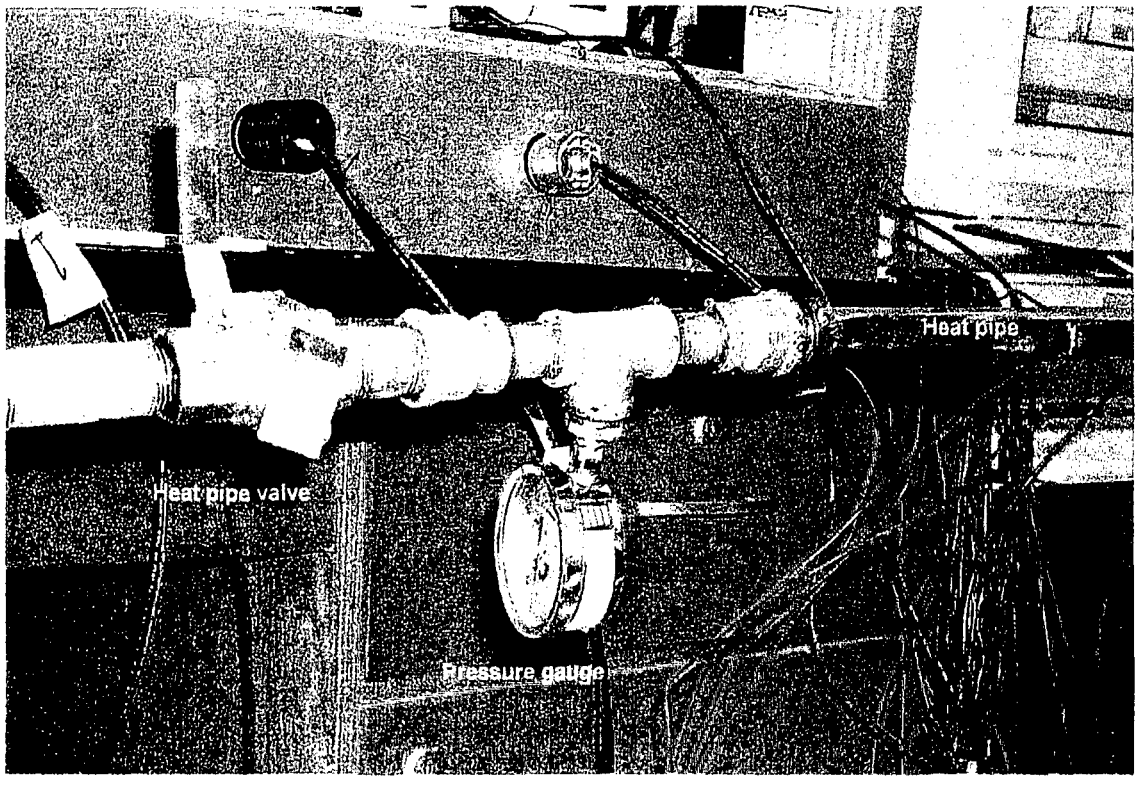

Figure 22. Analog Pressure Gauge

Again, it is important to note that the valve used was specially rated for high vacuum service. A regular valve would not be capable of holding the high vacuum states that occur in evacuation and when the heat pipe is properly charged but not operating.

Since testing at various angles to the horizontal is an important part of the test criteria, it was necessary to design a test stand such that the heat pipe was capable of rotating through the required angles while remaining free to natural convection. For this, a wooden stand was designed that consisted of two legs fixed to a flat base. See Figure 23 to view the stand with heat pipe mounted. Attached to the stand were two clamps to hold the heat pipe in place while being able to rotate it. These were made from two C-Clamps welded together by a steel bar. From this bar protruded a threaded screw, which was fixed to the bar. This screw went through a wooden bearing block and the test stand legs, and was attached on the other side of the leg by a wing nut and a washer. The wing nut could be loosened and tightened to move the clamps through the various angles about the screw. This assembly rotated the heat pipe through the required test angles. Figure 24 shows the clamps mounted to the heat pipe with PVC feet attached. These PVC feet served not only to spread the load, but also to insulate the clamps from the heat pipe so that the clamps could not become a heat sink.

Temperature data were recorded in two ways. The first was via the infrared camera videography, pictured in section 6. The other means was by an array of thermocouples. The

placement of the thermocouples on the heat pipe are shown in Figure 25. Figure 26 shows how the thermocouples actually looked when mounted on the heat pipe. The numbers of the thermocouple locations correspond to their assigned numbers in the data collection software. The thermocouples were wired into the same data acquisition junction boxes used by the Wattmeters. There were 8 junction boxes with 8 channels each for a total of 64 channels of data sampling. However, only 43 were used (39 thermocouples plus four Wattmeters). To see how the system is configured, see Figure 27.

Figure 23. Heat Pipe Test Stand

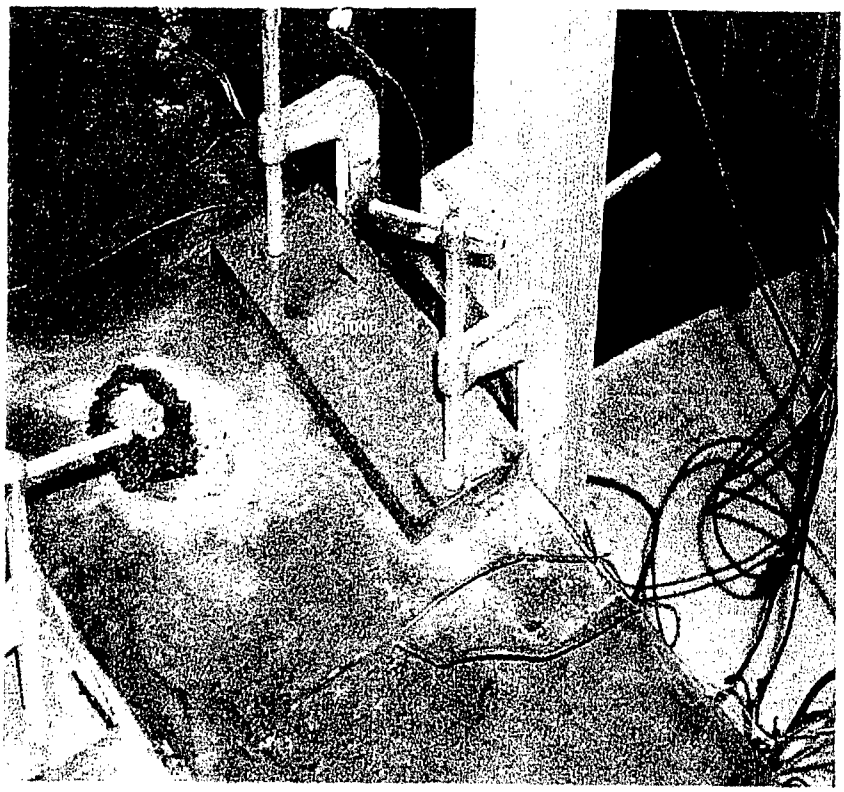

Figure 24. Heat Pipe Mounted to Clamp

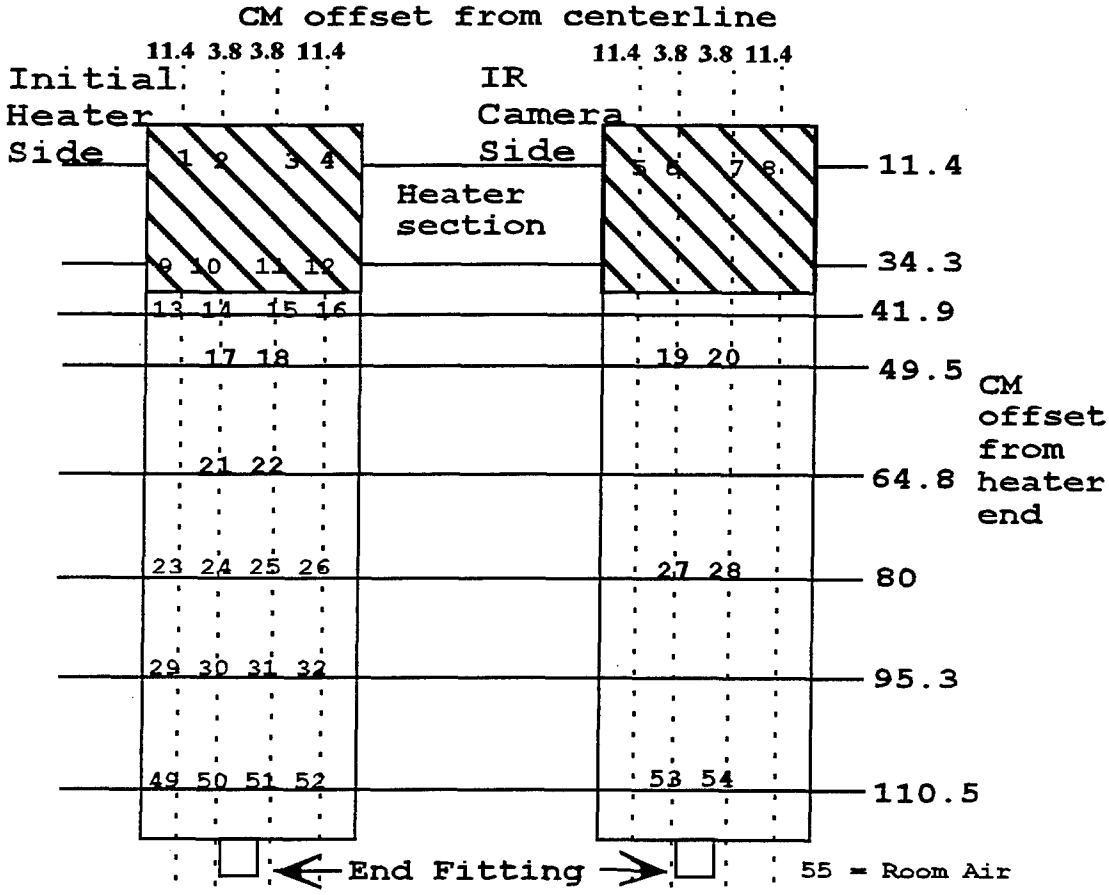

Figure 25. Thermocouple Placement by Number

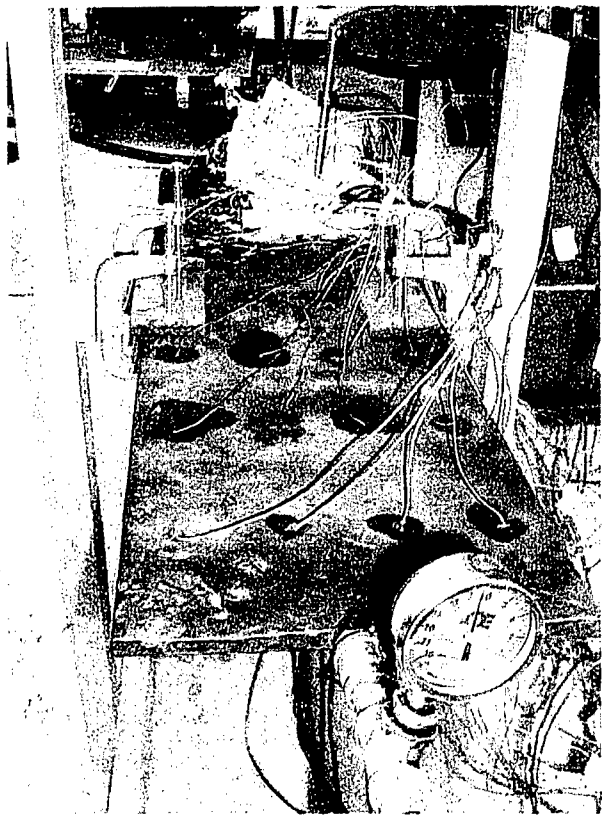

Figure 26. View of Attached Thermocouples

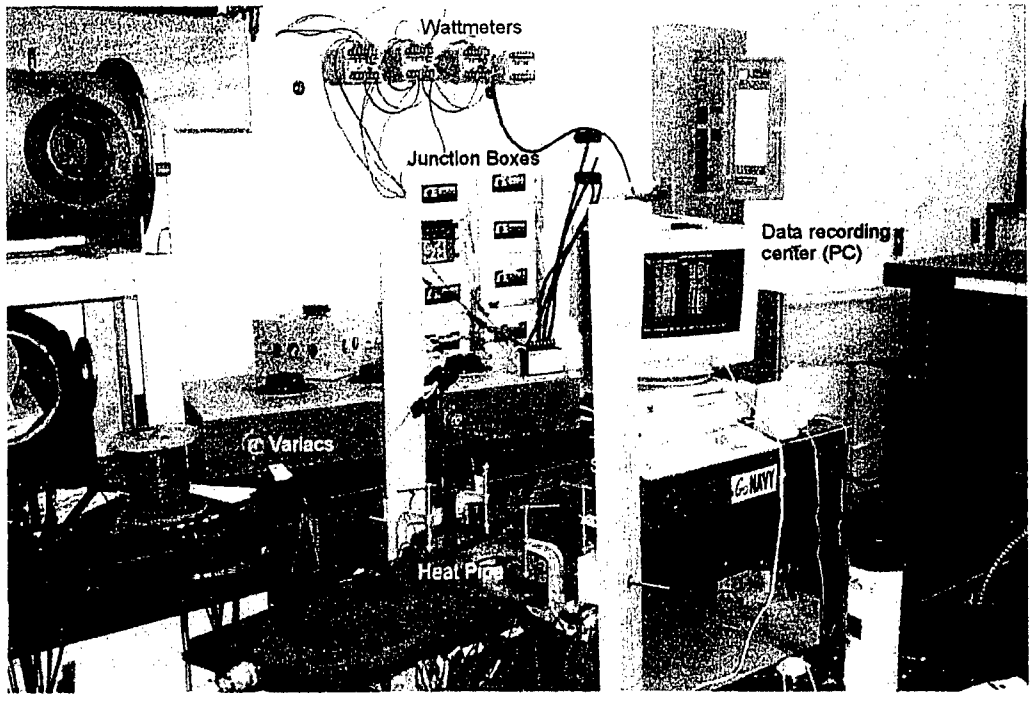

Figure 27. Testing Setup

8.2 EXPERIMENTAL PROCEDURE

The heat pipe went through tests at different orientations. Figure 28 shows the nomenclature for the different orientations.

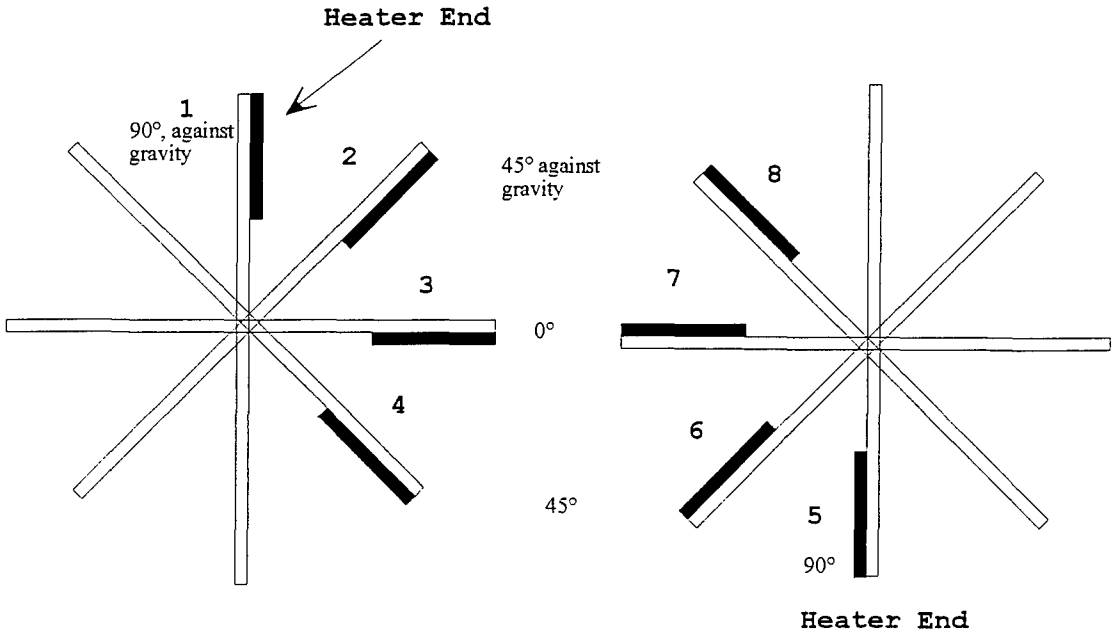

Figure 28. Testing Orientations

The testing criteria for the symmetric heating case (all heaters mounted on one side, covering entire width of heat pipe) was as follows:

1. With 100% fluid charge, test orientations 2,3,4,5,6, and 7 heating slowly to at least 400 Watts (more if conditions allow), allowing heat pipe to reach equilibrium temperature for each heat input.
2. With 125% fluid charge, test orientations 3,4,5, and 7 heating with at least 400W allowing equilibrium conditions.

3. With 75% charge, test orientations 3,4, and 5 heating with at least 400W allowing equilibrium conditions.
4. Mounting the heaters in the asymmetric configuration (see Figure 20), test heat pipe with 100% fluid charge in orientations 3,4,and 5 heating slowly to as high a heat input as possible, allowing for equilibrium between heating increases.
5. For all runs, data is to be collected over time by data acquisition software, which records continuously, and the infrared camera, which records at the user's discretion.
6. Take video and still photographs of interesting phenomena via the infrared camera.

9.0 DATA ANALYSIS

The experiments detailed in chapter 8.0 were completed. However, some calculations had to be performed before the data could be properly analyzed.

A fin, whether it is an isothermal heat pipe fin or a conventional fin, rejects heat to the ambient by means of convection and thermal radiation. These heat rejection modes are represented by equations 9.1 and 9.2, respectively (Kreith and Brohn, 1997). In equation 9.1, h is the convection coefficient [W/(m K)], A is the surface area of the body, and ΔT is the temperature difference between the hot body and its surroundings. In equation 9.2, σ is the Stefan-Boltzmann constant, ε is surface emissivity (percent radiated as compared to an ideal emitter), T_h is the temperature of the radiating body, and T_{amb} is the ambient environment temperature.

$$Q_{conv} = hA\Delta T \tag{9.1}$$

$$Q_{rad} = \sigma \varepsilon A\left(T_h^4 - T_{amb}^4\right) \tag{9.2}$$

For radiation heat transfer, the emissivity is set to .95, a value experimentally determined for the heat pipe using the infrared camera and thermocouple measurements. This was done by comparison of thermocouple measurement to infrared measurement. Emissivity is adjusted in the infrared camera data menu until the temperatures seen by the infrared camera match the temperatures recorded by the thermocouples.

Tables and equations used in solving the combined convection-radiation heat rejection problem are shown in Appendix 5. Figure 29 shows the heat transfer rejection modes for a given heat input (Watts) assuming all heat is transferred into the heat pipe (Cerza, 1999).

From Figure 29 it is seen that both radiation and convection are important modes of heat transfer for the heat pipe. To determine if the heat pipe was properly functioning as a heat pipe, it can be compared to a conventional fin. A fin is an extended surface that enhances heat transfer by increasing the heat transfer surface area, such as the aluminum fins on an automobile radiator. Thermal energy is input to the fin at one end. The energy then conducts through the fin to the colder end. As the energy conducts through the fin it is rejected to the ambient surroundings by convection and radiation (in this case). Since convection and radiation are of the same order of magnitude for the heat input range of these experiments, the simpler convection model is used with a convection heat transfer coefficient, h, equal to twice that of the value for convection only, thus taking the radiation heat rejection mode into account. Steady-state fin temperature along the fin length can then be calculated for a rectangular fin by equation 9.3.

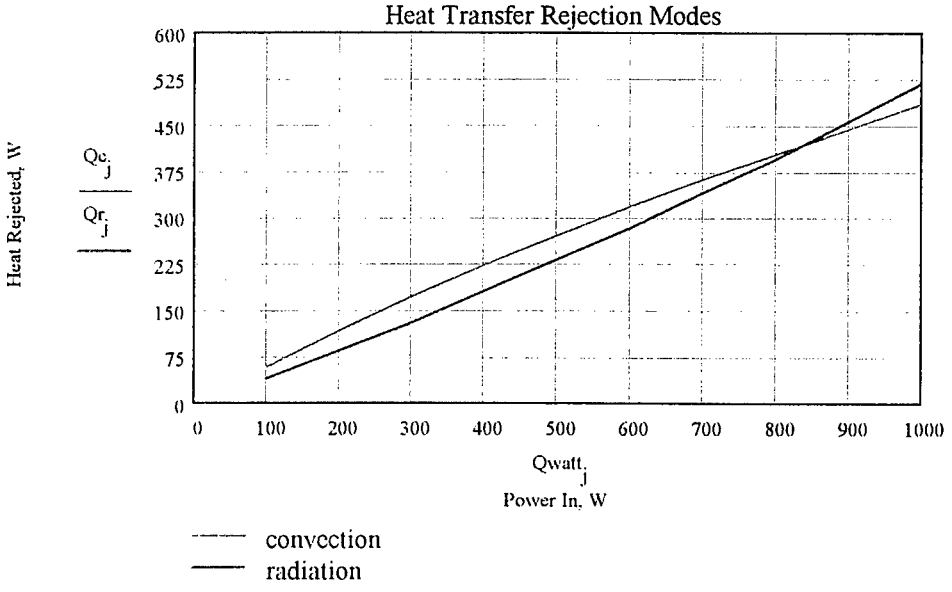

Figure 29. Heat Transfer Rejection Modes for Heat Input

$$T_{ss} = \left[T_{amb} + \left(\frac{Q_{in}}{kA_x m} \right) e^{-mx} \right] \tag{9.3}$$

where m is found with equation 9.3 as follows:

$$m = \left(\frac{hP}{kA_x} \right)^{\frac{1}{2}} \tag{9.4}$$

and P is the perimeter of the fin, A_x is the cross-sectional area in the x-direction.

The previous fin analysis is for a conventional fin. The heat pipe fin temperature is approximately isothermal along the fin length. Equation 9.5 represents the steady-state, isothermal heat pipe fin relation:

$$Q_{in} = hA(T - T_{amb}) + \sigma \varepsilon A(T^4 - T_{amb}^4) \tag{9.5}$$

Equation 9.5 is a fourth order polynomial equation for the temperature T. The solution to equation 9.5 is the positive real root of equation 9.5 assuming that T is unique and greater than T_{amb}.

9.1 HEAT PIPE VERIFICATION

Figure 30 shows a plot of a conventional fin vs the experimental data for the USNA flat heat pipe at a 400W steady-state condition with 100% fluid charge.

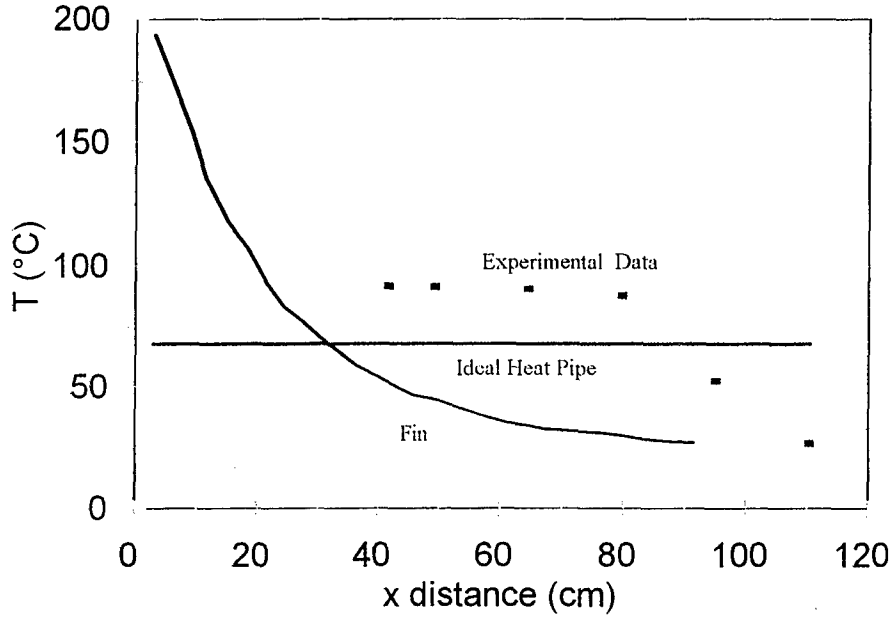

Figure 30. Standard Fin vs Ideal Heat Pipe Fin and Actual Heat Pipe (400 W Steady-State, Horizontal)

As one can see from the experimental data plot, the heat pipe was not isothermal, but had about a 60°C temperature drop from the beginning of the heat pipe to the end. However, a portion of the heat pipe was nearly isothermal. It can be assumed that the heat pipe is performing as a heat pipe for the first 80 cm away from the heater section and not as a conventional fin since the temperatures of the experimental data are close compared to the theoretical heat pipe case. Figure 31 shows an infrared camera photograph of the heat pipe in the horizontal (3) position (not yet reached steady-state with 125% charge). This clearly shows that although there are some serious end effects involved, a large region of the heat pipe is fairly isothermal. It is believed that some air leaked into the heat pipe and caused the end effects (cooler temperature pockets) by blocking a portion of the condenser region. At higher heat inputs (such as pictured in Figure 31), the air would be compressed into the end fitting by the water vapor, causing the cold region to recede, making the heat pipe surface closer to isothermal. The cold spot in the middle of the photo corresponds to a section of epoxy used to seal a leak. It is an insulator, and is therefore colder than the metal of the heat

pipe. The clamps that hold the heat pipe to the test stand also insulate and therefore are shown to be cooler than the heat pipe. Figure 32 is a graph corresponding to the photo in Figure 31, the best isothermal profile achieved by the USNA flat heat pipe.

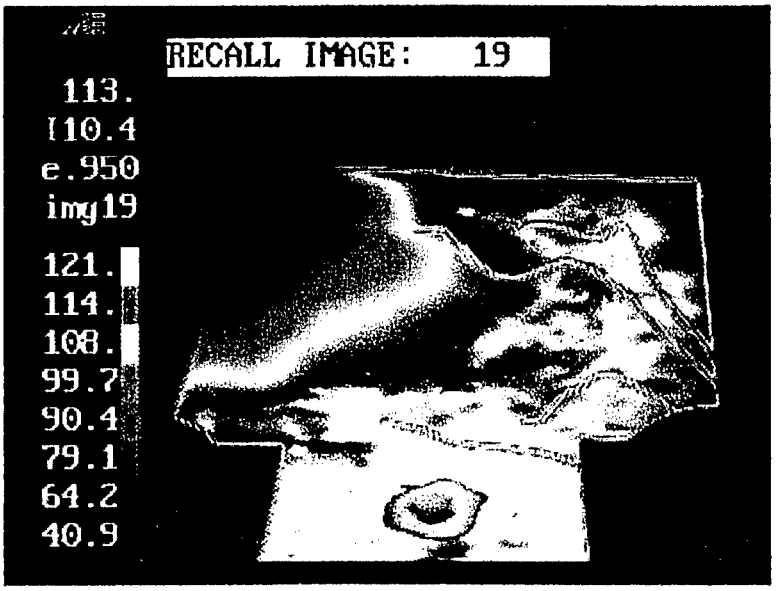

Figure 31. IR Photo of Horizontal Heat Pipe, 800W, 125% Charge

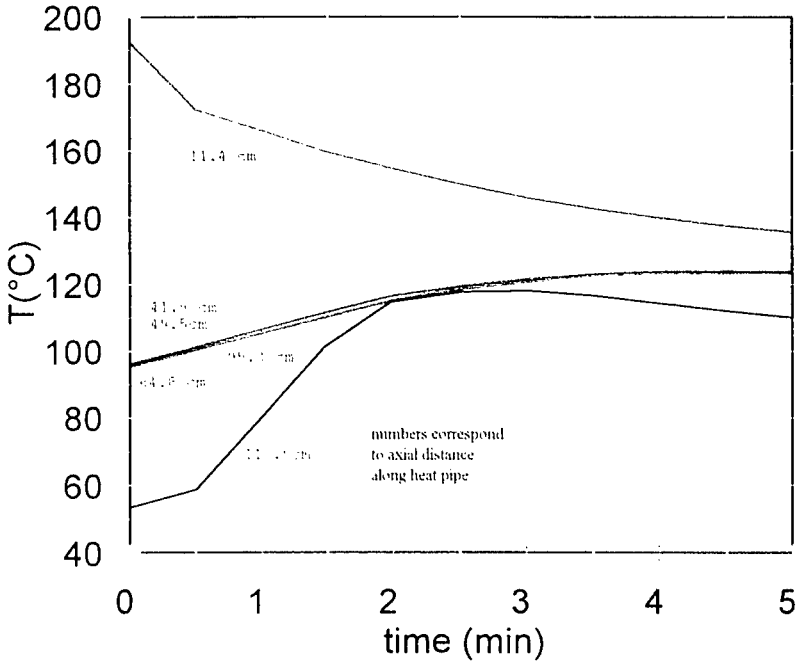

Figure 32. Near Isothermal Case Temperature Vs Time, Horizontal, 600W, 100% Charge

9.2 EFFECTS OF ORIENTATION ON HEAT PIPES

The convection coefficient, h, utilized in equation 9.5 change for flat plates with their heated side facing downwards in accordance with their orientation. Equations 9.6 and 9.7 can be used to solve for the convection coefficient at a given angle of orientation, θ, from the vertical. In equation 9.6, $N\overline{u}$ is the Nusselt number, a dimensionless heat transfer coefficient that is the ratio of convection heat transfer to conduction in a fluid layer of thickness L. Gr_l and Pr are the Grashof and Prandtl numbers, respectively. The Grashof number is the ratio of buoyancy to viscous forces, and the Prandtl number is the ratio of molecular momentum diffusivity to thermal diffusivity (Kreith and Brohn, 1997).

(9.6)

$$h = \frac{kN\overline{u}}{L}$$

(9.7)

$$N\overline{u} = .56(Gr_l \Pr \cos\theta)^{\frac{1}{4}}$$

Note: equation 9.7 is only valid for θ<90°

For the 90° case, equation 9.8 is to be used, where Ra_l is the Rayleigh number, which is the product of the Grashof and Prandtl numbers (Kreith and Brohn, 1997).

(9.8)

$$N\overline{u} = .15(Ra_l)^{\frac{1}{3}}$$

Although the convection coefficient would be slightly higher for the heated side facing upwards due to the interaction of buoyancy and momentum effects in natural convection, this case will be treated as if the convection coefficient is uniform for both sides of the heat pipe. By looking at equation 9.7, one can see that convection coefficients decline as the angle increases. Therefore, at orientations approaching the horizontal, to reject the same amount of heat, the surface temperature of the heat pipe must rise (equation 9.1). Using equation 9.7, a theoretical plot of isothermal flat heat pipe temperature versus angle orientation was made and compared against experimental data collected for the 400W steady-state condition with 100% charge (Figure 33). The experimental data is relatively close to the theoretical values.

When an orientation angle other than horizontal was introduced, the heat pipe did not demonstrate isothermal behavior until the heat input was increased to near 600W. Figure 34 shows the best isothermal profile reached for the vertical orientation (position 5). Figure 34 depicts the sides of the heat pipe as much hotter than the middle portion. This condition

existed for all inclined cases. Figure 34 shows a temperature difference of about 27°C from the hottest part to the coolest part of the condenser section. The data corresponding to Figure 34 was the closest to a theoretical heat pipe of any of the inclined test cases. Figure 35 shows a start-up condition (transient effect) for this orientation (position 5) at a lower power setting of 400W. Note the large temperature gradient across the heat pipe.

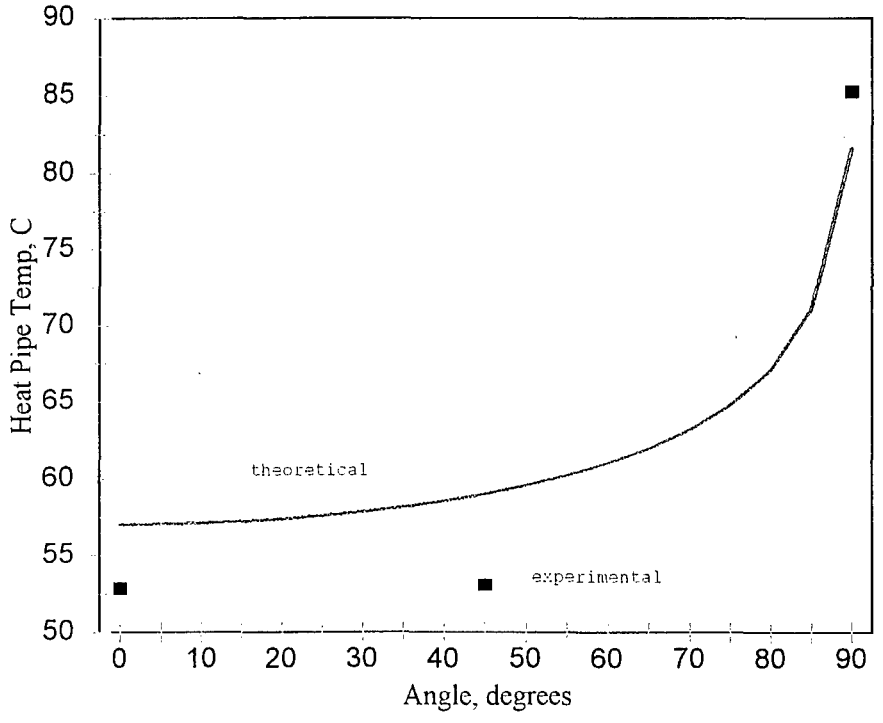

Figure 33. Heat Pipe Temperature vs Angle, 400W

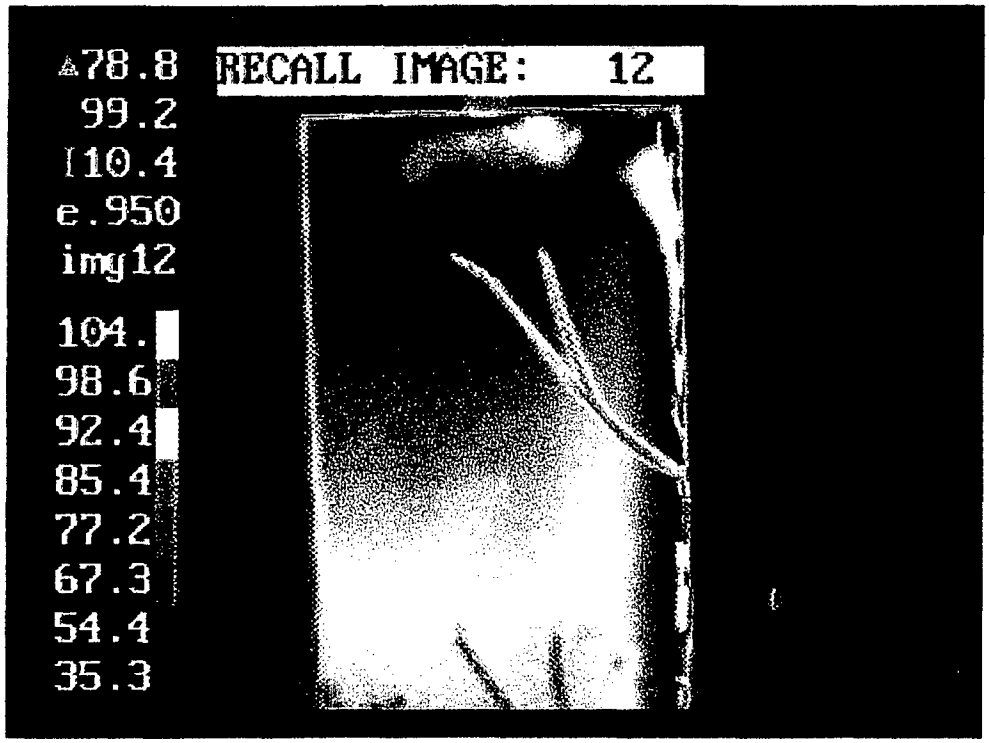

Figure 34. IR Photograph, Vertical (5), 600W

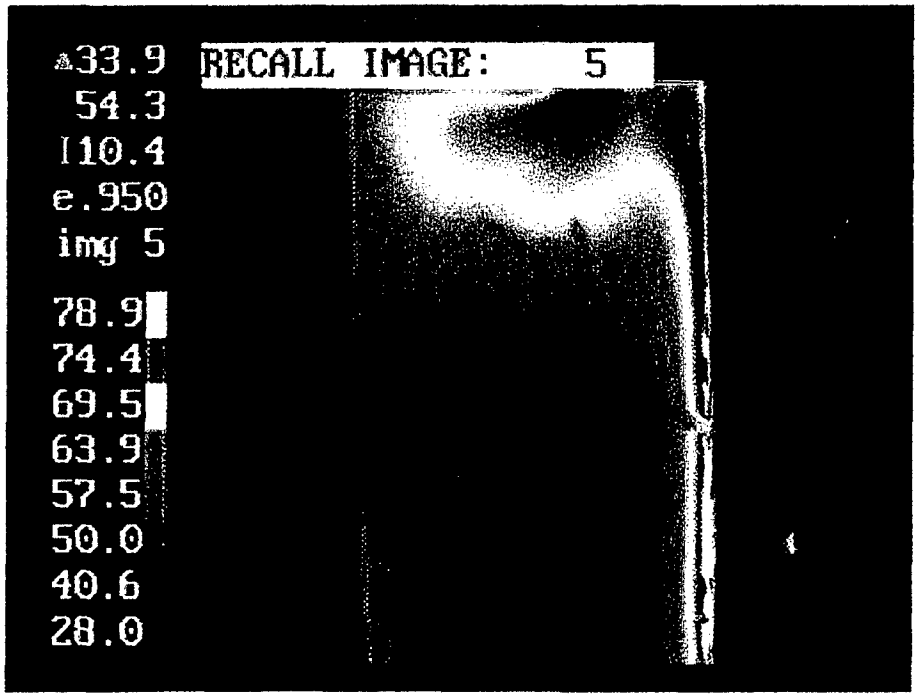

Figure 35. Vertical Gradient, 400W, 125% Charge

Only one case was tested with the condenser end lower than the evaporator end. This was orientation 2. The heat pipe did not function properly, acting as a fin. This is because the maximum vertical capillary pumping height achievable by the wick is around five cm. Therefore, no water could be delivered to the evaporator region via the wick (its height was greater than five cm above the end of the heat pipe) and the evaporator section remained dry. Without the circulation of the working fluid, the heat pipe does not function as a phase change device, but acts as a conventional fin. Only the horizontal tests performed well, and this will be explained in section 9.6.

9.3 EFFECTS OF VARYING CHARGE

To compare the effects of varying charges, each charge experiment was conducted at a 400W heat input. The experiments were allowed to reach a steady-state condition for orientations 3, 4, and 5. The horizontal cases produced the best data and are presented for comparison. Figures 36, 37, and 38 show the data plots of the each case, 125% charge, 100% charge, and 75% charge in sequence. Figure 39 depicts the three charges plotted against each other on the same graph for a uniform heat input over time.

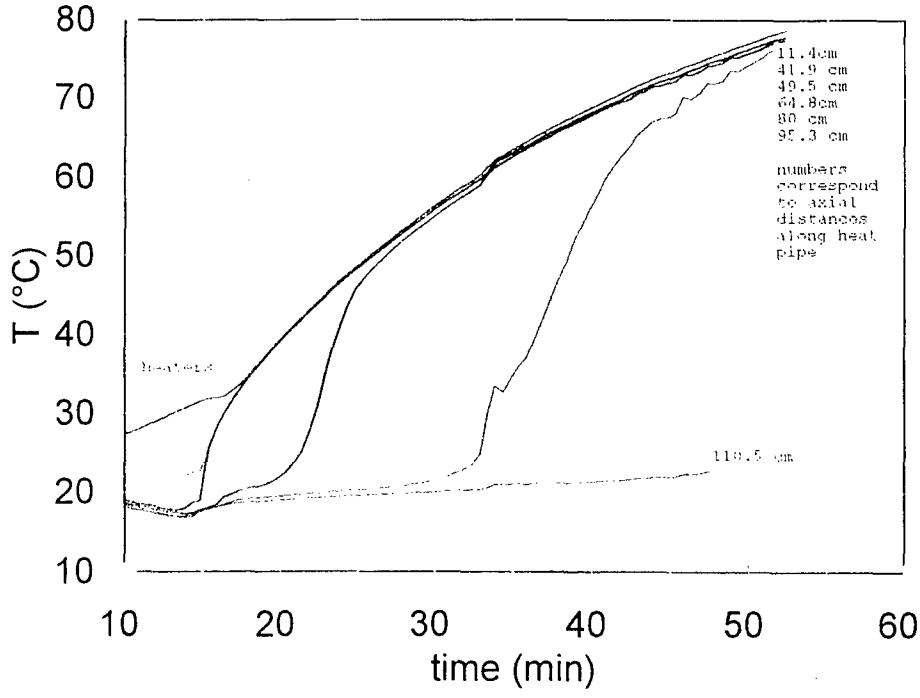

Figure 36. Temperature vs Time, 400W 125% Charge

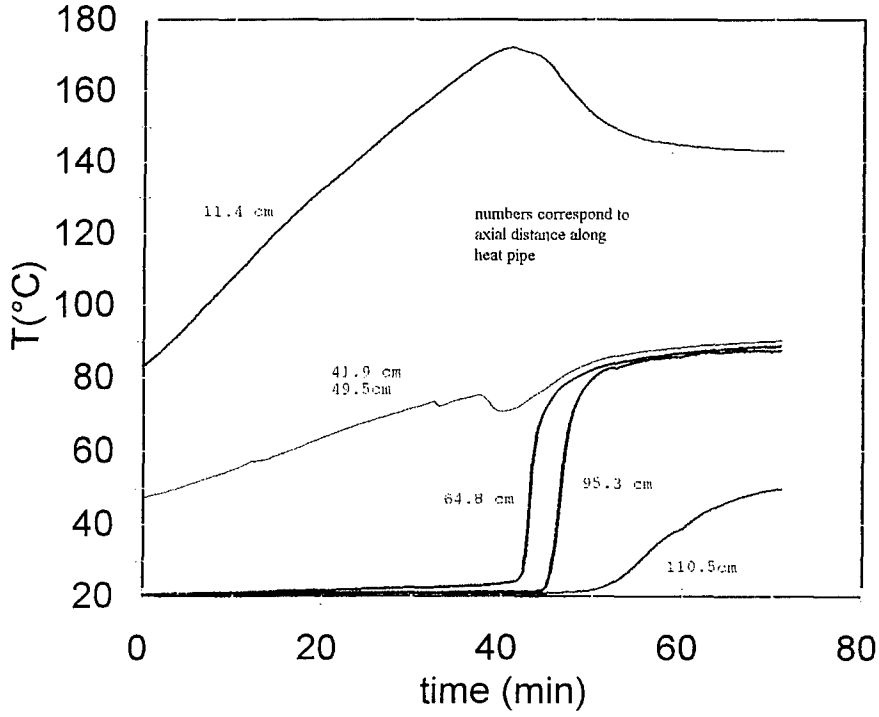

Figure 37. Temperature vs Time, 400W, 100% Charge

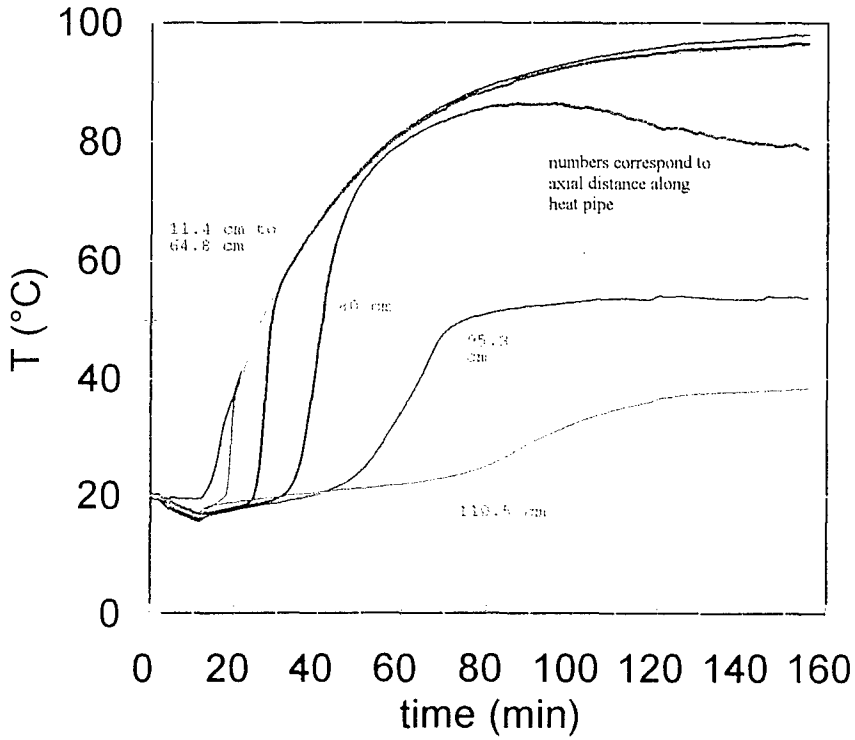

Figure 38. Temperature vs time, 400W, 75% Charge

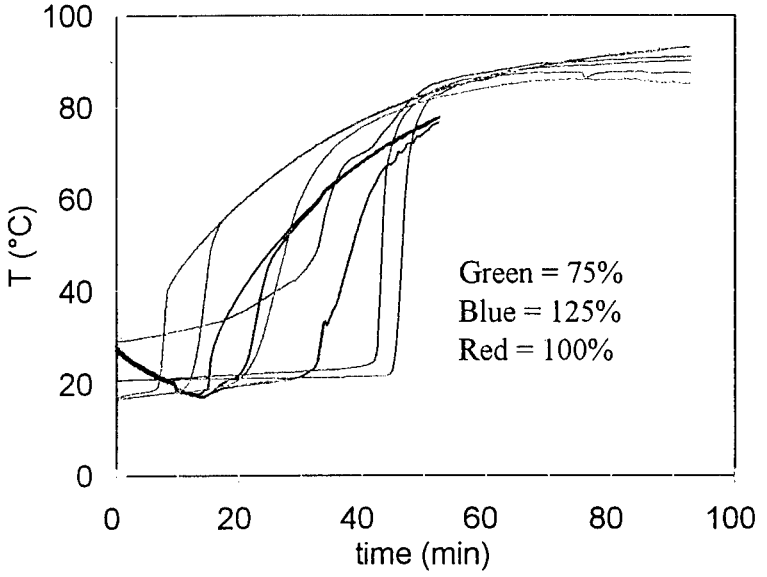

Figure 39. Varying Charges Temperature Vs. Time, 400W, Horizontal

Although the differences in effects are not very pronounced, it is apparent that the 75% charge case displays the quickest response time. This is because there is less water in the heat pipe and therefore less energy to be absorbed, allowing the heat pipe to attain steady state. However, notice that not all of the heat pipe in the 75% charging case achieves the same operating temperatures. This could be due to a lack of fluid in the wick required to circulate the necessary heat to activate the full heat pipe or the presence of air in the heat pipe (gas loading).

The 100% charging case has the best traditional heat pipe response. When a location encounters the condensing vapor front, it changes temperature rapidly to the saturation temperature corresponding to the internal saturation pressure. However, it takes longer for the 100% charging case to reach isothermal conditions along the length of the heat pipe than the 125% case. This is due to the presence of air, as once it is compressed further towards the end of the heat pipe the temperature at the location it previously occupied increasing rapidly. Also, the 100% charging case achieves the best near-isothermal condition, as all locations except the end are within a few degrees of each other at the steady-state condition. The divergent line on the top of the plot, corresponding to 11.4cm, does not necessarily make the heat pipe non-isothermal. This curve corresponds to thermocouples on the back of the heater side, and are therefore more representative of the heater temperatures. The thermocouples were reading an averaged temperature of the hot heaters and the inside evaporator section of the heat pipe. Hence, they would indicate higher temperatures than the thermocouples on the condenser end of the heat pipe. This curve can therefore be ignored.

The 125% charging case theoretically should take more time for all locations to reach an isothermal condition. This is because there may be some liquid flooding in the evaporator section, and until it is vaporized, there can be no menisci in the wick and therefore no capillary pumping action. The 125% charging case does reach a near isothermal case when it reaches steady-state, though it heats up faster than the 100% charge. This is not fully understood, though it is likely that the 100% charging case was conducted with more air present in the heat pipe than the 125% charging case, which required more time to compress the air towards the end of the heat pipe.

9.4 START-UP CONDITIONS

Before a heat pipe can reach a steady-state condition, the energy it is receives as heat input must heat all of the mass that comprises the heat pipe (fluid, screen, vessel wall, etc.) to the steady-state temperatures. The USNA heat pipe with a heat input of 400 W would respond as shown in Figure 40. Figure 40 compares closely to Figure 37, the 400W start-up case for a 100% charge. The experimental case reaches a slightly higher temperature in the activated regions. This is because in order to compensate for inactive regions which are at a lower temperature the active regions must get hotter to reject the input heat. However, both graphs reach an approximate steady-state condition at around one hour. Therefore, Figure 40 represents a good model.

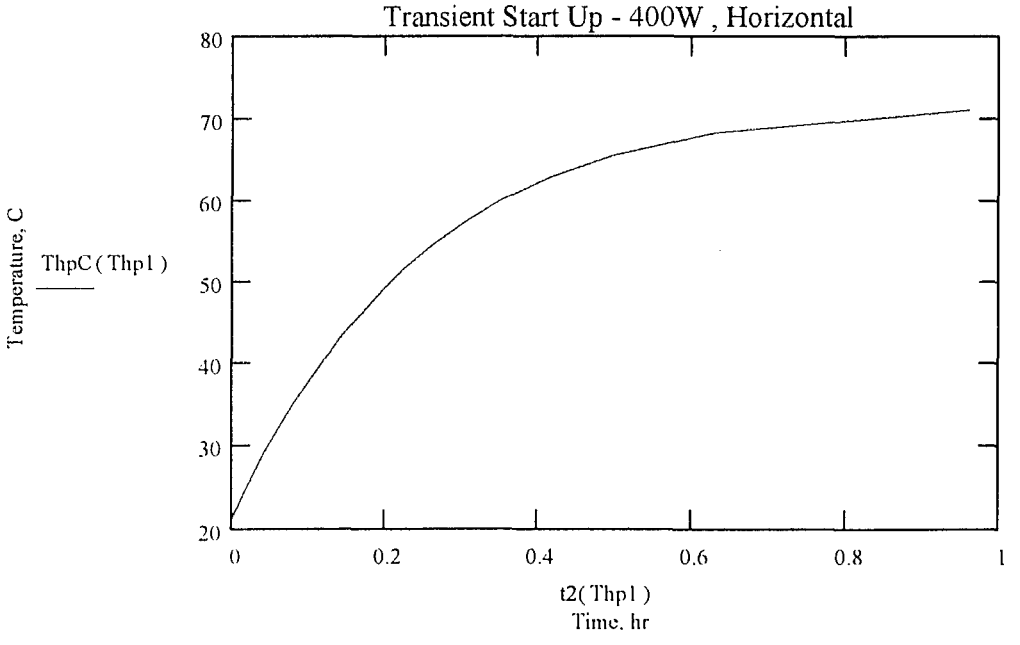

Figure 40. Theoretical Heat Pipe Start-Up

Another aspect of startup is shown in Figure 41. Figure 41 includes a plot of the heaters, which is the top trace in this graph. It is interesting to note that when heat is applied, the heaters' response time is rapid. The heat pipe slowly activates more regions, and when many are activated, the temperature of the heater drops because heat is being more effectively transferred over a large area.

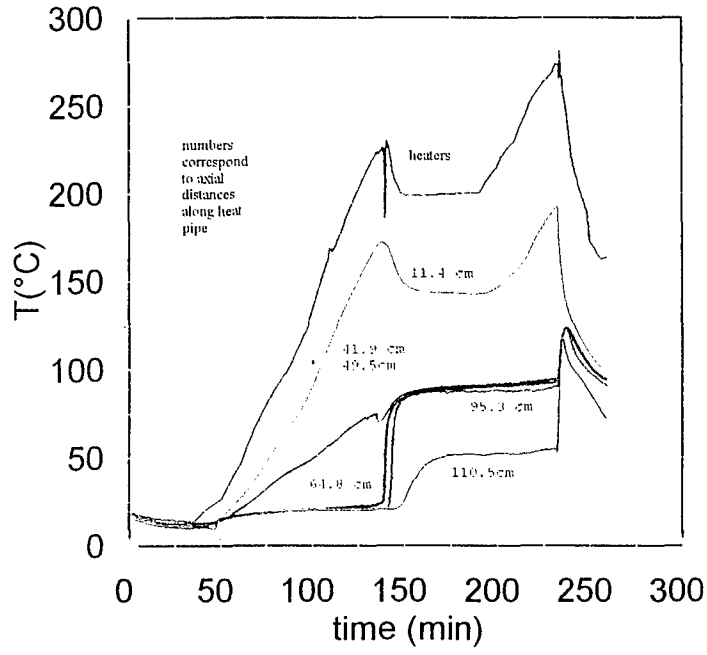

Figure 41. Temperature vs Time for 100% Charge, 400-800W, Horizontal

9.5 ASYMMETRIC CASES

Two cases of asymmetric heating will be discussed: the response of the heat pipe when inclined, and the response when horizontal. When horizontal and at a low heat input, only the condenser area opposite the heater section activated, as seen in Figure 42. However, as the heat input rises, the heat pipe condenser region begins to become more active as seen by the increasing size of the higher temperature section of the condenser surface. Figures 43 and 44 shows the heat pipe's thermal profile when the heat input is raised. This performance is indicative of having a non-condensable gas, such as air, in the heat pipe. If the USNA heat pipe performed as a theoretically perfect heat pipe without non-condensable gases inside, then all the condenser surface in the asymmetric (or any) case would reach an isothermal state.

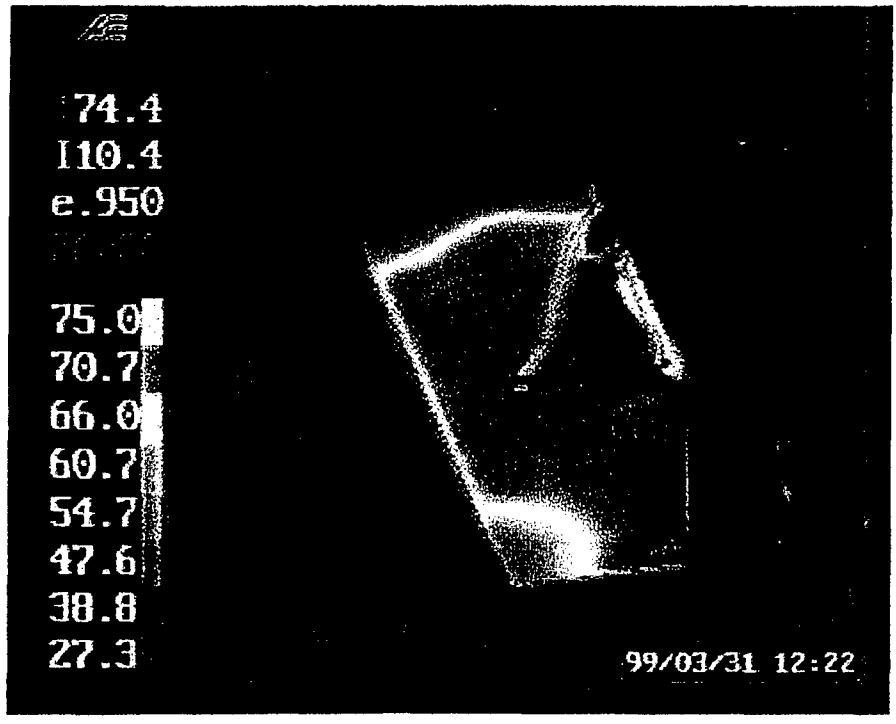

Figure 42. Asymmetric, Horizontal, 200W

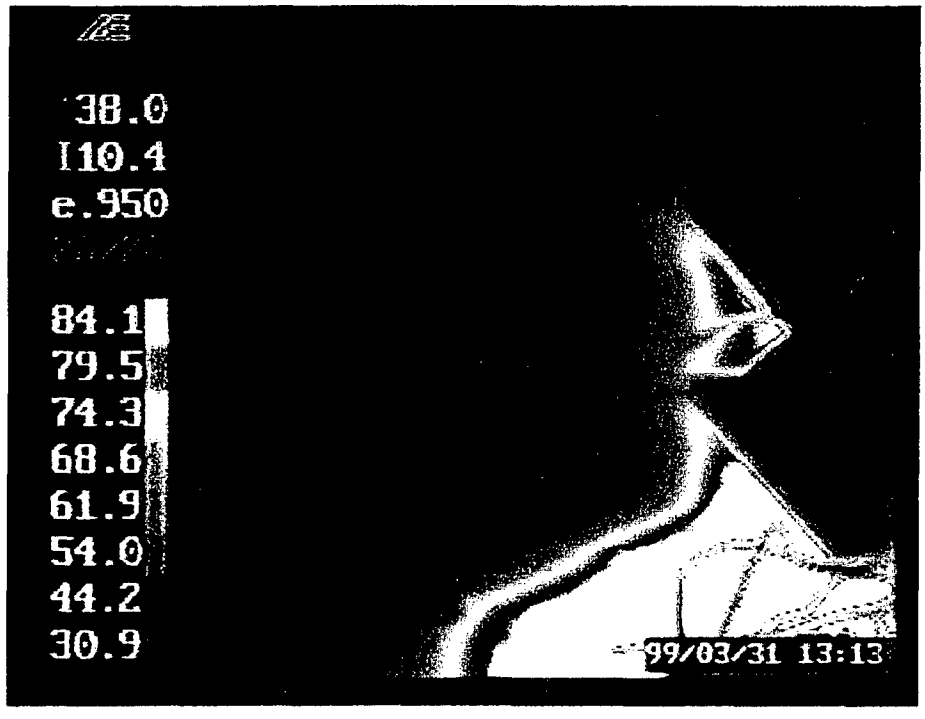

Figure 43. Asymmetric, Horizontal, 400W

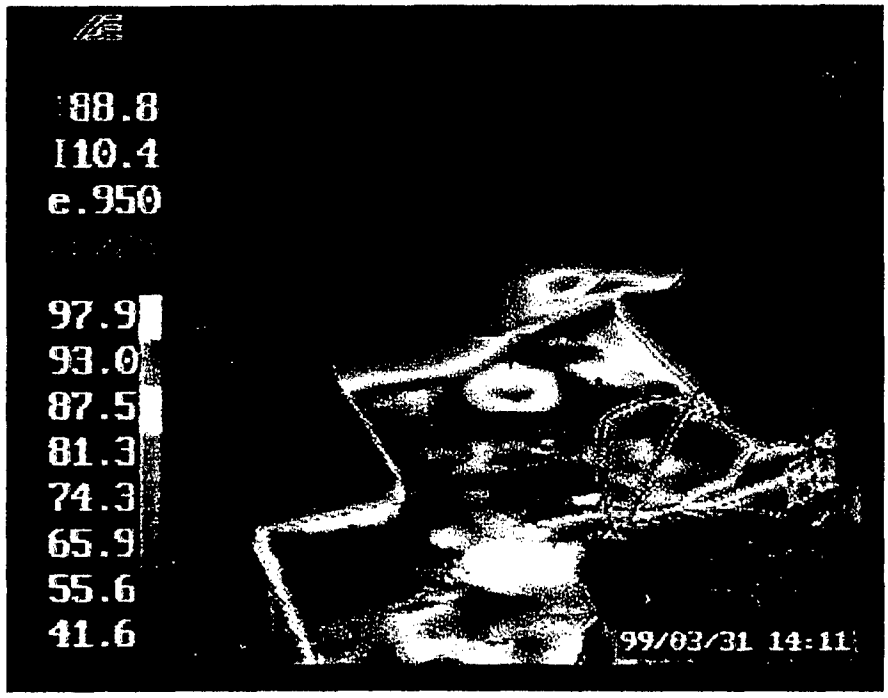

Figure 44. Asymmetric, Horizontal, 600W

The inclined cases did not perform as well as was hoped. The condenser side adjacent to the heaters never fully activated, and the more developed profile remained the "side-climbing" phenomenon that was observed in early inclined cases. Figure 45 shows the side near the heater section, and Figure 46 shows the larger area's thermal profile.

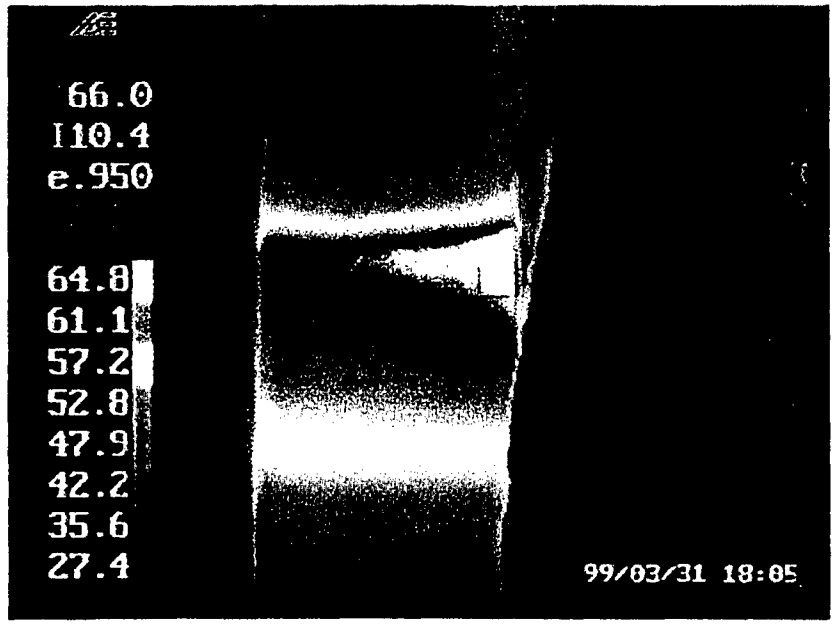

Figure 45. Asymmetric, Inclined, 400W

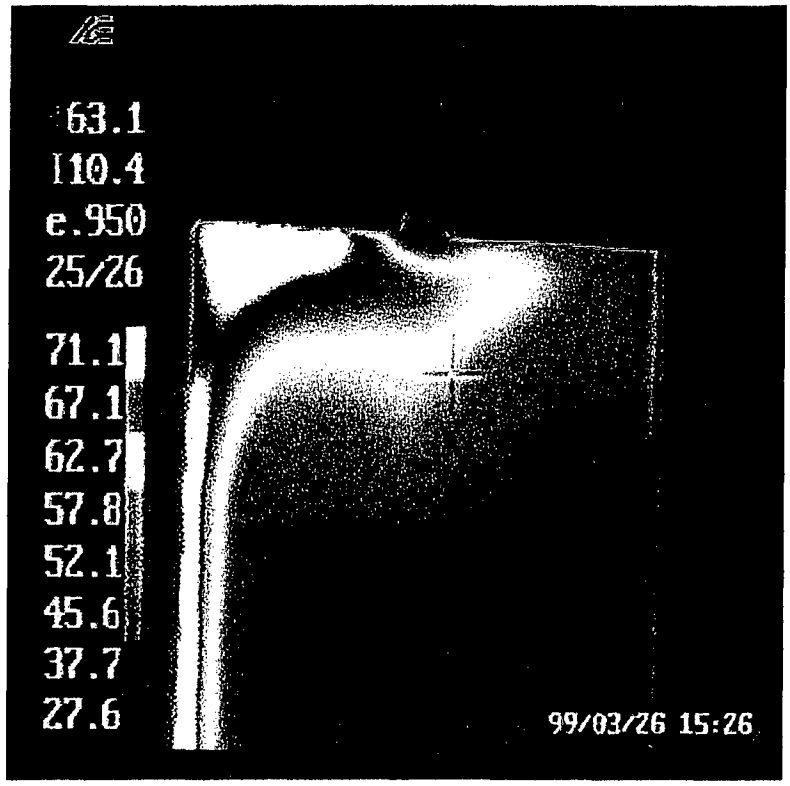

Figure 46. Asymmetric, Inclined, 400W

9.6 VARIABLE CONDUCTANCE HEAT PIPES

A variable conductance heat pipe is a heat pipe that operates with a certain amount of non-condensable gas loading. It is called variable conductance due to the effect that gas loading has. At low heat inputs, the gas blocks off a large portion of the condenser region, raising the temperature for the part that can be utilized. At higher powers, less of the condenser is blocked off as the gas is compressed more against the end of the heat pipe.

The maximum temperature drop across the wick (including liquid) and vessel wall was calculated to be less than 1.1°C for a heat input rate of 500W. Therefore, we cannot use excess fluid to explain the large temperature gradients. Only entrapped air in the heat pipe could be causing such a gradient. Observe Figures 36-38, and note that the end temperatures all remain much, much lower than the activated regions. These are areas inside the heat pipe that are covered with gas and the water vapor could not push the gas out of the way in order to have an active condenser section. Therefore, very little heat is transferred in that region and it remains much colder

10.0 CONCLUSIONS

Overall, this project was successful in determining the usefulness of flat heat pipes for thermophotovoltaic energy conversion.

10.1 GOALS MET

The following criteria were set for the project:

1. Design and construct the heat pipe entirely out of Monel 400.
2. Exhibit two-dimensional heat transfer behavior.
3. Feature ultimate dimensions of 4 feet long (1.22 m) by 1 foot wide (30.48 cm) by ½ inch thick (1.27 cm).
4. Maintain an operating temperature of up to 212°F (100°C).
5. Possess a means of internal support for structural rigidity without sacrificing two-dimensional flow capabilities.
6. Operate without the presence of any noncondensable gases, such as air, inside of the heat pipe (gas loading).

The project had the following experimental and theoretical goals:

1. Monitor the condenser region temperature profile as closely as possible, via thermocouples and infrared video camera.
2. Test asymmetric heating conditions and differing heat inputs.
3. Test performance at different heat inputs, fluid charges, and varying inclination angles.
4. Modify important heat pipe equations for flat geometry.
5. Model experimental and theoretical heat pipe performance against a conventional fin of the same dimensions.
6. Analyze experimental data to determine overall performance and feasibility of flat heat pipes for a TPV energy conversion system.

The goals were met as follows:

- A flat heat pipe of the set dimensions was designed entirely of Monel 400.
- The flat heat pipe was successfully constructed using pin spacers as internal supports and operated without biasing flow direction.
- Using water as a working fluid, an operating temperature in excess of 100°C was achieved.
- The heat pipe's temperature profile was monitored and recorded closely.

- Asymmetric tests were conducted and clearly demonstrated that a heat pipe can maintain an isothermal condenser area despite a nonuniform heat application.
- A 100% charge performed the best, achieving the most uniform temperature profile.
- Increasing angle of orientation from horizontal requires a higher surface temperature in the condenser region to reject the same amount of heat the vertical orientation.
- The horizontal angle of orientation performed closest to a theoretical heat pipe, achieving the most near isothermal profile.
- Cylindrical heat pipe equations were modified to flat geometry to design flat heat pipes.
- Heat pipes were modelled against fins so that heat pipe advantages could be better illustrated as an isothermal emitter and to verify experimental operation as a heat pipe
- The heat pipe did not operate completely without gas loading. However, even in the presence of gas loading, it is possible to maintain a near isothermal condenser surface.
- It has been demonstrated that a flat heat pipe can maintain a large isothermal surface, with either a uniform (symmetric case) or nonuniform (asymmetric case) application of heat.
- A flat heat pipe can effectively serve as an emitter for a thermophotovoltaic energy conversion system.

10.2 RECOMMENDATIONS

The following are recommendations based on the data gathered by this project:

- Retest heat pipe without gas loading.
- Test higher heat fluxes (near capillary limit) to verify heat pipe's full heat transport capabilities.
- Develop transient models for multidimensional behaviors, such as large temperature gradient in inclined cases and temperature oscillations.

References

Ashcroft, John, High Temperature Heat Pipe Primer, Internal Report, Knolls Atomic Power Laboratory. September, 1997.

Borowsky, E. W., and R. J. Dziendziel, Thermophotovoltaics Primer, Internal Report. Knolls Atomic Power Laboratory, 1996.

Cerza, M. R., lecture notes, "Heat Pipes-A Design Guide." 1998.

Cerza, M.R., flat heat pipe derivations and modelling, 1999.

Chi, S. W., Heat Pipe Theory and Practice, Washington, D. C.: Hemisphere, 1976.

Dunn, P. D., and D. A. Reay, Heat Pipes, Oxford: Pergamon, 1976.

Erickson, Timothy, "Design and Construction of a Thermophotovoltaic Energy Conversion System Using Combustion Gases from a T-58 Gas Turbine." Trident Scholar Report. U.S. Naval Academy. May, 1997.

Faghri, Amir, Heat Pipe Science and Technology, Washington, D. C.: Taylor and Francis, 1995.

Kreith, Frank, and M. S. Brohn, Heat Transfer, Boston: PWS Publishing Company, 1997.

Lindler, K.W. Discussions on Thermophotovoltaic Cell Efficiency. 1999.

Peterson, G.P., An Introduction to Heat Pipes; Modelling, Testing and Applications, New York: Wiley and Sons, 1994.

Singer, Ferdinand L., Strength of Materials, New York: Harper and Row, 1962.

APPENDICES

	Page
APPENDIX 1 - CAPILLARY LIMIT DERIVATIONS	69
APPENDIX 2 - BOILING LIMIT DERIVATION	84
APPENDIX 3 - SONIC LIMIT DERIVATION	88
APPENDIX 4 - DEFLECTION DERIVATIONS AND SPREADSHEET	89
APPENDIX 5 - MATHCAD MODELLING OF FIN VS HEAT PIPE	94

APPENDIX 1 - CAPILLARY LIMIT DERIVATIONS

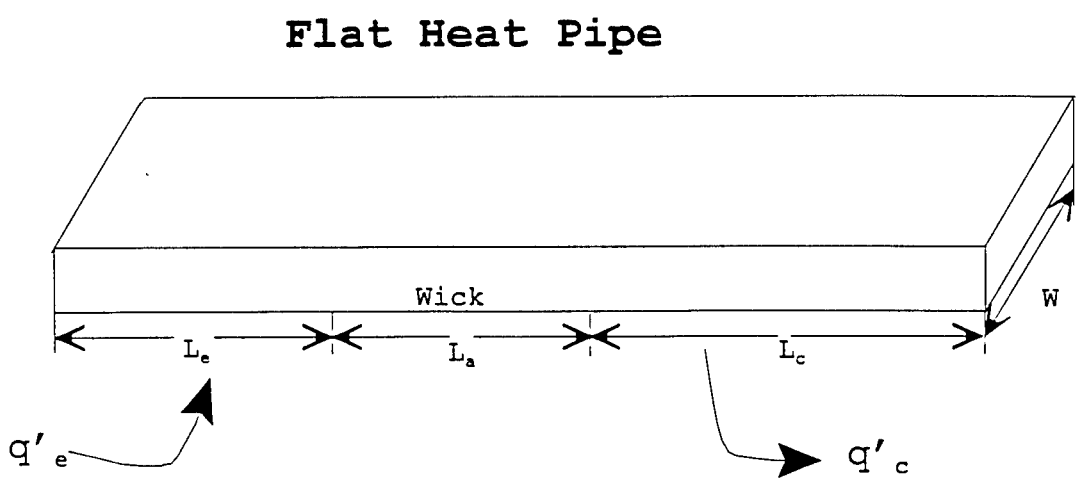

$$q'_e = \frac{q_e}{L_e W} = \text{heat flux into evaporator}$$

$$q'_C = \frac{q_c}{L_c W} = \text{heat flux out from condenser}$$

qe = qc at steady state = $\dot{m} h_{fg}$

$$\dot{m} = \frac{q_e}{h_{fg}} = \rho_g \left(W h_v\right) \bar{V}_{gU} \ , \quad \bar{V}_{gU} \text{ is the upward velocity from wick}$$

$$\dot{m} = \rho_g \left(W h_v\right) \bar{V}_{gD} \ , \quad \bar{V}_{gD} \text{ is the downward vapor flow in vapor space}$$

$$\dot{m} = \rho_f \left(W h_L\right) \bar{V}_L \varphi \ , \ \bar{V}_L \text{ is the liquid flow through wick,}$$

φ = porosity

Capillary Limit (neglect boiling incipience) for horizontal case

$$\Delta P_{\max} = P_v - P_L = \frac{2\sigma}{r_w}$$

$$P_v = P_{sat}$$

applying the Clapeyron relationship:

$$\left.\frac{dP}{dT}\right)_{sat} = \frac{h_{fg}}{Tv_{fg}}$$

since v_f is small, $v_{fg} = v_g$

therefore

$$\frac{dP}{dT} \cong \frac{h_{fg}}{Tv_g} = \frac{h_{fg}P_g}{RT^2}$$

integrating from P_v, T_f to P_L, T_L

$$\ln\left(\frac{P_v}{P_L}\right) = -\frac{h_{fg}}{R}\frac{1}{T}\Bigg|_{T_L}^{T_v}$$

recall

$$P_v = P_{sat} = P_L + \frac{2\sigma}{r_w}$$

$$\ln\left(\frac{P_v}{P_L}\right) = \ln\left[1+\frac{2\sigma}{r_W P_L}\right] \approx \frac{2\sigma}{r_W P_L}$$ If this term is small

now $P_L = P_{sat}$, $T_v T_L \approx T_{sat}^2$

$$\frac{2\sigma}{r_W P_{sat}} \approx \frac{h_{fg}}{RT_{sat}^2}\left(T_{sat} - T_L\right)$$

$$\left(T_{sat} - T_L\right) \approx \frac{2\sigma R T_{sat}^2}{h_{fg} r_W P_{sat}}$$

let $r_w = r_{eff}$, an effective pore radius

$$\Delta P_{max} = P_v - P_L = \frac{2\sigma}{r_{eff}}$$

$$(T_{sat} - T_L) \approx \frac{2\sigma R T_{sat}^2}{h_{fg} r_{eff} P_{sat}}$$

Pressure in Flat Heat Pipe

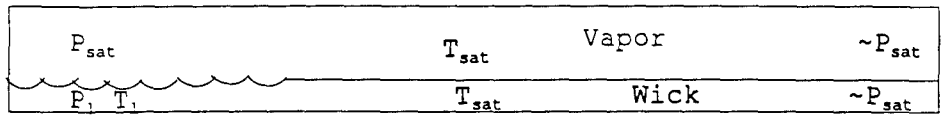

Liquid - Vapor Path

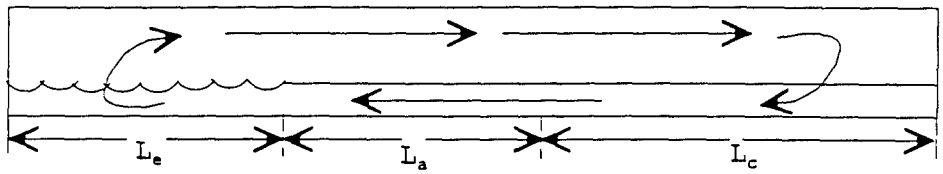

$$\Delta P_{max} = \Delta P_{vapor} + \Delta P_{liquid}$$

but the path is some averaged path estimate of averaged path:

$$\overline{L} = \frac{L_e}{2} + L_a + \frac{L_c}{2}$$

for no adiabatic section, as in USNA fhp

$$\overline{L} = \frac{L_e + L_c}{2}$$

Flat Plate Pressure Loss, Laminar Flow

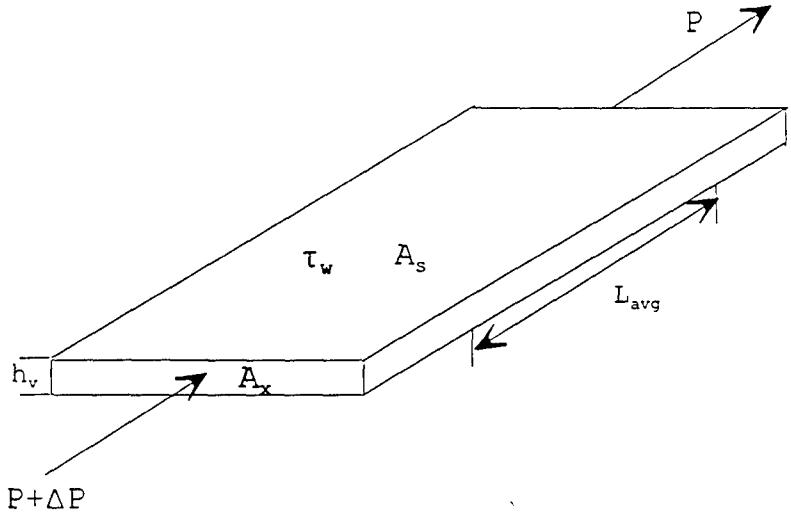

$$(P + \Delta P)A_x - PA_x = \tau_W 2W\overline{L}$$

$$\Delta P = \frac{2\tau_w \overline{L}}{h_v}$$

where

$$f \equiv \frac{\tau_w}{5\rho_v \bar{V}_{vD}^2}$$

need f in terms of average vapor velocity

Fluid Flow (Pouseuille) - Laminar

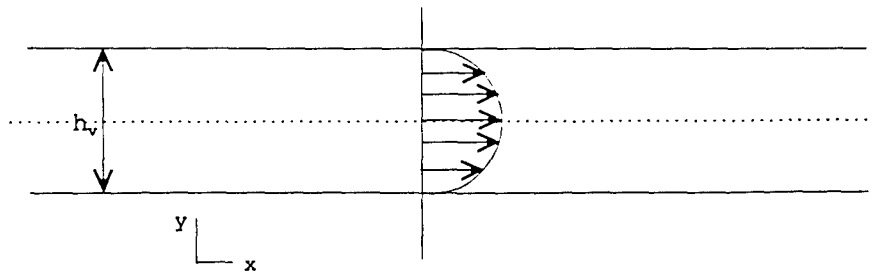

$$-\frac{dP}{dx} = G = \mu \frac{d^2u}{dy^2}$$

$$u = \frac{Gy^2}{2\mu} + Ay + B$$

Boundary Conditions

at y=0, u=0

$$\text{at } y = \frac{h_v}{2}, \frac{\partial u}{\partial y} = 0$$

Applying Boundary Conditions,

$$u = \frac{\left(\frac{dP}{dx}\right)}{2\mu}\left[h_v y - y^2\right]$$

then,

$$\text{find } \bar{V}_{vD} = \frac{\int_0^{h_v} u dy}{h_v}$$

$$\bar{V}_{vD} = \frac{\frac{dP}{dx} h_v^2}{12\mu}$$

$$\text{so, } \frac{dP}{dx} = \frac{12\mu \bar{V}_{vD}}{h_v^2} = \frac{\Delta P}{\bar{L}}$$

let $\mathrm{Re}_f \equiv \frac{\rho_v \bar{V}_{vD} h_v}{\mu_v}$, film Reynold's number

$$f_f = \frac{12}{\mathrm{Re}_f}$$

Pressure Loss Through Vapor assuming laminar flow

$$\Delta P_v = \left(\tfrac{1}{2}\rho_v \bar{V}_{vD}^2\right)\frac{24}{\mathrm{Re}_f}\frac{\bar{L}}{h_v}$$

$$\dot{m} = \rho_v \bar{V}_{vD} W h_v = \frac{q_e}{h_{fg}}$$

where $A_v = Wh_v$ (Vapor Flow Area)

$$\Delta P_v = \frac{12\dot{m}\bar{L}\mu_v}{\rho_v h_v^2 A_v} = \frac{12 q_e \bar{L}\mu_v}{\rho_v h_v^2 A_v h_{fg}}$$

where

$$h_v = \delta_v$$

So,

$$\Delta P_v = \frac{12 q_e \bar{L}\mu_v}{\rho_v \delta_v^2 A_v h_{fg}}$$

Vapor Flow (Find effective L)

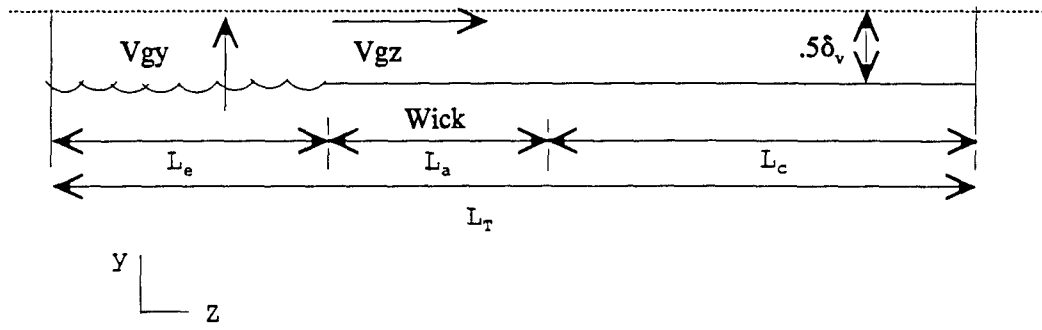

$$\text{Assume } \mathrm{Re}_\delta = \frac{\rho_v \delta_v \bar{V}_{gy}}{\mu_v} << 1$$

$$\text{let } \left.\frac{dP}{dz}\right)_v = -\frac{12 q_e \mu_v}{\rho_v \delta_v^2 A_v h_{fg}} = -\frac{12 \dot{m} \mu_v}{\rho_v \delta_v^2 A_v}$$

for mass flow in z direction,

$$\dot{m}_z = \frac{z}{L_e}\frac{q_e}{h_{fg}}, 0 \le z \le L_e$$

$$\dot{m}_z = \frac{q_e}{h_{fg}}, L_e \le z \le L_e + L_a$$

$$\dot{m}_z = \frac{L_T - z}{L_T - (L_e + L_a)}\left(\frac{q_e}{h_{fg}}\right), L_e + L_a \le z \le L_T$$

$$\frac{dP}{dz} = -B\left[\frac{z}{L_e} + 1 + \frac{(L_T - z)}{L_T - (L_e + L_a)}\right]$$

where

$$B = \frac{12\mu_v q_e}{\rho_v \delta_v^2 A_v h_{fg}}$$

integrating both sides,

$$P_v(L_T) - P_v(0) = -B\left\{\left[\frac{z^2}{2L_e}\right]_0^{L_e} + (z)_{L_e}^{L_e+L_a} + \left[\frac{L_T - \frac{z^2}{2}}{L_c}\right]_{L_e+L_a}^{L_T}\right\}$$

this simplifies to:

$$P_v(L_T) - P_v(0) = \frac{12\mu_v q_e}{\rho_v \delta_v^2 A_v h_{fg}}\left(\frac{L_e}{2} + L_a + \frac{L_c}{2}\right)$$

which is the pressure loss in the vapor space where:

$$\left(\frac{L_e}{2} + L_a + \frac{L_c}{2}\right) = \overline{L}$$

Flow through Porous Media

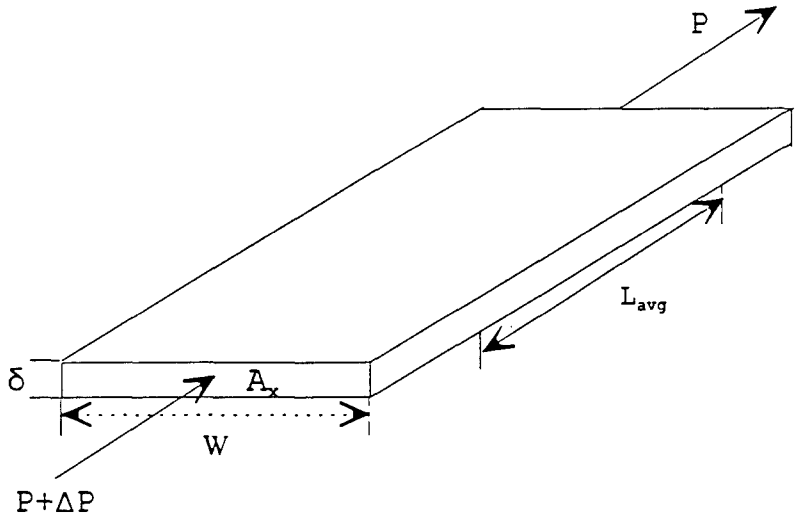

For Flat Plate (non-porous) channel:

$$\Delta P_v = \frac{12\dot{m}\bar{L}\mu}{\rho\delta^2 A}$$

$$A = W\delta$$

$$\Delta P = \tfrac{1}{2}\rho V^2 2f\tfrac{\bar{L}}{\delta}$$

recall,

$$f \equiv \frac{12}{\mathrm{Re}_\delta} = \frac{12\mu}{\rho V\delta}$$

therefore

$$\frac{\Delta P}{\bar{L}} = \frac{12\mu V}{\delta^2}$$

and

$$\frac{dP}{dx} = \frac{12\mu\bar{V}}{\delta^2}$$

For porous media,

$\bar{V}_L$ = average velocity through wick

$\bar{V}_{pL}$ = average velocity through pores

and A_x = open area (pore area) where A_L = wick area

φ, porosity, is defined as:

$$\varphi = \frac{A_x}{A_L} = \frac{\bar{V}_L}{\bar{V}_{pL}}$$

$$\frac{dP}{dx} = -\frac{\mu_L \dot{m}_L}{\rho_L A_L K}$$

K = permeability (m^2)

Also, for flow through porous media,

$$\Delta P A_x = \tau_W A_s$$

where A_s is total wetted surface area of wick

$$f = \frac{\tau_W}{\frac{1}{2}\rho\bar{V}_{pL}^2}$$

substituting,

$$\Delta P A_x = \left(\tfrac{1}{2}\rho \bar{V}_{pL}^2\right) f A_s$$

simplifies to approximately

$$\frac{dP}{dx} = -\left(\tfrac{1}{2}\rho \bar{V}_{pL}^2\right) f \frac{\frac{A_s}{L}}{A_x}$$

set this equal to the earlier result,

$$\frac{dP}{dx} = -\frac{\mu_L \dot{m}_L}{\rho_L A_L K}$$

$$\left(\tfrac{1}{2}\rho \bar{V}_{pL}^2\right) f \frac{\frac{A_s}{L}}{A_x} = \frac{\mu_L \dot{m}_L}{\rho_L A_L K}$$

solving for K,

$$K = \frac{2\mu\varphi A_x}{\rho \bar{V}_{pL} f(\frac{A_s}{L})}$$

however, using permeability equation for cylindrical porous media and approximating with D_h, hydraulic radius is a valid approximation:

$$K = \frac{\varphi D_h^2}{32}$$

to find liquid pressure drop in heat pipes, use this K along with the following equation:

$$\frac{dP}{dx} = -\frac{\mu_L \dot{m}_L}{\rho_L A_L K}$$

Capillary Limit -One Side heated

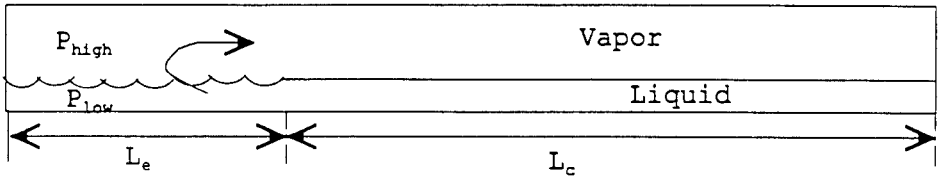

Steady state limit

$$\dot{m}_L = \dot{m}_v = \frac{\dot{q}_e}{h_{fg}}$$

max capillary pumping head (neglect gravity)

$$\Delta P_{cap_{\max}} = \frac{2\sigma}{r_{eff}}$$

$$\Delta P_{cap} = \Delta P_v + \Delta P_L$$

$$\text{let } \overline{L} = \frac{L_e + L_c}{2}$$

$$\Delta P_{cap} = \frac{dP}{dx}dx\bigg|_v + \frac{dP}{dx}dx\bigg|_L$$

$$\Delta P_{cap} = \frac{12\mu_v \dot{m}}{\rho_v A_v \delta_v^2}\overline{L} + \frac{12\mu_L \dot{m}}{\rho_L A_L K}\overline{L}$$

$$\frac{2\sigma}{r_{eff}} = \frac{\dot{q}_e}{h_{fg}}\overline{L}\left\{\frac{12\mu_v}{\rho_v A_v \delta_v^2} + \frac{\mu_L}{\rho_L A_L K}\right\}$$

therefore, capillary limit, one side heated is:

$$\dot{q}_e\Big)_{cap_{limit}} = \frac{2\sigma h_{fg}}{r_{eff}\overline{L}}\left\{\frac{12\mu_v}{\rho_v A_v \delta_v^2} + \frac{\mu_L}{\rho_L A_L K}\right\}^{-1}$$

Capillary Limit, Both Sides Heated

$$\Delta P_v = f_v \dot{m}$$

and

$$\Delta P_{L1} = f_{L1} \dot{m}_{L1},$$

$$\Delta P_{L2} = f_{L2} \dot{m}_{L2}$$

$$\Delta P_T = f_T \dot{m} = f_v \dot{m} + f_{Le} \dot{m}$$

$$\Delta P_T = f_T \dot{m} = f_v \dot{m} + f_{Le} (\dot{m}_{L1} + \dot{m}_{L2})$$

letting $\Delta P_{L1} = \Delta P_{L2}$

$$\Delta P_T - \Delta P_v = f_{Le} \Delta P_L \left(\frac{1}{f_{L1}} + \frac{1}{f_{L2}} \right)$$

where

$$f_v = \frac{12 \mu_v}{\rho_v A_v \delta_v^2} \overline{L}$$

and

$$f_{L1} = f_{L2} = \frac{\mu_L}{\rho_L A_L K} \overline{L}$$

therefore

$$\Delta P_T = \dot{m} \left[f_v + \frac{f_L}{2} \right] = \dot{m} \overline{L} \left[\frac{12 \mu_v}{\rho_v A_v \delta_v^2} + \frac{\mu_L}{2 \rho_L A_L K} \right]$$

and, **Capillary Limit for 2 sides heated:**

$$\dot{q}_e \Big)_{cap_{\lim it}} = \frac{2 \sigma h_{fg}}{r_{eff} \overline{L}} \left[\frac{12 \mu_v}{\rho_v A_v \delta_v^2} + \frac{\mu_L}{2 \rho_L A_L K} \right]^{-1}$$

Appendix 2 - BOILING LIMIT DERIVATION

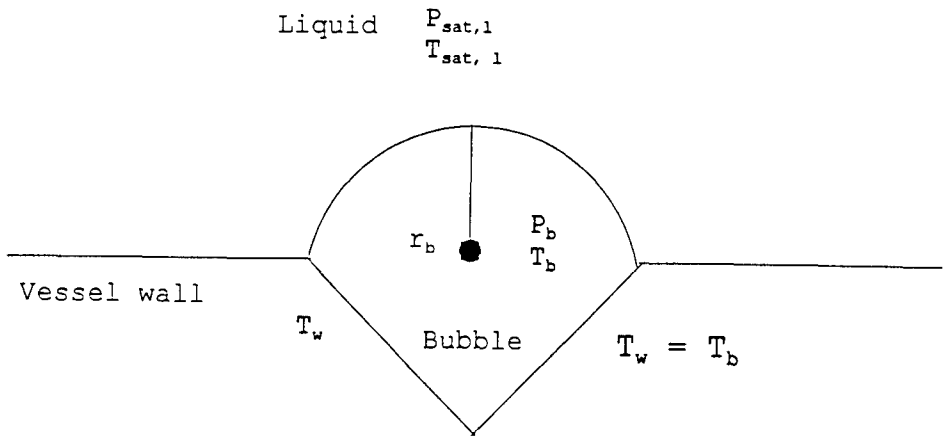

$$dP = \frac{2\sigma}{r_b}$$, r_b = effective bubble radius

Clapeyron Equation:

$$\left.\frac{dP}{dT}\right)_{sat} = \frac{h_{fg}}{Tv_{fg}}$$

$$v_{fg} = v_g + v_f \text{ (small)} = v_g$$

$$v_g = v_b = (RT_b) / P_b, \quad P_b = P$$

$$\left.\frac{dP}{dT}\right)_{sat} = \frac{h_{fg}P}{RT^2}$$

$$\int_{P_{sat,l}}^{P_b} \frac{dP}{P} = \frac{h_{fg}}{R} \int_{T_{sat,l}}^{T_b} \frac{dT}{T^2}$$

recall,

$$P_b = P_{sat,l} + \frac{2\sigma}{r_b}$$

so

$$\ln(P_{sat,l} + \tfrac{2\sigma}{r}) - \ln(P_{sat,l}) = -\tfrac{h_{fg}}{R}\left[\tfrac{1}{T_b} - \tfrac{1}{T_{sat,l}}\right]$$

where

$$\ln(P_{sat,l} + \tfrac{2\sigma}{r}) - \ln(P_{sat,l}) \approx \frac{2\sigma}{rP_{sat,l}}$$

$$\frac{2\sigma}{P_{sat,l}r} = -\frac{h_{fg}}{R}\left[\frac{T_{sat,l} - T_b}{T_{sat,l}T_b}\right]$$

$$T_{sat,l} \approx T_b \approx T_{sat}$$

Therefore, wall temperature difference required for nucleation

$$T_b - T_{sat,l} = \frac{R2\sigma T_{sat,l}^2}{h_{fg}P_{sat,l}r_b}$$

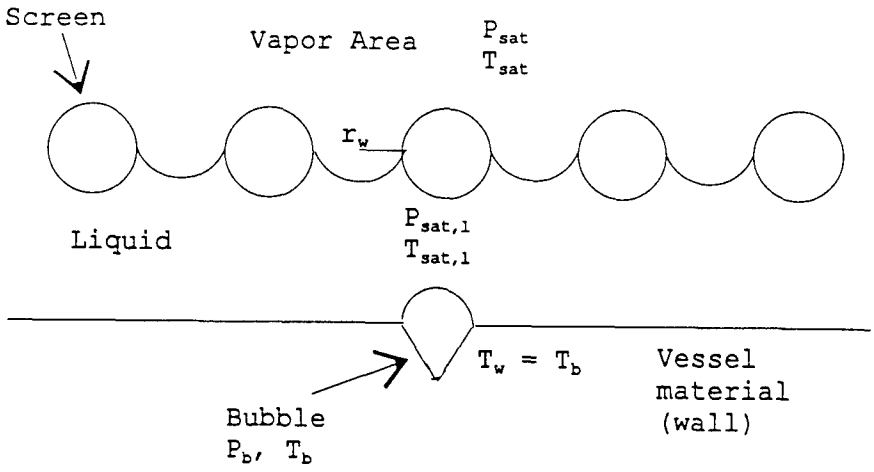

Note: $r_b << r_w$

Applied to heat pipe wick

Boiling Onset in Heat Pipe

ΔP from vessel wall to vapor area:

$$P_b - P_{sat} = (P_b - P_{sat,l}) - (P_{sat} - P_{sat,l})$$

$$P_b - P_{sat} = 2\sigma\left[\frac{1}{r_b} - \frac{1}{r_w}\right]$$

Using Clapeyron Criteria for boiling

$$\Delta T_{crit} = T_w - T_{sat} = \frac{2\sigma R T_{sat}^2}{P_{sat} h_{fg}} \left[\frac{1}{r_b} - \frac{1}{r_w} \right]$$

Heat into heat pipe is transferred by conduction,

$$Q_{cond} = \frac{kA\Delta T}{\Delta x}$$

therefore, boiling limit is reached when

$$Q_b = UA_v \Delta T_{crit}$$

where U, the overall heat transfer coefficient is found by:

$$U = \left[\frac{t_v}{k_w} + \frac{t_w}{k_{eff}} \right]^{-1}$$

where t_v is vessel thickness and t_w is wick thickness

therefore,

$$Q_b = \frac{2 A_v R T_{sat}^2}{P_{sat} h_{fg}} \left[\frac{1}{r_b} - \frac{1}{r_w} \right] \left[\frac{t_v}{k_w} + \frac{t_w}{k_{eff}} \right]^{-1}$$

APPENDIX 3 - SONIC LIMIT DERIVATION

at steady-state:

$$Q = \dot{m} h_{fg}$$

where $\dot{m} = \rho A V$

also max velocity (sonic) for constant area duct is:

$$V_{\max} = \sqrt{kRT_{local}}$$

substituting,

$$Q_{sonic} = h_{fg} \rho_v A_v \sqrt{kRT_{local}}$$

APPENDIX 4 - DEFLECTION DERIVATIONS AND SPREADSHEET

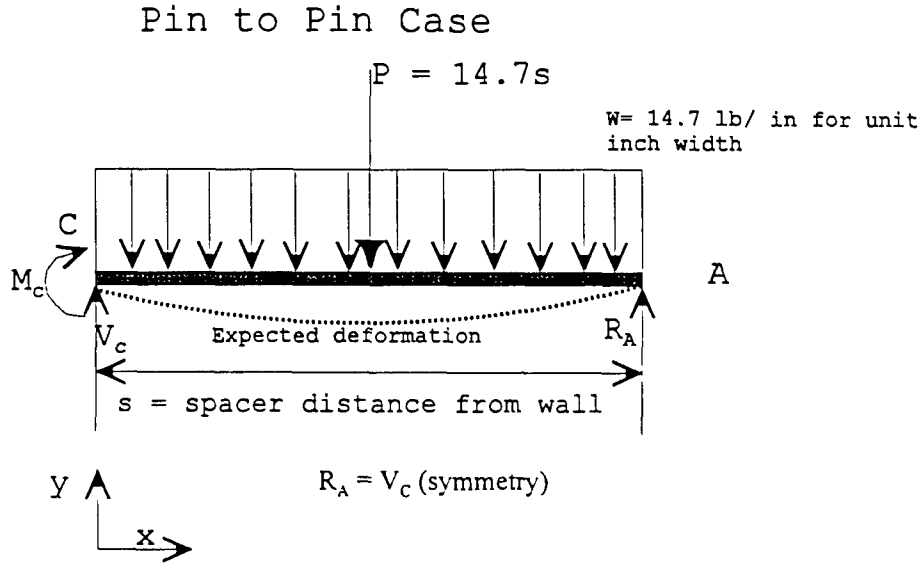

Equation 1: $$EI\frac{d^2v}{dx^2} = R_A x - 7.35x^2$$

Equation 2: $$EI\frac{dv}{dx} = \frac{R_A}{2}x^2 - \frac{7.35}{3}x^3 + C_1$$

Equation 3 : $$EIv = \frac{R_A}{6}x^3 - \frac{7.35}{12}x^4 + C_1 x + C_2$$

Boundary Conditions

at x = 0, v = 0. Therefore $C_2 = 0$

at x = s/2, dv/dx =0

$$C_1 = -.6125s^3$$

knowing that v_{max} is at x = s/2 and solving equation 3:

$$v_{max} = \frac{-.191405s^4}{EI}$$

Sidewall to Pin Case

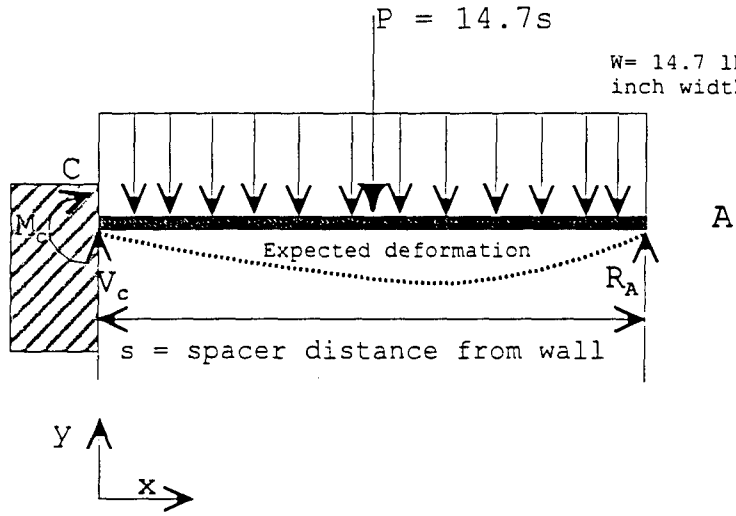

Equation 1 $$EI\frac{d^2v}{dx^2} = M_c + V_c x - \frac{Wx^2}{2}$$

Equation 2 $$EI\frac{dv}{dx} = M_c x + \frac{V_c}{2}x^2 - \frac{Wx^3}{6} + C_1$$

Equation 3 $$EIv = \frac{M_c}{2}x^2 + \frac{V_c}{6}x^3 - \frac{W}{24}x^4 + C_1 x + C_2$$

Boundary Conditions
at x = 0, v = 0, dv/dx = 0
therefore $C_1 = 0 = C_2$

To find M_C and V_C, use equations 1 and 3 and at A, M = 0 and v = 0

$$M_C = -1.8375s$$

$$V_C = 9.1875s$$

solving for max deflection (dv/dx = 0) using equation 2

v_{max} at x = .57846483s

substituting into equation 3

$$v_{max} = \frac{.22785s^4 - .30747s^3}{EI}$$

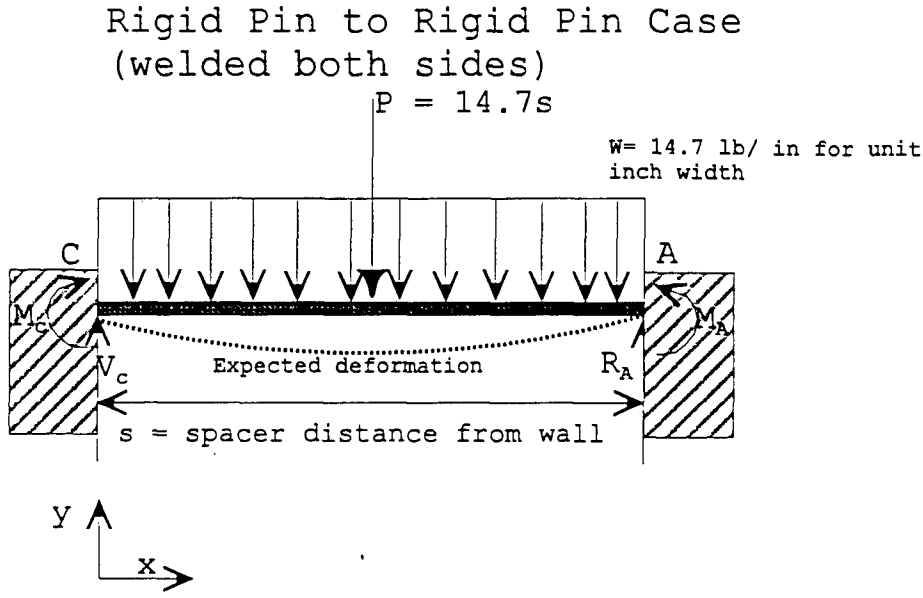

Using Ferdindand Singer's Strength of Materials (1962):

$$M_A = M_C = \frac{Ws^2}{12}$$

And

$$v_{max} = \frac{Ws^4}{384EI}$$

Materials

	psipsi EG	psi Yield T	psi Yield C	psi Ult T	psi Ult C	Poisson's
Monel						
R-400	2.6E+07	9.4E+06	3.5E+04	8.0E+04		0.295
R-405	2.6E+07	9.4E+06	7.4E+04	8.3E+04		0.32
K-500	2.6E+07	9.4E+06	1.2E+05	1.6E+05		0.32
SS 304	2.80E+07		5.50E+04	1.00E+05		0.3
1040	3.00E+07		5.43E+04	8.55E+04		0.3

for unit inch width

Desired deflection = 0.0625

Spacing 1040 Material, Thickness

	0.035	**0.04**	**0.045**	**0.05**	**0.055**	**0.06**	**0.065**
0.1	-0.0000	-0.0000	-0.0000	-0.0000	-0.0000	-0.0000	-0.0000
0.2	-0.0000	-0.0000	-0.0000	-0.0000	-0.0000	-0.0000	-0.0000
0.3	-0.0000	-0.0000	-0.0000	-0.0000	-0.0000	-0.0000	-0.0000
0.4	-0.0000	-0.0000	-0.0000	-0.0000	-0.0000	-0.0000	-0.0000
0.5	-0.0000	-0.0000	-0.0000	-0.0000	-0.0000	-0.0000	-0.0000
0.6	-0.0000	-0.0000	-0.0000	-0.0000	-0.0000	-0.0000	-0.0000
0.7	-0.0000	-0.0000	-0.0000	-0.0000	-0.0000	-0.0000	-0.0000
0.8	-0.0001	-0.0000	-0.0000	-0.0000	-0.0000	-0.0000	-0.0000
0.9	-0.0001	-0.0001	-0.0000	-0.0000	-0.0000	-0.0000	-0.0000
1	-0.0001	-0.0001	-0.0001	-0.0000	-0.0000	-0.0000	-0.0000
1.1	-0.0002	-0.0001	-0.0001	-0.0001	-0.0001	-0.0000	-0.0000
1.2	-0.0003	-0.0002	-0.0001	-0.0001	-0.0001	-0.0001	-0.0000
1.3	-0.0004	-0.0003	-0.0002	-0.0001	-0.0001	-0.0001	-0.0001
1.4	-0.0005	-0.0003	-0.0002	-0.0002	-0.0001	-0.0001	-0.0001
1.5	-0.0007	-0.0005	-0.0003	-0.0002	-0.0002	-0.0001	-0.0001
1.6	-0.0009	-0.0006	-0.0004	-0.0003	-0.0002	-0.0002	-0.0001
1.7	-0.0011	-0.0007	-0.0005	-0.0004	-0.0003	-0.0002	-0.0002
1.8	-0.0014	-0.0009	-0.0007	-0.0005	-0.0004	-0.0003	-0.0002
1.9	-0.0017	-0.0012	-0.0008	-0.0006	-0.0004	-0.0003	-0.0003
2	-0.0021	-0.0014	-0.0010	-0.0007	-0.0006	-0.0004	-0.0003
2.1	-0.0026	-0.0017	-0.0012	-0.0009	-0.0007	-0.0005	-0.0004
2.2	-0.0031	-0.0021	-0.0015	-0.0011	-0.0008	-0.0006	-0.0005
2.3	-0.0037	-0.0025	-0.0018	-0.0013	-0.0010	-0.0007	-0.0006
2.4	-0.0044	-0.0030	-0.0021	-0.0015	-0.0011	-0.0009	-0.0007
2.5	-0.0052	-0.0035	-0.0025	-0.0018	-0.0013	-0.0010	-0.0008
2.6	-0.0061	-0.0041	-0.0029	-0.0021	-0.0016	-0.0012	-0.0010
2.7	-0.0071	-0.0048	-0.0033	-0.0024	-0.0018	-0.0014	-0.0011
2.8	-0.0082	-0.0055	-0.0039	-0.0028	-0.0021	-0.0016	-0.0013
2.9	-0.0095	-0.0063	-0.0045	-0.0032	-0.0024	-0.0019	-0.0015
3	-0.0108	-0.0073	-0.0051	-0.0037	-0.0028	-0.0022	-0.0017
3.1	-0.0124	-0.0083	-0.0058	-0.0042	-0.0032	-0.0025	-0.0019

APPENDIX 5 - MATHCAD MODELLING OF FIN VS HEAT PIPE

Fin Analysis - convection only - steady state

$j := 1..10$ $\quad k := 150$ $\quad Ax := \frac{.1}{12} \cdot 1$

$h := 1.5$ $\quad P := 2 + \frac{1}{12}$

$m := \left(\frac{h \cdot P}{k \cdot Ax}\right)^{0.5}$ $\quad T_{room} := 70$ $\quad Q_j := 100 - 3.412 \cdot j$ $\quad Qwatt_j := \frac{Q_j}{3.412}$

$$T(j,x) := \left[\left[T_{room} + \left(\frac{Q_j}{k \cdot Ax \cdot m}\right) \cdot \exp(-m \cdot x)\right] - 32\right] \cdot \frac{5}{9}$$

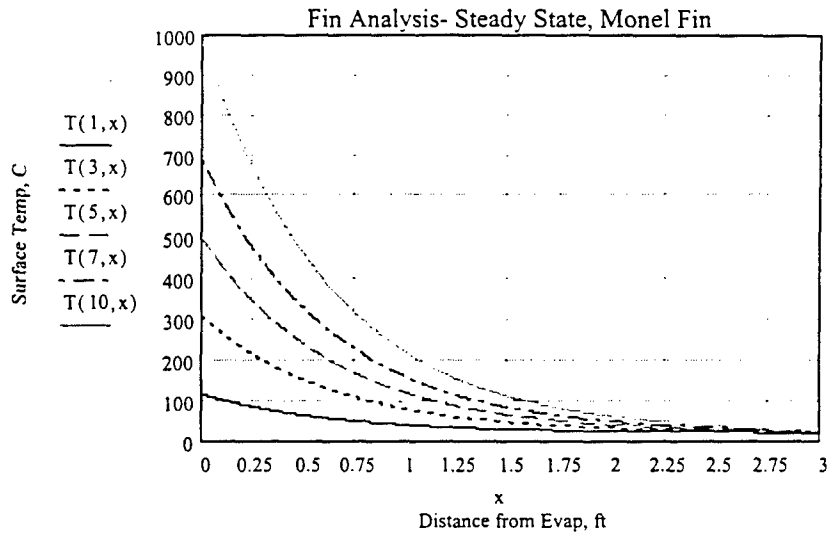

Tsat, isothermal steady state heat pipe analysis with radiation and convection.

$\sigma := 0.171810^{-8}$ $\quad \varepsilon := 0.95$ $\quad As := 6$ $\quad T_{roomk} := 70 + 460$

$Qconv(T_{ss}) := h \cdot As \cdot (T_{ss} - T_{roomk})$ $\quad Qrad(T_{ss}) := (\sigma \cdot \varepsilon \cdot As) \cdot (T_{ss}^{4} - T_{roomk}^{4})$

$T_{ss} := 460$

$T_{s1}(j) := root(Q_j - Qconv(T_{ss}) - Qrad(T_{ss}), T_{ss})$ $\quad Ts_j := [(T_{s1}(j) - 460) - 32] \cdot \frac{5}{9}$

$Qc_j := \frac{Qconv(T_{s1}(j))}{3.412}$ $\quad Qr_j := \frac{Qrad(T_{s1}(j))}{3.412}$

$Qwatt_j$ W	Ts_j C	Qc_j W	Qr_j W
100	33.572	59.163	40.837
200	45.422	115.426	84.574
300	56.704	168.995	131.005
400	67.461	220.066	179.934
500	77.73	268.824	231.176
600	87.548	315.44	284.56
700	96.949	360.075	339.925
800	105.964	402.875	397.125
900	114.619	443.973	456.027
$1 \cdot 10^3$	122.943	483.492	516.508

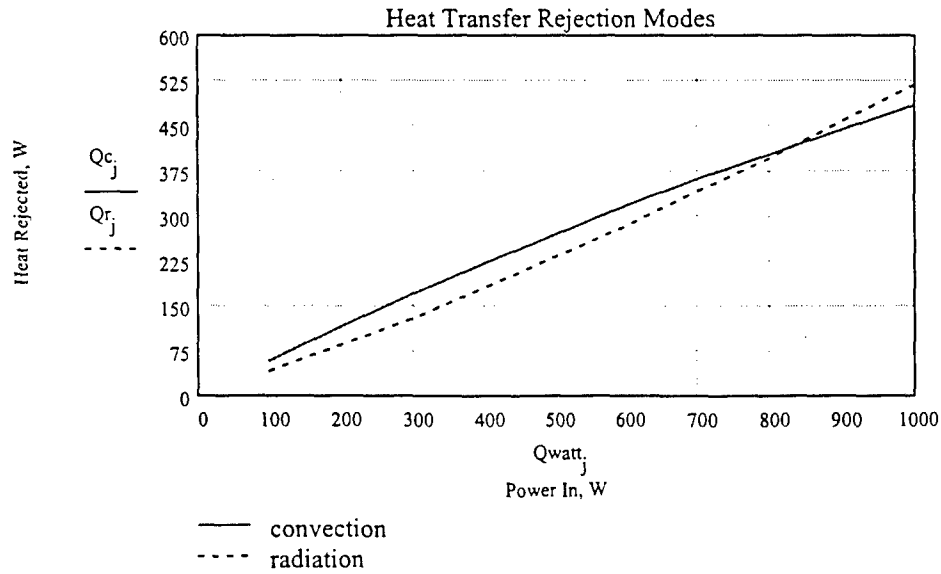

Steady state heat pipe, combined convection and radiation modes, variation of heff with angle of inclination. Q in = 400W

$n := 0 .. 18$

$theta_n := (n) \cdot 5$

$$heff := \begin{bmatrix} 4.124 \\ 4.120 \\ 4.108 \\ 4.088 \\ 4.060 \\ 4.023 \\ 3.978 \\ 3.923 \\ 3.858 \\ 3.781 \\ 3.692 \\ 3.589 \\ 3.468 \\ 3.325 \\ 3.154 \\ 2.941 \\ 2.662 \\ 2.241 \\ 1.355 \end{bmatrix}$$

$$Qconv1(T_{ss}, n) := \left(heff_n \cdot \frac{3.412}{3.28^2} \cdot 1.8\right) \cdot As \cdot (T_{ss} - T_{roomk})$$

$$Qrad1(T_{ss}) := (\sigma \cdot \varepsilon \cdot As) \cdot (T_{ss}^4 - T_{roomk}^4)$$

$T_{ss} := 460$

$T_{s2}(n) := root(Q_4 - Qconv1(T_{ss}, n) - Qrad1(T$

$Ts2\_ang_n := \left[(T_{s2}(n) - 460) - 32\right] \cdot \frac{5}{9}$

$Q_4 = 1.365 \cdot 10^3$

$Ts2\_ang =$

57.023
57.045
57.111
57.222
57.378
57.587
57.843
58.162
58.544
59.008
59.556
60.21
61.005
61.984
63.214

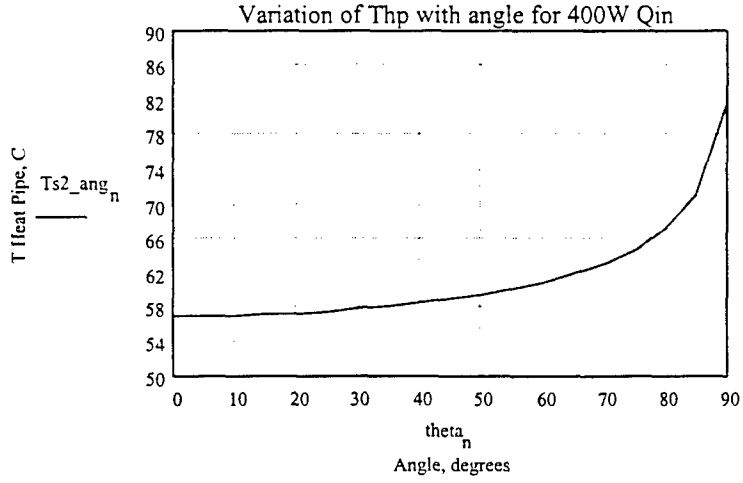

Transient lumped parameter heat pipe fin model- Monel and water masses are combined with appropriate specific heat. The heat Pipe temperature is assumed to be isothermal.

$$0 = m \cdot c \cdot \frac{d}{dt} Trad(t) - Q + h \cdot A \cdot (Trad(t) - Tref) + A \cdot \sigma \cdot \varepsilon \cdot \left(Trad(t)^4 - Tref^4\right)$$

$m := 3.85$ $c := 1$ $h := 1.23$ $Q_4 = 1.365 \cdot 10^3$ $As = 6$

$Thp1 := 530, 535 .. 620$

$$t2(Thp1) := m \cdot c \cdot \left[\int_{530}^{Thp1} \frac{1}{\left[Q_4 - h \cdot As \cdot (Trad - 530) - As \cdot \sigma \cdot \varepsilon \cdot \left(Trad^4 - 530^4\right)\right]} dTrad \right]$$

$$ThpC(Thp1) := (Thp1 - 460 - 32) \cdot \frac{5}{9}$$

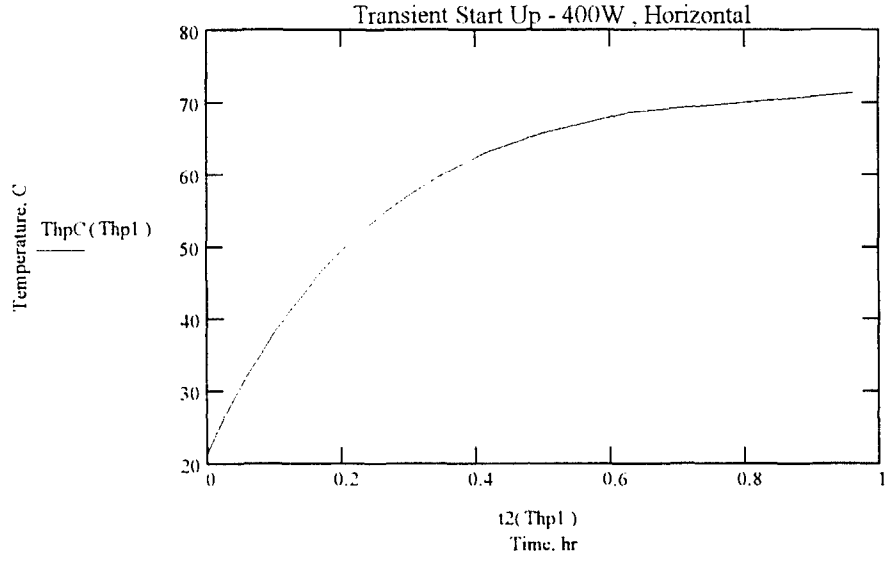

Fin Analysis - convection only (assume radiation losses are close to convection losses) see other analysis - steady state, so h is approximately 3.

$j := 1 .. 10$ $\quad k := 150$ $\quad Ax := \frac{.1}{12} \cdot 1$

$h := 3$ $\quad P := 2 + \frac{1}{12}$

$m := \left(\frac{h \cdot P}{k \cdot Ax}\right)^{0.5}$ $\quad T_{room} := 70$ $\quad Q_j := 100 \cdot 3.412 \cdot j$ $\quad Qwatt_j := \frac{Q_j}{3.412}$

$Thpipe(x) := 68.$ $\quad T(j, x) := \left[\left[T_{room} + \left(\frac{Q_j}{k \cdot Ax \cdot m}\right) \cdot \exp(-m \cdot x)\right] - 32\right] \cdot \frac{5}{9}$

$cm(x) := \frac{x}{3.28} \cdot 100$

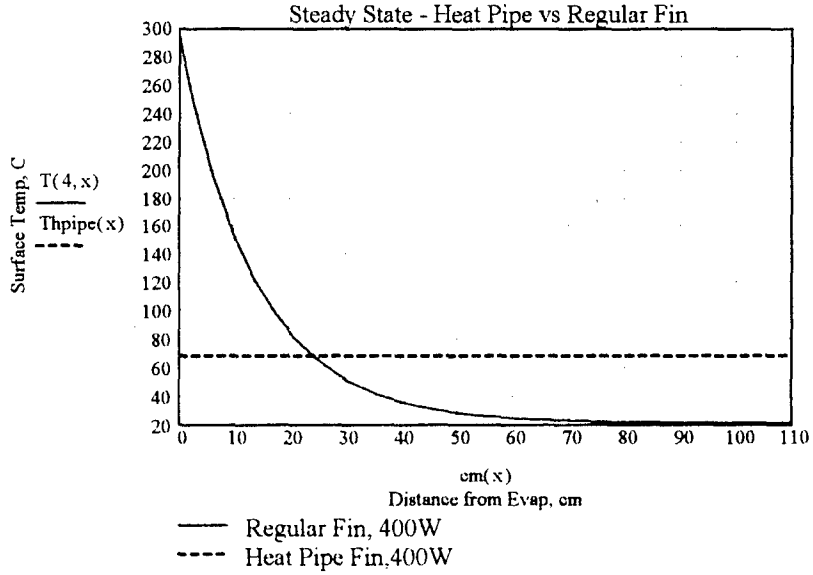

ACKNOWLEDGMENTS

Special Thanks to:

Gene Miller, who welded both heat pipes and developed much of the fabrication procedures

Tom Price, who coordinated all work with USNA Technical Support Department (TSD) as well as:

Greg Denevan and Michel Baden, who helped with all of the purchasing

Louis Becnel
Ronald Hanner
Charlie Popp
Bob Banks
Dale Boyer
Bob Disque

and

USNA TSD
CADIG
Purchasing Dept.
Los Alamos National Laboratory
Knolls Atomic Power Laboratory